Recirculating Ocean Gyres

Nicholas M. J. Hall,
Space and Atmospheric Physics Group,
Imperial College,
London SW7 2AZ.

December 1989

A thesis submitted for the degree of
Doctor of Philosophy, University of London
and the
Diploma of Imperial College.

Abstract

The north-west corners of the major ocean basins are characterised by seaward jets, flanked by tight, non-linear gyres exhibiting closed potential vorticity contours. At deep levels, isolated from surface forcing, areas of homogeneous potential vorticity are apparent. Following a review of pertinent theories and observations, a model is presented describing these 'recirculation' regions, extending the quasi-geostrophic layer models of Marshall and Nurser (1986, 1988) to the continuously stratified two dimensional case.

The study is diagnostic, concentrating on numerical inversions of idealised potential vorticity distributions in a vertical, meridional section through a free inertial gyre. An iterative approach is used to find the 'bowl' of the circulation: the free boundary between the deep recirculating homogenised water and the stagnant water below. A quasi-geostrophic model is presented first, forced by potential vorticity anomalies in the upper layers. Later, the Ertel potential vorticity is inverted in an isopycnal coordinate model, 'forced' by prescribing the depth of the uppermost coordinate surface, chosen to represent the depth of the main thermocline.

It is shown that the homogenised recirculation has a finite depth penetration, possibly not extending to the ocean floor. In cases where the flow reaches the bottom, the recirculation can be divided into two regions: a 'core' region, where bottom currents exist and a baroclinic 'fringe' to the south. The surface intensified part of the eastward jet is recirculated in the broad, westward flowing fringe, while the component of the transport returned within the core itself is largely depth independent.

The enhanced mass transport of the Gulf Stream can be accounted for by the models. Its magnitude is sensitive to the surface forcing imposed. For realistic parameters, the core carries the greater proportion of the transport.

The structure of the recirculation is dependent on the value assumed for the deep homogeneous potential vorticity. If a positive deep potential vorticity anomaly is imposed, the upper level gyre interface moves northwards while a cyclonic gyre becomes dominant in the bottom flow. If the anomaly exceeds a certain limit, solutions can no longer be found.

For Lily

Acknowledgements

I would like to thank my supervisor, John Marshall, and everyone in the Atmospheric Physics Group, particularly George Nurser, for their help and advice. This work was supported by the Natural Environment Research Council of the United Kingdom.

Contents

List of Figures

Chapter 1

Review of Theories

1.1 Introduction

A major component of the observed large scale ocean circulation can be attributed to the driving force of the wind. The precise mechanism is subtle but the end result is intuitive. Blocked by the continents, the water circulates in closed gyres. During the late 40s and early 50s, theories were developed to explain the nature of the wind driven circulation. A duality emerged. On the one hand there were forced dissipative models such as that of Stommel (1948), where the momentum imparted by the wind is dissipated in a frictional boundary layer. On the other hand, Fofonoff's (1954) model had no wind forcing or friction, but free flow closed by non-linear boundary currents. In the latter model, the role of forcing and dissipation is relegated to a fine tuning effect, determining the intensity of the free circulation (Niiler, 1966). In this thesis, attention is concentrated on the 'recirculation' regions found in the north western corners of the world's oceans, which are modelled as free inertial gyres.

The dynamics of these two archetypal theories are best understood in terms of vorticity. In the forced / dissipative regime, vorticity is supplied and extracted by the wind stress and friction in a continuing cycle, offsetting changes in planetary vorticity as the fluid moves meridionally. In an unforced, 'inertial' regime, the flow follows closed absolute vorticity contours.

The ocean circulation has considerable depth dependence and if this vertical structure is to be modelled, the effects of vortex stretching must be taken into account. Vorticity

theory must give way to potential vorticity theory. Various forms of potential vorticity shall be used in what follows, but they are all based on either the Ertel potential vorticity,

$$Q = -\frac{(f+\xi)}{\rho}\frac{\partial \rho}{\partial z} \tag{1.1.1}$$

or the quasi-geostrophic form,

$$q = \beta y + \nabla^2 \psi + f_0^2 \frac{\partial}{\partial z}\left(\frac{1}{N^2}\frac{\partial \psi}{\partial z}\right) \tag{1.1.2}$$

where f is the coriolis parameter; ξ the relative vorticity*; ρ is density; y and z are northward and upward cartesian coordinates; f_0 and β are the values of f and its meridional gradient at $y = 0$; ψ is the horizontal streamfunction and N is the Brunt Vaisalla frequency.

In an incompressible baroclinic ocean, the following conservation laws apply for steady, adiabatic flow:

$$\left.\begin{aligned} \mathbf{u}.\nabla\rho &= 0 \\ \mathbf{u}.\nabla Q &= 0 \end{aligned}\right\} \tag{1.1.3}$$

where $\mathbf{u}$ is the velocity, (u, v, w) (in directions x, y, z where x is to the east). Equations (1.1.3) form a starting point for all theories of the vertical structure of ocean gyres, but alone, they are not sufficient to pose the problem fully. In the last decade several theories have emerged which satisfy (1.1.3) in radically different ways. A new duality now exists between 'ventilated' models (Luyten, Pedlosky and Stommel, 1983) and unventilated models (Rhines and Young, 1982a). In the former, potential vorticity is set at a surface density outcrop and then conserved as fluid is subducted into the main thermocline. In the latter, deep flow is confined to regions where potential vorticity contours have closed off on themselves, resulting in the homogenisation of potential vorticity by small (synoptic) scale eddies.

Again, the duality can be resolved by considering different regions. Marshall and Nurser (1986, 1988) (hereafter MN and MN2), Greatbatch (1987), Cessi, Ierley and Young (1987) (hereafter CIY) and Cessi (1988) have all made use of the facts that homogenisation occurs within closed Q contours, and that these closed Q contours are a feature of the recirculating gyres associated with strong seaward jets such as the Gulf Stream and Kuroshio extensions. The resulting models depict these recirculation regions as free inertial gyres with homogeneous potential vorticity at deep, isolated levels.

* vertical component

The work presented in this thesis is an extension of these theories to a vertically continuous model, which is then used to examine the structure and transport of these gyres. Idealised distributions of potential vorticity are inverted to find the flow in a vertical, meridional section through a free inertial gyre. In particular, solutions are sought for the 'bowl' of the circulation: the free boundary representing the depth of penetration of the deep homogenised gyre.

The remainder of this chapter is a review of the classical theories of the steady, gyre scale ocean circulation. Particular emphasis is given to the role of eddies in equilibrating these steady flows, especially through their effect on the large scale Q distribution. Attention is focussed on the ramifications for non-linear free gyres of sub-basin scale.

In chapter 2, the observations relevant to the recirculation region are discussed. Hydrographic sections and current meter measurements are presented and the characteristic Q fields at different depths are analysed.

In chapter 3, a brief review is given of theories which have attempted to describe the vertical structure of these observations. Previous models of the vertical structure of free, non-linear gyres with idealised Q distributions are discussed in detail and the results from eddy resolving numerical models are surveyed.

Chapter 4 contains the author's extensions to these models. A continuous two dimensional model is presented, based on numerical inversions of idealised quasi-geostrophic potential vorticity distributions. The method of solution for both the flow and its depth extent is described and the results are presented and analysed. Comparisons are made with simple theory, observations and general circulation models.

Chapter 5 is an extension of this work to an asymmetric two gyre system in which the value of the deep homogeneous q and the position of the eastward jet are allowed to vary. The quasi-geostrophic inversions presented up to this point are the subject of a paper by the author (Hall, 1990).

In chapter 6, a new formulation is presented in which the restrictions of quasi-geostrophy are discarded and a geostrophic form of the Ertel potential vorticity is inverted. This allows much closer comparison with the observations shown in chapter 2. In particular, the sensitivity of the solutions to the position of the thermocline and the bottom isopycnal is investigated and an inversion is presented which has been forced with real data.

1.2 Homogeneous Theories of the Ocean Circulation

Much of the early theoretical effort in oceanography was concentrated on understanding how surface winds could drive the observed general circulation. Figure (1.1) shows the surface currents of the Atlantic Ocean from a long term compilation of measurements and ship reports (Defant, 1961). The first thing to note about these observations is the existence of closed circulation patterns or gyres. Another striking feature is the strong, narrow boundary currents which complete these gyres on the western sides of every major ocean basin in both hemispheres. A brief review is presented below of the key theories which have been put forward to explain these phenomena.

(a) Basic Driving Mechanisms: Ekman and Sverdrup Transports

Surface currents were a puzzle for navigators and oceanographers during the early part of this century. The correlation between mean winds and mean currents, as measured by ship drift was very poor. It was Ekman (1905) who took the first step towards explaining this conundrum. In an Ekman surface boundary layer the momentum balance is

$$f\hat{\mathbf{k}}_{\wedge}\mathbf{v} + \frac{1}{\rho_0}\nabla p = \frac{1}{\rho_0}\frac{\partial \vec{\tau}}{\partial z} \tag{1.2.1}$$

where $\hat{\mathbf{k}}$ is a vertical unit vector, $\mathbf{v}$ is the horizontal velocity, (u, v), ρ_0 is density, ∇p is the horizontal pressure gradient and $\vec{\tau}$ is the horizontal stress acting at depth z due to vertical momentum transfer from the surface wind. It is now standard theory to model $\vec{\tau}$ as proportional to the vertical shear of the horizontal current, a parameterisation of turbulent vertical momentum transfer. The resulting solution of (1.2.1) is the 'Ekman spiral'. The dominant balance at the surface is between the wind stress and the coriolis force, resulting in a surface drift to the right (in the northern hemisphere) of the prevailing wind direction. Below the surface layer, the direct effect of the wind stress is diminished and the flow is in geostrophic balance with the large scale pressure gradient. We shall see below that the Ekman layer is instrumental in setting up this pressure gradient.

The mean winds blowing over a northern hemisphere ocean take the form of polar and equatorial easterlies and mid-latitude westerlies. If the integrated mass transport of the Ekman layer is to the right of the mean winds, this results in a convergent mass transport in sub-tropical regions and a divergence in sub-polar regions, evident in figure (1.1).

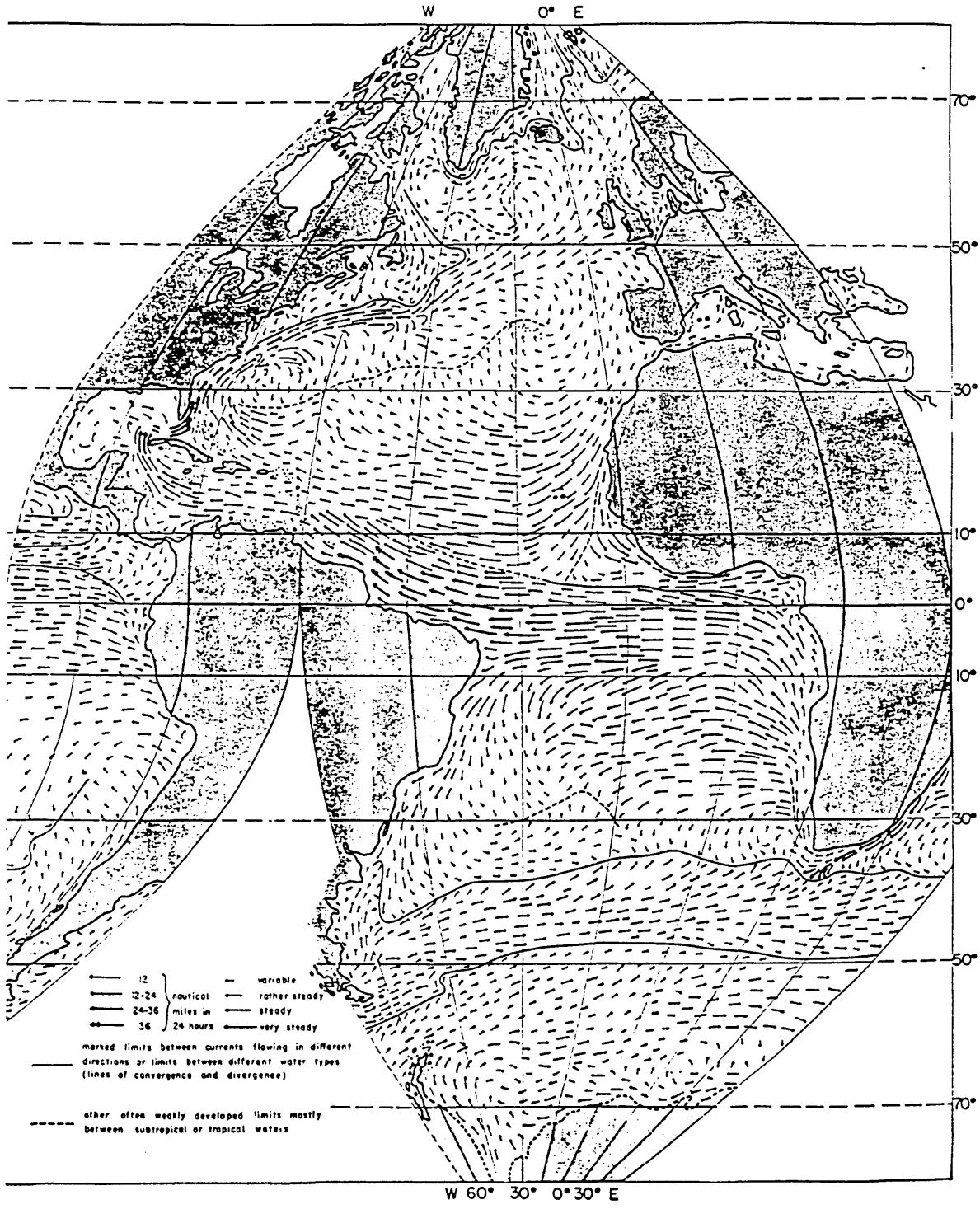

Figure 1.1: Surface currents in the Atlantic Ocean from a long term compilation of measurements and ship reports. From Defant (1961).

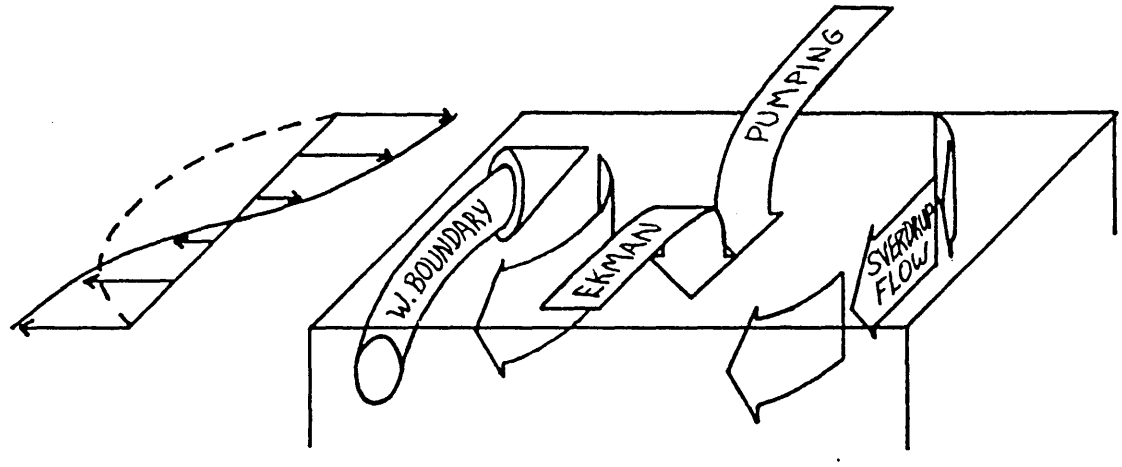

Figure 1.2: A schematic diagram representing the character of the basin scale gyres of the world's oceans. The prevailing winds depicted to the left of the picture give rise to the Ekman pumping field shown, and hence the southward Sverdrup flow. The gyre is closed by a strong western boundary current.

Through mass conservation this implies sub-tropical downwelling (Ekman pumping) and sub-polar upwelling (Ekman suction). This is represented schematically in figure (1.2).

One can envisage the above process having no effect at all on the general circulation of the ocean, with the wind simply driving a slow overturning motion in a shallow layer ($\sim$ 100m) at the ocean surface. However, there are more constraints to satisfy than mass conservation. The vorticity equation must also be satisfied.

The steady horizontal momentum equation is

$$\mathbf{v}.\nabla\mathbf{v} + f\hat{\mathbf{k}}_\wedge\mathbf{v} + \frac{1}{\rho_0}\nabla p = \frac{1}{\rho_0}\frac{\partial\vec{\tau}}{\partial z} - \mathbf{F} \tag{1.2.2}$$

where $\mathbf{F}$ is a frictional drag. Eliminating the pressure by taking the curl, and combining with the continuity equation,

$$\frac{\partial u}{\partial x} + \frac{\partial v}{\partial y} + \frac{\partial w}{\partial z} = 0 \tag{1.2.3}$$

one obtains the vorticity equation,

$$\mathbf{v}.\nabla(f+\xi) = f\frac{\partial w}{\partial z} + \frac{1}{\rho_0}\frac{\partial}{\partial z}\hat{\mathbf{k}}.\nabla_\wedge\vec{\tau} - \hat{\mathbf{k}}.\nabla_\wedge\mathbf{F} \tag{1.2.4}$$

where $\xi = \nabla_\wedge\mathbf{v}$ and has been neglected relative to f when undifferentiated.

Equation (1.2.4) states that the rate of change of vorticity for a fluid parcel is equal to the vortex stretching; plus the vorticity supplied by vertical momentum transfer from

the surface wind; minus that removed by friction. If (1.2.4) is integrated from the surface to a depth, d, at which $\vec{\tau} = w = 0$ (the depth of the wind driven gyre) then, neglecting both friction and the advection of relative vorticity, we obtain Sverdrup's (1947) mass transport equation,

$$\beta \int_{-d}^{0} v dz = \frac{1}{\rho_0} \hat{\mathbf{k}}.\nabla_{\wedge}\vec{\tau_s} \tag{1.2.5}$$

where $\vec{\tau_s}$ is the surface wind stress. If this integral is performed over the region between the base of the Ekman layer, where the vertical velocity is w_E, and $-d$, neglecting the transport within the Ekman layer itself, the right hand side of (1.2.5) can be replaced by fw_E, giving an equation for the transport in the thermocline in terms of the Ekman pumping velocity, w_E.

We are now in a position to compare the magnitude of velocity required by (1.2.5) with the meridional velocity required simply to maintain a divergent Ekman layer (from (1.2.3)). The former is of the order

$$v \sim \frac{f}{\beta d} w_E$$

while the latter is

$$v \sim \frac{L_y}{d} w_E$$

where L_y is the meridional scale of the circulation. The ratio of these two velocities is the ratio of the radius of the Earth to the horizontal scale of the gyre. So it can be seen that due to the constraints imposed by the vorticity equation, Ekman pumping has the effect of forcing a rapid non-divergent horizontal flow which is considerably stronger than the surface Ekman drift.

Sverdrup used (1.2.5) to clarify further the relationship between currents and winds. It is important to note that it is the curl of the wind stress which determines the transport rather than the wind stress itself. Equation (1.2.5) predicts southward transport in regions of anticyclonic wind stress curl (sub-tropical gyre) and northward transport in regions of cyclonic wind stress curl (sub-polar gyre). If the circulation of the gyres is to reflect the sign of the vorticity input by the wind stress, then they must be closed by meridional boundary currents running along the western side of the ocean. Therefore the Sverdrup transport is consistent with the western intensification seen in figure (1.1), although (1.2.5) cannot account for it explicitly.

Through continuity, it can be seen that maxima and minima of the eastward component of $\vec{\tau_s}$, where meridional transport is zero, correspond to zonal transport to the east and west respectively. These latitudes mark the gyre boundaries, and herein lies the explanation of how an eastward tropical counter current can exist against a prevailing easterly wind, in the region of trade wind minima known as the Doldrums.

Extensions of (1.2.5) to allow explicit representation of western boundary closures will be considered in the next section.

(b) Frictional and Non-Linear Boundary Closures

It can be readily shown that (1.2.5) cannot support a western boundary current by writing it in terms of a mass transport streamfunction, Ψ, defined by

$$\int_{-d}^{0} u\,dz = -\frac{\partial \Psi}{\partial y}, \qquad \int_{-d}^{0} v\,dz = \frac{\partial \Psi}{\partial x} \tag{1.2.6}$$

then, for purely zonal winds, we obtain

$$\frac{\partial \Psi}{\partial x} = -\frac{1}{\rho_0 \beta}\frac{\partial \vec{\tau_s}}{\partial y} \tag{1.2.7}$$

which has a solution linear in x and therefore unable to furnish the repeated values of Ψ necessary for a closed circulation.

To proceed to a full theory, second order (frictional) or non-linear (advection) terms must be included in the equations of momentum and vorticity. It must be noted, however, that non-linear terms alone cannot act as dissipation for the input of vorticity through the wind stress curl.

Stommel (1948) constructed a model with rectangular geometry and a $\Psi = 0$ boundary condition, prohibiting flow through the walls. A sinusoidal zonal wind profile was chosen to represent easterly winds to the south and westerlies to the north, the curl of this quantity having a single maximum at the middle latitude of the basin and decreasing to zero at the latitudinal boundaries. The model is therefore just a single anticyclonic gyre. Friction was represented by a linear drag law in the momentum equation:

$$\mathbf{F} = R\mathbf{v} \tag{1.2.8}$$

where R is a coefficient of friction. In the depth integral, this form for $\mathbf{F}$ can be associated with the effect of bottom friction.

Equation (1.2.7) now becomes

$$\beta\frac{\partial\Psi}{\partial x} = -\frac{\tau_0\pi}{\rho_0 L_y}\sin\left(\frac{\pi y}{L_y}\right) - R\nabla^2\Psi \tag{1.2.9}$$

where τ_0 is a constant and L_y is the meridional extent of the basin. It is the left hand side of (1.2.9), due to the variation of Coriolis parameter with latitude, that is entirely responsible for the western intensification seen in the solution (figure (1.3a)). Equation (1.2.9) cannot support eastern boundary currents because $\partial\Psi/\partial x$ is negative except in the frictional boundary layer while Ψ is positive everywhere.

An alternative to this type of friction is that used by Munk (1950). In recognition of the fact that currents almost vanish towards the ocean floor, Munk discarded the idea of bottom friction and instead postulated that lateral friction in small scale eddies was the dominant dissipative process. This was parameterised in terms of the gradient of velocity rather than the velocity itself by analogy with molecular viscosity, to give a dissipative term in (1.2.2) of the form

$$\mathbf{F} = -\nu\nabla^2\mathbf{v} \tag{1.2.10}$$

where ν is the kinematic viscosity coefficient, assumed to be independent of position. This gives a replacement of the Laplacian term in (1.2.9) by

$$+\nu\nabla^4\Psi \quad \text{or} \quad +\nu\nabla^2\Xi$$

where $\nabla^4 = \frac{\partial^4}{\partial x^4} + 2\frac{\partial^4}{\partial x^2\partial y^2} + \frac{\partial^4}{\partial y^4}$ and Ξ is the relative vorticity of the mass transport. The adoption of this form of dissipation term is consistent with the idea of relative vorticity being fluxed laterally down-gradient by eddies. The applicability of this to the ocean will be discussed in the following section. The equation to be solved is now fourth order and thus requires further boundary conditions in addition to those used by Stommel. A no slip condition was chosen, consistent with a mechanism whereby eddy vorticity is transferred laterally and destroyed by friction at the coasts. Originally Munk used the same rectangular basin as Stommel but realistic annual mean zonal winds were used to drive the model. Munk and Carrier (1950) reproduced the work with a triangular basin for better comparison with observations and this can be seen in figure (1.3b).

Both the linear dissipative models described above are successful in reproducing the observed surface flow patterns to a certain extent, particularly in their representation of

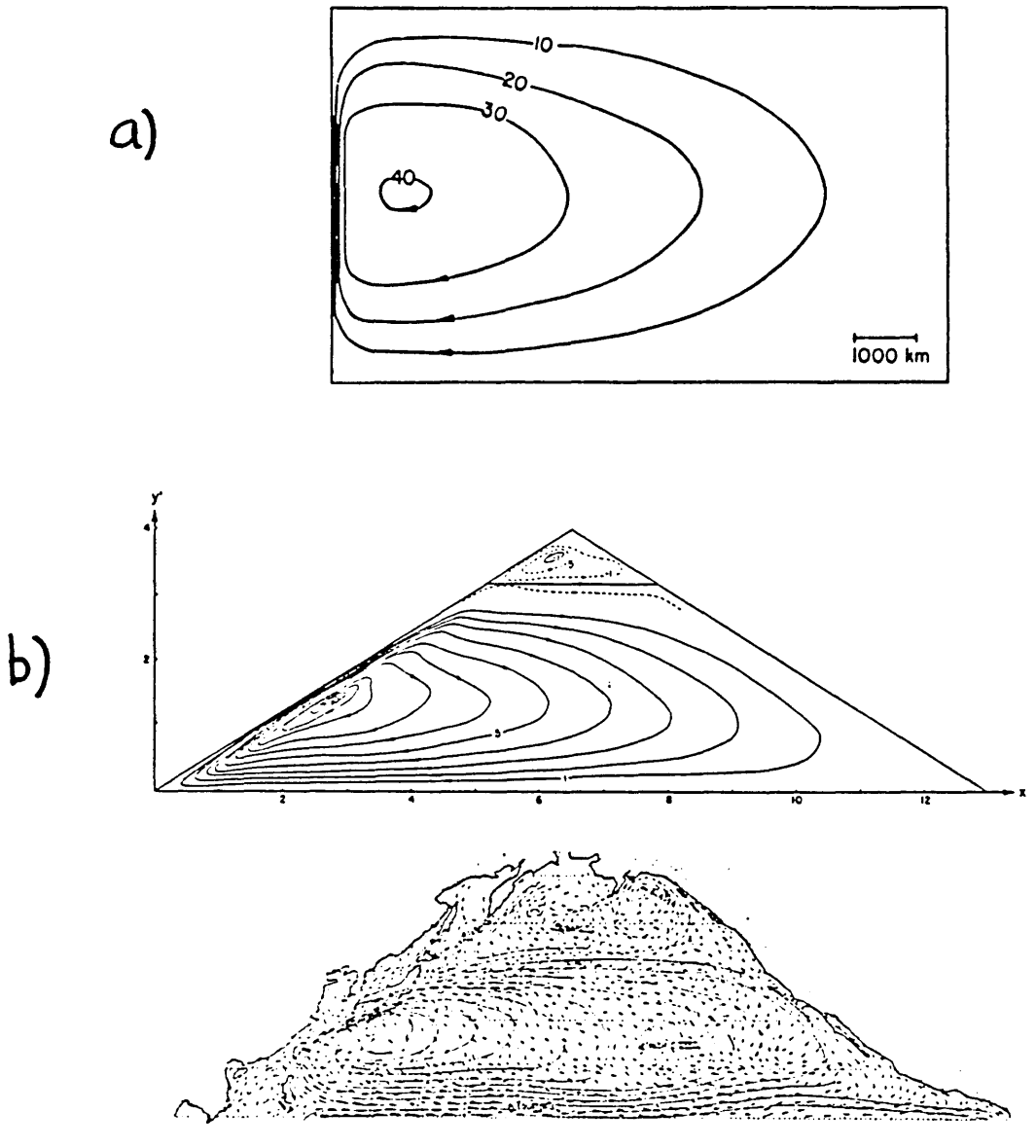

Figure 1.3: The results of the classical linear ocean circulation theories of Stommel (1948) (a) and Munk and Carrier (1950) (b). The latter is compared with observations of the Pacific surface currents.

the western boundary current. They fail, however, to give this current the correct width, needing a viscosity coefficient much larger than observed by independent means to do so. Also, the mass transport in the boundary current predicted by the models is only about half the observed value. It can be seen from figure (1.3b) that the models even fail qualitatively due to their inability to represent the seaward extensions of the western boundary currents observed in both the Atlantic and Pacific oceans.

These weaknesses in the frictional models correspond to the strengths of the non-linear models. Non-linear terms can introduce seaward jets and flow strengths in excess of those implied by linear theories, accounting for the mismatch of the latter with observed current strengths. The key difference between these two paradigms lies in the geometry of the contours of absolute vorticity, η (where $\eta = f + \xi$). In the linear models, contours of η always connect with the meridional boundaries. Flow is forced across them by wind stress in the interior and friction in the western boundary current, changing its value of η as it goes. In the unforced, non-linear limit, η contours coincide exactly with streamlines and η is materially conserved.

Fofonoff (1954) proposed a model in which all wind stress forcing and frictional dissipation was neglected, and the coriolis term, βv, was balanced purely by the advection of relative vorticity. Thus, equating the left hand side of (1.2.4) to zero, we obtain

$$J(\psi, \eta) = 0 \tag{1.2.11}$$

Here $\eta = f_0 + \beta y + \nabla^2\psi$ and $J(\psi, \eta)$ is the Jacobean of ψ and η, $(= \frac{\partial\psi}{\partial x}\frac{\partial\eta}{\partial y} - \frac{\partial\psi}{\partial y}\frac{\partial\eta}{\partial x})$ and represents the advection of η. Equation (1.2.11) implies that there is a functional relationship between ψ and η and to proceed further it is necessary to specify this relationship. For analytical convenience Fofonoff chose a linear form:

$$\eta = \eta_0 + c\psi \tag{1.2.12}$$

where η_0 and c are constants, and solved for ψ in a rectangular basin requiring $\psi = 0$ on the boundaries. The solution is shown in figure (1.4). It is characterised by a strong eastward flowing jet and a broad westward return flow. To complete the circulation there are symmetrical eastern and western boundary currents. Both the position of the jet and the strength of the flow are arbitrary in this model, depending on the values of η_0 and c respectively. The north-south asymmetry of the ocean circulation, which is absent from

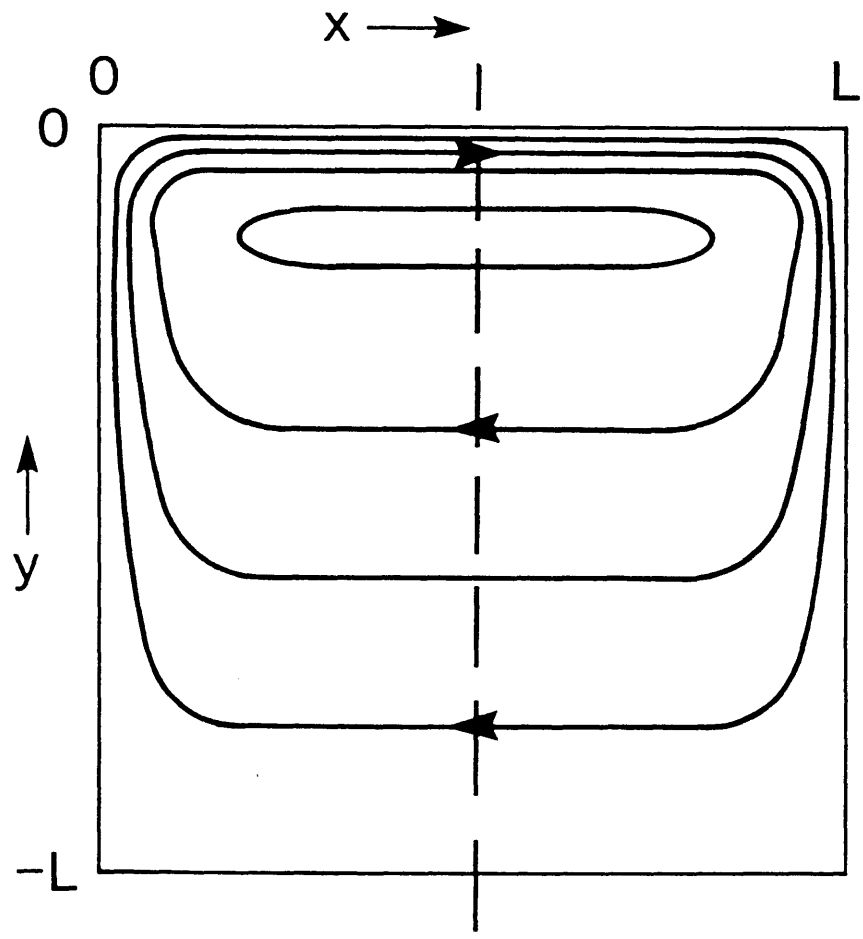

Figure 1.4: Fofonoff's (1954) solution for free non-linear flow in a rectangular basin. Weak, westward flow prevails over most of the gyre and relative vorticity is concentrated in the boundary layers and in the eastward jet to the north. The dashed meridian is a line of symmetry included for later reference.

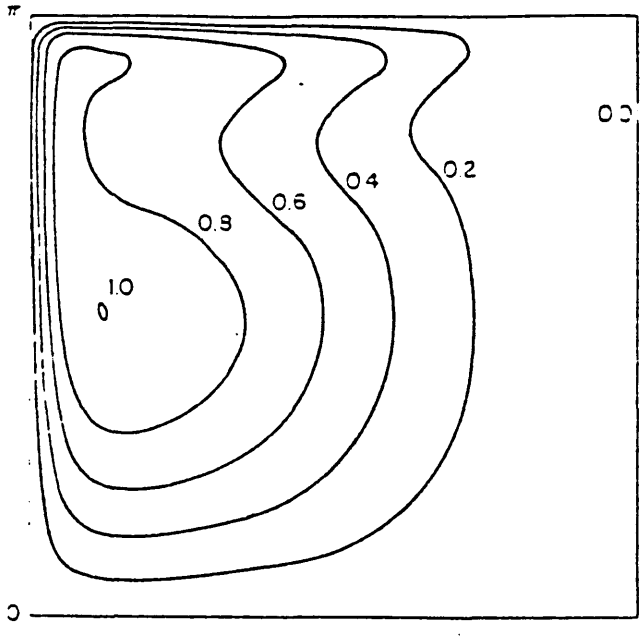

Figure 1.5: Streamlines from a numerical integration by Veronis (1966) in which a barotropic model is forced by wind stress and retarded by bottom friction in the same manner as Stommel's (1948) model, but with the non-linear terms also included.

the linear models, is well represented in a Fofonoff gyre, although the east-west symmetry is an unrealistic feature of the model. It was noted by MN that the limit represented by the Fofonoff gyre forms a useful reference point from which to study the recirculation regions. The work presented in this thesis is an investigation into the vertical structure of such regions in terms of baroclinic Fofonoff gyres.

Various attempts have been made to reconcile the two extremes presented above. Charney (1955) made a successful detailed comparison between observations and an unforced non-linear model of the western boundary area, supplied from the east with a prescribed realistic flow. Niiler (1966) showed that weak forcing and dissipation can in principle set the transport of a Fofonoff gyre (see next section). Figure (1.5) shows a numerical result due to Veronis (1966) in which frictional and non-linear terms are fully included. The basin scale flow adheres, broadly speaking, to the forced linear Sverdrup balance. However, an intense seaward jet exists in the north western corner, much of which is recirculated locally in a tight non-linear gyre more reminiscent of the Fofonoff mode.

1.3 The Role of Eddies in Shaping the Large Scale Flow

All the analyses presented so far have depicted the ocean as a quiescent fluid, circulating in a steady fashion. This is far from the truth. In reality the ocean is alive with transient eddies, produced by both barotropic and baroclinic instability, particularly in the intense jet regions where there are sharp gradients of potential vorticity. If one is to make a serious attempt to model the large scale circulation then small (synoptic) scale processes cannot be ignored. The effects of these eddies must be represented accurately, even if only through a generalisation of their collective effect on large scales, i.e. a parameterisation of their transfer properties in terms of large scale quantities.

For our purposes, an eddy can be defined as a deviation from a time mean field over $\sim$ 10 years, the time scale for the adjustment of the large scale baroclinic flow field to changes in large scale forcing. It should be remembered, however, that eddies exist as single coherent entities with characteristic spatial extents $\sim$ 100 km and lifetimes of several months. They are readily identified in satellite photographs of ocean colour or sea surface temperature and from experiments with drifting buoys. On these length scales, typical ocean velocities are less than 1 m/s, so the Rossby number is small and the eddies are well described by geostrophic dynamics.

The spatial extent of ocean eddies causes serious problems for both observationalists and numerical modellers. They exist on a length scale equal to the Rossby radius of deformation: $L_\rho = NH/f = \sqrt{g'H_1}/f$ where H is a depth scale for the motion and g' is the reduced gravity. This is the scale at which vortex stretching and relative vorticity advection play an equal role in the creation of vorticity locally. It is several hundred times smaller than a typical ocean basin. Equivalent systems in the atmosphere, which is more strongly stratified, are 2000 km wide, posing no such problems. The parameterisation of small scale processes is therefore particularly important in ocean modelling.

If we are to assess the transfer properties of geostrophic eddies in quasi-two dimensional turbulent flow, it is useful to talk in terms of a quantity which is conserved by the horizontal flow. Such a quantity is the quasi-geostrophic potential vorticity, q. The other advantage of using q is that given boundary conditions, it specifies the flow. Therefore any hypothesis as to the nature of eddy transfers of q in terms of the mean q field can form a dynamical closure for the mean flow.

(a) Scale Evolution of Geostrophic Turbulence

Turbulent flow, as distinct from wave like flow, is associated with the irreversible deformation of q contours. Theoretical arguments are presented by Rhines (1979) to illustrate the way the spatial scales of energy and enstrophy ($= \frac{1}{2}q^2$) evolve in turbulent flow. If the enstrophy is associated mainly with vorticity and the velocity structure is represented as a sum of wave components then the integral conservation laws for energy and enstrophy can be written as follows:

$$\begin{array}{lll} \text{Energy} & \int_0^\infty E dk & = \text{constant} \\ \text{Enstrophy} & \int_0^\infty k^2 E dk & = \text{constant} \end{array} \tag{1.3.1}$$

where k is the wavenumber, E is the energy ($= \frac{1}{2}(\nabla\psi)^2$) and enstrophy is $\frac{1}{2}(\nabla^2\psi)^2 = -k^2 E$. The only way that both these integrals can be preserved at their constant value is if energy migrates to larger scales while enstrophy cascades to smaller scales. What happens physically is that eddies stretch out the q contours, increasing the average q gradients and thus creating a finer scale structure in the q field. Small scale dissipative processes then break these contours leading to dissipation of enstrophy at very small scales. This effect can be seen in figure (1.6). The process is eventually slowed by the increasing disparity in scales between the straining eddies and the strained eddies. The streamfunction shows no such collapse to small scales (the ∇^{-2} can be regarded as a smoothing operator). Rather, the ψ field becomes smoother as filaments of q are stretched.

Further strong constraints are imposed on these processes by the presence of vortex stretching, bottom topography and by the background planetary vorticity gradient. The enstrophy cascade can be halted as chaotic turbulence degenerates into organised Rossby waves with a length scale appropriate to $k^2 \sim \beta/u$.

(b) Transfer Properties of Eddies

If a closure is to be found for geostrophic turbulence, the systematic effect of eddies on the mean flow must be understood. This can be achieved by considering the way in which eddies re-shape the large scale q field through turbulent fluxes.

The equation expressing the conservation of potential vorticity is

$$\frac{\partial q}{\partial t} + \mathbf{v}.\nabla q = \mathcal{F} - \mathcal{D} \tag{1.3.2}$$

Figure 1.6: Contours of constant vorticity in a barotropic, two dimensional turbulence experiment. The stretching out of contours can be seen. From Rhines (1979).

where $\mathcal{F}$ and $\mathcal{D}$ are sources and sinks of potential vorticity. The fields can be split into time mean and eddy components:

$$\begin{aligned} q &= \bar{q} + q' \\ \mathbf{v} &= \bar{\mathbf{v}} + \mathbf{v}' \\ \mathcal{F} &= \overline{\mathcal{F}} \\ \mathcal{D} &= \overline{\mathcal{D}} + \mathcal{D}' \end{aligned} \tag{1.3.3}$$

where overbar and prime denote mean and perturbation. Substituting these into (1.3.2), multiplying by q' and time averaging, the eddy enstrophy equation is formed.

$$\frac{\partial}{\partial t}\left(\frac{1}{2}\overline{q'^2}\right) + \bar{\mathbf{v}}.\nabla\frac{1}{2}\overline{q'^2} + \overline{\mathbf{v}'q'}.\nabla\bar{q} = -\overline{\mathcal{D}'q'} \tag{1.3.4}$$

Equation (1.3.4) states that the eddy enstrophy change undergone by a fluid parcel is the result of eddy q fluxes across mean q contours and frictional dissipation at small scales.

For example, at the entrance to an atmospheric storm track, where eddy enstrophy is increasing along streamlines, there must be a flux of eddy potential vorticity down the mean q gradient. Eddy enstrophy is dissipated in storm track exit regions either through

up-gradient q fluxes or through the cascade process described above whereby energy is returned to the mean flow (see Hoskins, 1983, Illari and Marshall, 1983).

However, such examples from the atmosphere are of limited use in the ocean, where there is a mean meridional velocity and strong curvature of q and ψ contours. In the ocean, eddies are spawned in the intense jet regions and decay over a much larger area. To understand their large scale transfer properties it is useful to split the eddy flux into divergent and non-divergent parts, a method pioneered by Lau and Wallace (1979). By doing this, assuming that the mean flow is almost free, i.e. $\bar{q} = \bar{q}(\bar{\psi})$, Marshall and Shutts (1981) rewrote (1.3.4) as

$$\bar{\mathbf{v}}.\nabla\tfrac{1}{2}\overline{q'^2} + (\overline{\mathbf{v}'q'})_{rot}.\nabla\bar{q} = 0 \tag{1.3.5a}$$

$$\tfrac{\partial}{\partial t}(\tfrac{1}{2}\overline{q'^2}) + (\overline{\mathbf{v}'q'} - (\overline{\mathbf{v}'q'})_{rot}).\nabla\bar{q} = -\overline{\mathcal{D}'q'} \tag{1.3.5b}$$

where $(\overline{\mathbf{v}'q'})_{rot} = \tfrac{1}{2}\hat{\mathbf{k}}\wedge\nabla(\tfrac{d\bar{\psi}}{d\bar{q}}\overline{q'^2})$. Equations (1.3.5) demonstrate that the advection of eddy enstrophy by the mean flow (1.3.5a) is associated with a purely rotational eddy q flux which cannot alter the large scale field. If local eddy enstrophy is in a steady state, (1.3.5b) shows that in an enstrophy cascade, the divergent eddy q flux, which is capable of acting on the large scale, is directed down the mean q gradient.

We are now able to replace the frictional dissipation employed in the previous section with a more realistic eddy vorticity flux. Green (1970) introduced a diffusive parameterisation for the gross effects of eddy potential vorticity transfer. The above arguments suggest that there is some justice in using such a parameterisation for local time mean eddy fluxes as well. We therefore write

$$\overline{\mathbf{v}'q'} = -\kappa\nabla\bar{q} \tag{1.3.6}$$

where κ is the an eddy transfer coefficient.

Marshall (1984) shows that redistribution of potential vorticity alone is capable of maintaining equilibrium in a symmetrical two gyre system. Vorticity is supplied to the sub-polar gyre and extracted from the sub-tropical gyre by the wind. It is carried down-gradient between the two by divergent eddy flux. Frictional processes are only necessary at very small scales to halt the enstrophy cascade. Marshall's model is barotropic so the closure is mathematically identical to that of Munk (1950). However, the physical emphasis is completely different: Munk envisages a lateral vorticity transfer to the boundaries,

where momentum is destroyed; Marshall adopts a different boundary condition, allowing flow on the boundaries and relies on the double gyre system for equilibration.

(c) Potential Vorticity Homogenisation

A down-gradient eddy transfer of potential vorticity obviously acts to erode mean potential vorticity gradients. In the absence of sources of q, and within closed q contours, this erosion can continue unimpeded, resulting in gyre scale regions of uniform q. Potential vorticity cannot be transported across density surfaces except by diabatic processes. This serves to reduce the dimensionality of the problem. If the density surface one is considering does not outcrop at the surface, the region can be considered isolated from surface forcing. Rhines and Young (1982b) put forward a theory for such regions. The equation of motion for steady, unforced flow is

$$J(\psi, q) = -\nabla.\overline{\mathbf{v}'q'} = \nabla.\kappa\nabla\overline{q} \tag{1.3.7}$$

Integrating (1.3.7) within a closed streamline, the left hand side vanishes and the equation becomes

$$\oint \kappa\nabla\overline{q}.\hat{\mathbf{n}}\, dl = 0 \tag{1.3.8}$$

where $\hat{\mathbf{n}}$ is a unit vector normal to the ψ contour. Using

$$\hat{\mathbf{n}} = \frac{\nabla\overline{\psi}}{|\nabla\overline{\psi}|} \quad \text{and} \quad \nabla\overline{q} = \frac{d\overline{q}}{d\overline{\psi}}\nabla\overline{\psi} \tag{1.3.9}$$

one obtains

$$\frac{d\overline{q}}{d\overline{\psi}} \oint \kappa|\nabla\overline{\psi}|dl = 0\ . \tag{1.3.10}$$

which implies that $\overline{q}$ is uniform wherever there is flow, isolated from forcing.

These gyre scale regions of uniform q can be seen in the observations and in eddy resolving numerical models (see chapter 3). The theories of the vertical structure of the recirculation region presented in this thesis invoke their existence.

(d) Equilibration of Almost Free Gyres

Even if the direct contribution of eddies to the vorticity budget is small, they can have a controlling effect on the mean flow. Niiler (1966) made use of weak forcing and dissipation to remove the indeterminacy of the transport in a barotropic Fofonoff gyre. He adopted

a free, inertial zero order flow, with forcing and dissipation acting as first order effects. The equations for such steady, almost free flow are

$$\begin{aligned} J(\overline{\psi},\overline{\eta}) &= 0 \\ J(\psi',\overline{\eta}) + J(\overline{\psi},\eta') &= \mathcal{F}' - \mathcal{D}' \end{aligned} \tag{1.3.11}$$

A prime now denotes an eddy which is weak compared to the mean flow. As before, a linear relationship is assumed between $\overline{\eta}$ and $\overline{\psi}$ giving

$$f_0 + \beta y + \nabla^2\overline{\psi} = \overline{\eta}_0 + \frac{d\overline{\eta}}{d\overline{\psi}}\overline{\psi} \tag{1.3.12}$$

This is identical to (1.2.12), the equation of a Fofonoff gyre. The strength of the flow is set by integrating (1.3.11) over the area enclosed by a streamline. The result is an integral balance between forcing and dissipation.

$$\iint \mathcal{F}'\,dx\,dy = \iint \mathcal{D}'\,dx\,dy \tag{1.3.13}$$

If $\mathcal{F}' = \frac{1}{\rho_0}\hat{\mathbf{k}}.\nabla_\wedge\vec{\tau}$ and a bottom friction parameterisation is used: $\mathcal{D}' = R\nabla^2\overline{\psi}$ as in (1.2.8), then (1.3.13) can be written

$$\frac{1}{\rho_0}\oint_{\overline{\psi}} \vec{\tau}.d\mathbf{l} = R\oint_{\overline{\psi}} \overline{\mathbf{v}}.d\mathbf{l} \tag{1.3.14}$$

Frictional dissipation takes place primarily in the boundary layers, where velocities are high, so the right hand side of (1.3.14) can be associated with a velocity scale for the inertial boundary layer. Niiler deduced that the boundary current velocity is almost an order of magnitude higher than that implied by linear theory. It can also be seen that (1.3.14) is consistent with the notion that the sense of the circulation must reflect the sign of the wind stress forcing, proving that bottom friction is capable of equilibrating an almost free gyre. However, problems occur when this mechanism is replaced by down-gradient fluxing of η. If dissipation is modelled as the eddy transfer of eddy vorticity: $\mathcal{D}' = -\nabla.(\kappa\nabla\overline{\eta})$ (c.f. (1.3.7)) then, using (1.3.9), (1.3.14) becomes

$$\frac{1}{\rho_0}\oint_{\overline{\psi}} \vec{\tau}.d\mathbf{l} = -\frac{d\overline{\eta}}{d\overline{\psi}}\oint_{\overline{\psi}} \kappa\overline{\mathbf{v}}.d\mathbf{l} \tag{1.3.15}$$

implying that if the sign of the circulation is to reflect the sign of the wind stress curl, $d\overline{\eta}/d\overline{\psi}$ must be negative. This can be understood qualitatively from figure (1.7) which shows an anticyclonic wind driven gyre with a balancing down-gradient eddy vorticity flux. But if this is the case then the solution to (1.3.12) becomes sinusoidal, meaning that

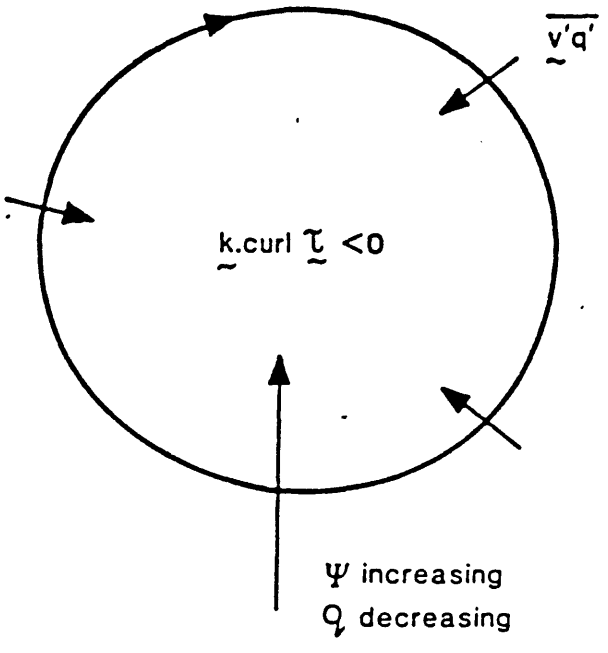

Figure 1.7: An anticyclonic gyre produced by anticyclonic wind stress. ψ increases into the gyre. The wind stress curl imparts negative vorticity to the gyre. For equilibrium, eddies must transfer positive vorticity into the gyre. Therefore, if eddies transfer q down-gradient, q must decrease into the gyre. So $dq/d\psi$ is negative. Taken from MN.

inertial boundary layers cannot exist. A solution to this paradox was proposed by MN, who couched the problem in terms of baroclinic flow, replacing the absolute vorticity, η, with quasi-geostrophic potential vorticity, q, as defined in (1.1.2). Thus (1.3.12) becomes

$$\beta y + \nabla^2\psi + f_0^2 \frac{\partial}{\partial z}\left(\frac{1}{N^2}\frac{\partial \psi}{\partial z}\right) = q_0 + \frac{dq}{d\psi}\psi \tag{1.3.16}$$

This equation can support inertial boundary layers even when $dq/d\psi$ is negative due to the presence of vortex stretching. So if lateral transfer of eddy potential vorticity is to equilibrate an almost free gyre, the flow must have some vertical structure. The precise nature of this vertical structure will be addressed in the following chapters.

Chapter 2

Observations of the Recirculation

2.1 The Circulation in Three Dimensions

As it flows through the Florida straits, the Gulf Stream is estimated to carry a mass transport of about 30 Sverdrups (Sv)(one Sv is 10^6 m^3s^{-1}). As it leaves the coast at Cape Hateras, this has intensified to $\sim$100 Sv. By the time it reaches 55^0 W, now flowing eastwards, the transport has risen to 150 Sv (see Richardson, 1985 for a review of transport estimates). We shall return to a quantitative discussion in section (2.4) and in chapters 4 and 6. Qualitatively, it is obvious that the large transports carried by the seaward jet cannot be representative of the transport of the basin scale circulation. Much of the excess water must be recirculated locally. The downstream acceleration described above is consistent with the inertial nature of the boundary layer, which gains cyclonic shear as the current moves northwards and planetary vorticity increases (see Stewart, 1964). An 'inertial recirculation' can therefore be postulated simply on the basis of maintaining the observed transport structure of the Gulf Stream. However, there is further evidence of a separate, locally recirculating gyre in the western north Atlantic.

Following an analysis of oxygen concentrations in the north Atlantic, Worthington (1962) identified two distinct circulations . Warm, relatively oxygen sparse Sargasso sea water was hypothesised to recirculate in an anticyclonic gyre confined to the western side of the Atlantic, the north Atlantic drift further east being returned in a separate gyre (also anticyclonic) to the north east. Figure (2.1) shows Worthington's (1976) suggested circulation scheme for the total flow in the north Atlantic. It was constructed on the basis

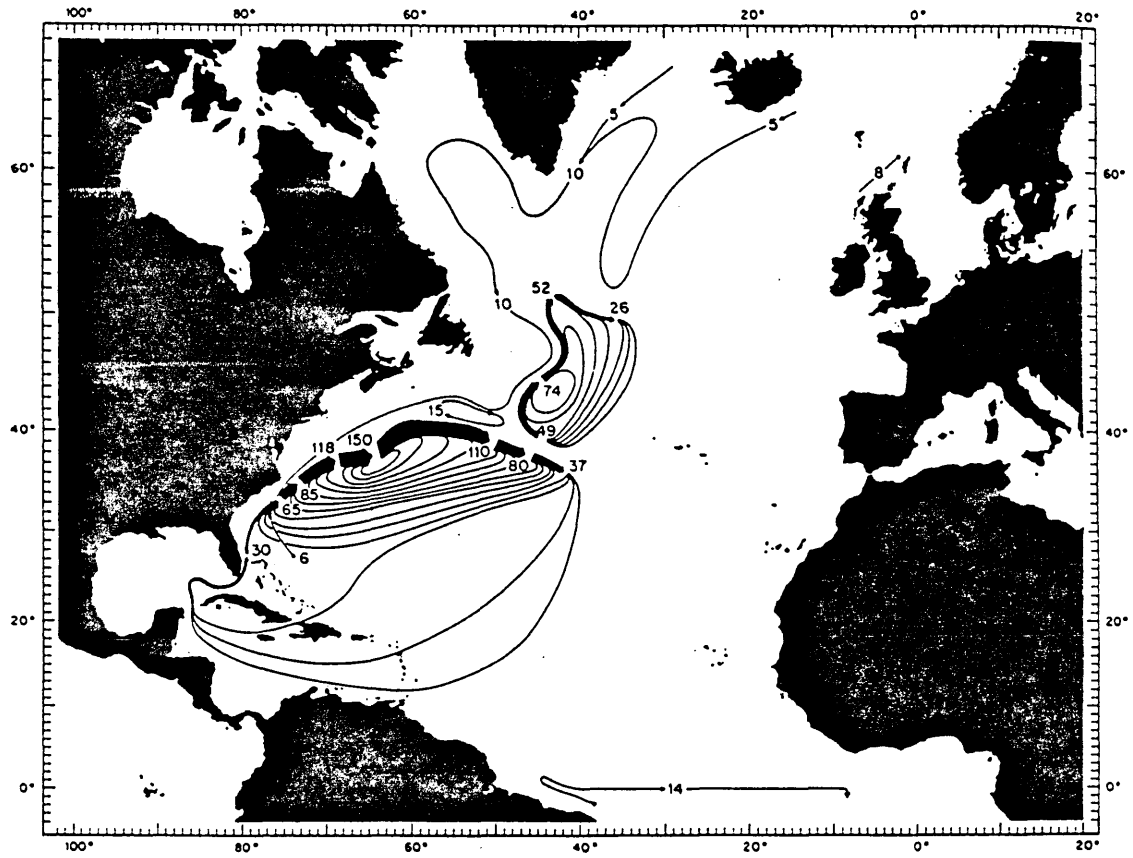

Figure 2.1: Worthington's (1976) circulation scheme for depth integrated flow in the north Atlantic. Contours show intervals of 10 Sv.

of material conservation of physical properties. Flow lines were drawn such that they did not cross clear water mass boundaries. The resulting scheme has been criticised (Clarke *et al*, 1980) for violating geostrophic balance. Furthermore, it is difficult to satisfy mass transport continuity in a gyre of this scale without allowing thermal forcing to modify the water mass to some extent (Luyten and Stommel, 1982). But even if some of the Gulf Stream water does end up far to the north, it seems that a large fraction of it stays in the western half of the basin, recirculating to the south. A fluid parcel in this gyre is thought to make many orbits on average, before its properties are significantly influenced by wind or thermal forcing. Much of the thermocline water circulating as shown in figure (2.1) has weak vertical gradients of temperature and density, and has correspondingly low potential vorticity. It is known as 18 degree water or 'mode' water and its importance is discussed in the next section.

In tandem with this southern recirculation gyre is a tight cyclonic recirculation to the north, returning Gulf Stream water to the west south of the Grand Banks of Newfoundland. The structure and transport of this gyre has been documented by Hogg (1983), Richardson (1985) and Hogg *et al* (1986). It is discussed further in sections (2.3) and (2.4), and a model is presented in chapter 5.

The non-linear nature of the recirculation is apparent from figure (2.2a) which shows a north Atlantic potential vorticity map compiled by Keffer (1985). At this level (σ_θ = 26.3 – 26.5) closed contours can be seen, forming free paths for the flow. These closed contours delineate the recirculation region. To the east of this region, the Q contours still show significant curvature but it can be seen that much of the water flows through the outcrop zone and is therefore influenced by surface forcing. This is the 'ventilated thermocline' (Luyten, Pedlosky and Stommel, 1983). A strong front is apparent, marking the position of the Gulf Stream and illustrating its baroclinically unstable nature. Just south of the Gulf Stream front is a strong minimum of potential vorticity. This is the mode water referred to above. There is considerable injection of potential vorticity into this layer through convective mid-gyre sources, violating the necessary conditions for potential vorticity homogenisation.

At deeper levels (figure (2.2b)) the water is largely isolated from direct mechanical and thermal forcing. Although the layer shown (σ_θ = 26.5 – 27.0) still outcrops, closed

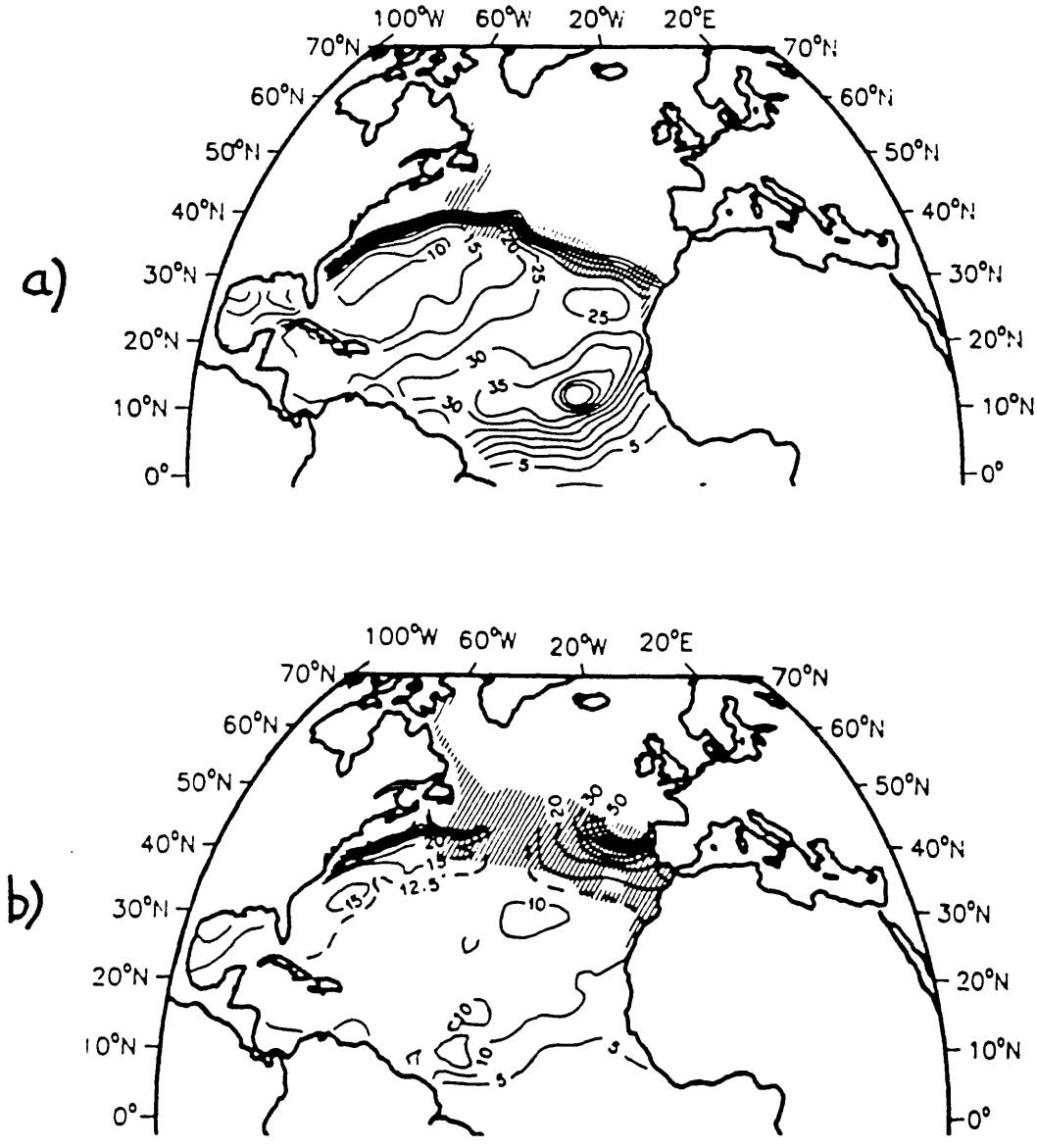

Figure 2.2: North Atlantic potential vorticity taken from Keffer (1985): (a) in the $\sigma_\theta = 26.3 - 26.5$ layer showing closed contours; (b) in the $\sigma_\theta = 26.5 - 27.0$ layer, showing homogeneous regions.

Q contours exist south of the outcrop, providing the opportunity for homogenisation as described in section (1.3c). At this level, the homogenisation has extended across most of the ocean basin. It should be noted that the appearance of such large scale homogeneity in Q could in part be due to a lack of contrast in boundary conditions, with the outcrop zone arranged in such a way that there is a limited range in the values of Q advected south (see Keffer, 1985).

There is a marked contrast, therefore, between flow regimes which are ventilated and those which are isolated. In ventilated regions, the potential vorticity is set at the outcrop and conserved downstream. In isolated regions, potential vorticity is not continually reset, so there is time for it to be redistributed by eddies, allowing free flow in a region of uniform Q set into the background beta gradient.

In the direct vicinity of the Gulf Stream, the homogenisation of properties extends across the stream itself in the deep water ($\sigma_\theta > 27.1$) (Bower, Rossby and Lillibridge, 1985). This contrasts with the strong front in both dynamical and passive properties at the surface, where the Gulf Stream has a continuous identity as a water mass boundary. The larger scale picture at this depth is more complicated, particularly in the north Atlantic. McDowell, Rhines and Keffer (1982) document open Q contours lying in a north east - south west orientation and providing pathways for source to sink flows of Mediterranean water and north Atlantic intermediate and deep waters. Such source to sink flows require a complicated depth structure to the currents in the eastern north Atlantic. By imposing the Sverdrup constraint, Saunders (1982) deduces northward flow between 300 and 1000 m depths at 48^0 N and 20^0 to 30^0 W, with southward flow extending to great depths below. The closure of this thermohaline mode of circulation takes place through deep convection in the norwegian sea. Some of the cold abyssal water formed in this region ends up in the western north Atlantic by means of the deep western boundary current (see figure (2.1)). The Pacific on the other hand, is more poorly ventilated and these denser layers do not outcrop to the north even in the winter. Consequently, potential vorticity still appears to be homogeneous on a large scale down to the base of the thermocline.

2.2 Mode Water and Anticyclogenesis

(a) Geographical Location and Formation of Mode Water

Another view of mode water is given in the hydrographic section of figure (2.3) which shows the 1956 Atlantis section at 50^0 W (McCartney, 1982). Figure (2.3a) shows contours of potential density with depth as the ordinate. The strong vertical shear at the Gulf Stream front is clearly apparent. To the south of this, centred on $\sigma_\theta = 26.5$, is a wedge of weak vertical gradient: a pycnostad. The pycnostad gets thicker towards the north as vortex stretching offsets planetary vorticity, maintaining the potential vorticity at a low value. The thermocline is at its deepest just south of the Gulf Stream. The pycnostad of figure (2.3a) translates into the region of low potential vorticity shown in figure (2.3b), a contour plot of potential vorticity with σ_θ as the ordinate. A sharp front exists at the latitude of the Gulf Stream. It is still sharper when relative vorticity is included in the calculations of Q (M. Hall, private communication).

The upper regions of the recirculation are characterised, then, by a region of low potential vorticity south of the Gulf Stream front, associated with a depression in the main thermocline.

McCartney (1982) documents the geographical location of two types of mode water: sub-tropical and sub-polar. It is the sub-tropical variety which forms Worthington's 18 degree water and resides within the recirculation. Sub-tropical mode water is formed when winter outbreaks of cold air from the continent cool the surface of the warm water just offshore of the Gulf Stream or Kuroshio. The resulting deep convection destroys the vertical stratification creating low potential vorticity water which is subducted into the main thermocline as the mixed layer retreats in the spring (Woods and Barkmann, 1988). Sarmiento (1983) estimates that the flux of water from the mixed layer into the thermocline in this region is as much as 40 Sv, exceeding the Ekman flux by a factor of 5. Once an east-west band of this low Q water is formed, it is advected round the gyre to the south and back west to fill the gyre in a sporadic uneven way.

In fact the distribution of mode water is highly variable in space and time. Talley and Raymer (1982) have recorded temporal variations in potential vorticity at one station. In the short term, they correspond to spatial variations over a few thousand km along the flow direction of the same order as the value of Q characteristic of mode water. The depth

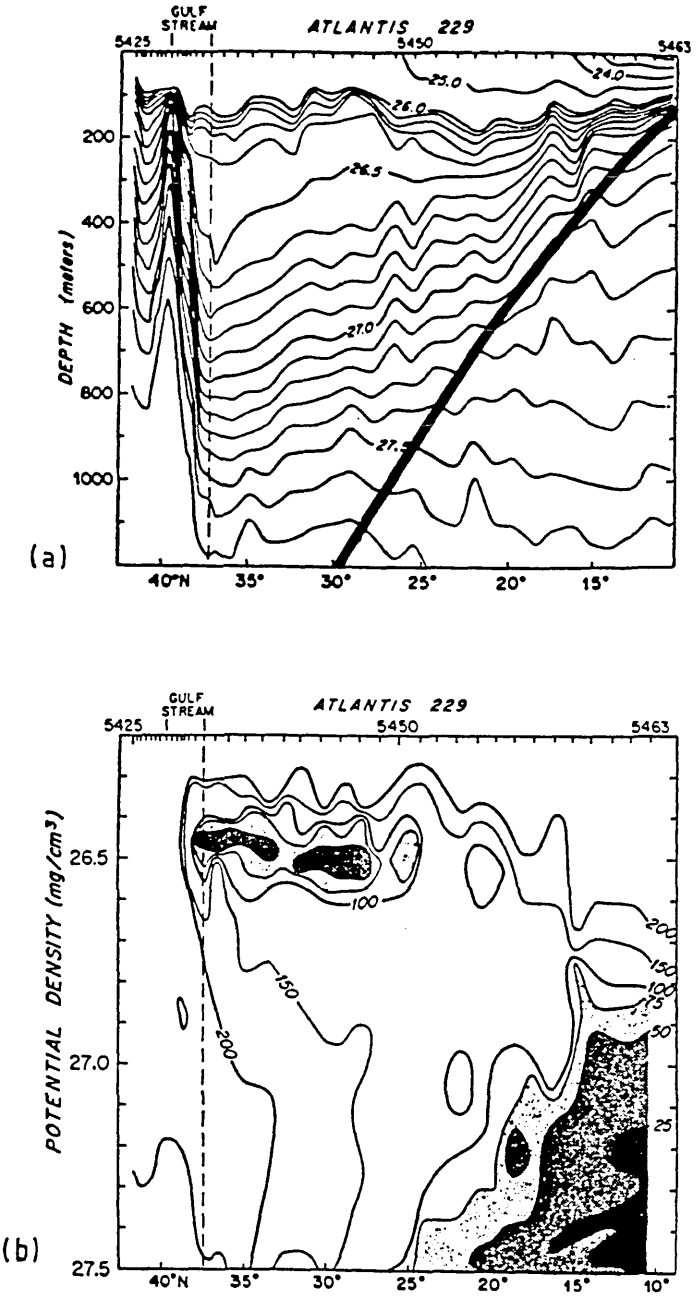

Figure 2.3: Meridional sections taken along 50^0 W by RV *Atlantis* between November 13 (north) and November 30 (south) 1956, taken from McCartney (1982). (a) Potential density in kg m^{-3} with depth as the ordinate. The mode water is centred on $\sigma_\theta = 26.5$. The bowl is marked as a thick line. (b) Potential vorticity in 10^{-12} m^{-1} s^{-1} with potential density as the ordinate. The low potential vorticity water has been shaded.

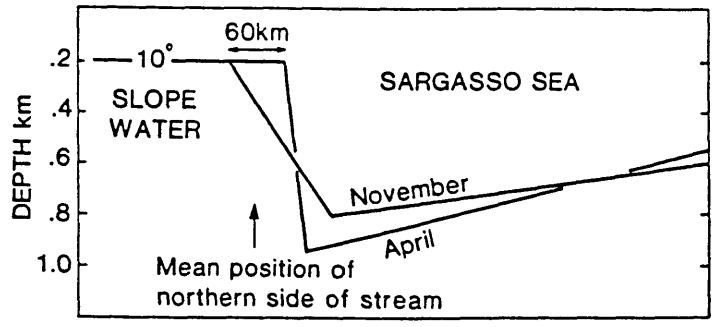

Figure 2.4: A schematic illustration of annual changes in the Gulf Stream position and interface shape. From Worthington (1976).

variation of the mode water is equally troublesome, spanning a range in σ_θ equal to the thickness of the mode water wedge. In the long term, the properties and abundance of mode water are not always constant, but can change suddenly after years of constancy in response to anomalous atmospheric conditions. Observations of this nature expose the limitations of steady state theories in the modelling of these gyres. The models presented in the following chapters can aid our understanding only if they are interpreted carefully (see section (3.3)).

(b) Anticyclogenesis

The intensity of the Gulf Stream system is observed to increase significantly following severe winters. This intensification has been dubbed 'anticyclogenesis' by Worthington (1972a, 1976) who attributes it to the surface cooling and subsequent convective overturning which follows winter cold air outbreaks. Halkin and Rossby (1985) and Fu *et al* (1986) present evidence of annual spring time intensification of the Gulf Stream. Increased volumes of mode water were generated after the particularly severe winter of 1976-77 (McCartney, Worthington and Raymer, 1980) and the Gulf Stream intensified considerably (Worthington, 1977). Figure (2.4) shows schematically the annual changes in the position of the Gulf Stream and the shape of the thermocline. It is deeper and steeper in the spring following the regeneration of mode water. Worthington talks of a 'fresh charge of energy' being given to the stream.

Whether this extra depression of the main thermocline is the result of thermal forcing, or simply due to increased wind stress during winter is a matter for conjecture. Worthington (1972b) describes a thermally direct meridional circulation with sinking water in the

region of maximum cooling and a broad region of upwelling to the south. Csanady (1982) has modelled the effect of this *differential* buoyancy loss in a simple two layer ocean and finds that the thermohaline circulation transfers streamwise momentum into the stream, thus intensifying it. The thermocline is distorted in a manner similar to that of figure (2.4). A relevant question to ask is: can this vertical circulation aid the Ekman pumping and actually increase the depth integrated transport ? There is an important difference between thermally induced vertical motion and Ekman pumping which is made clear by equation (1.2.5). The $f\frac{\partial w}{\partial z}$ term has disappeared in the vertical integral and has no effect on the vertically integrated velocity in the linear Sverdrup regime. It is only the wind stress which can set the transport in this case. The situation is more complicated in a non-linear recirculating gyre. The relative vorticity advection term in (1.2.4) is non-linear in velocity. If a thermally induced vertical velocity can redistribute this term in the vertical this may, therefore, lead to a change in the depth integrated velocity locally. Stommel and Veronis (1980) show that in a rotating baroclinic fluid, initially ageostrophic finite amplitude disturbances to density surfaces lead to non-zero barotropic transports in the subsequent geostrophically adjusted flow. The rotation of the fluid means that some of the available potential energy liberated by cooling feeds a depth independent transport, rather than a vertical secondary circulation. MN2 suggest that anticyclogenesis is a 'resonance' of the free Fofonoff mode and they model the intensified recirculation in terms of baroclinic Fofonoff gyres reaching down to the ocean floor. This model is described in detail in section (3.3).

The causes and effects pertaining to anticyclogenesis are not addressed directly in the work presented below. Rather, the effect of varying the volume of low potential vorticity water and the thermocline depression is studied in isolation from the driving mechanisms.

2.3 Deep Flow

Attention has so far been restricted chiefly to the main thermocline. Over most of the ocean the flow at deeper levels is weak. However, the deep abyssal flow is a very important part of the recirculation system. Figure (2.3b) shows a region of homogeneous potential vorticity descending to great depths. More recent data (McCartney, private communication) shows very weak isopycnal gradients of potential vorticity extending right to the

ocean floor. The homogeneous potential vorticity of figure (2.3b) matches closely onto areas where isopycnals are sloping, as seen in figure (2.3a). A bold line has been drawn on this figure demarking areas with sloping isopycnals from areas with relatively flat isopycnals. This is the 'bowl' of the circulation.

Within the bowl, there is baroclinic flow and uniform potential vorticity. Beneath the bowl, the water is stagnant, isopycnals are at their reference depth and the potential vorticity takes on its rest value. The above statement is an idealisation of the observations. This idealised model forms the basis of the work presented in this thesis.

Whether or not the bowl hits the bottom is an important question, as it determines the possibility of a barotropic (depth independent) component to the recirculation. This question is addressed theoretically in chapters 4 and 6. Observational evidence that the bowl does indeed hit the bottom in the north Atlantic is given by Schmitz (1980). Figure (2.5) shows his current meter data, from an array set out along 55^0 W. The westward return part of the flow at 36^0 N is almost independent of depth. The recirculation has a strong ($\sim$ 10 cm s^{-1}) barotropic component at this latitude.

These data also show a deep counter current beneath the axis of the eastward jet. The jet itself sweeps southwards with depth. In an analysis of further current meter data, Hogg (1983) reveals that the dominant recirculation gyre at 4 km depth is in fact cyclonic, and represents a southward expansion of the cyclonic recirculation found to the north of the Gulf Stream at the surface with a contribution to the westward flow also coming from the deep western boundary current (see Richardson, 1985). Both cyclonic and anticyclonic gyres are seen in figure (2.6), which shows a suggested circulation scheme for 4 km depth. The cyclonic gyre is clearly the larger of the two. This depth structure is modelled in terms of free homogeneous gyres in chapter 5.

As mentioned above, the Pacific is a poorly ventilated ocean compared to the north Atlantic and the main thermocline does not penetrate to such depth (see Worthington and Kawai, 1972). This can affect the depth penetration of the bowl, and will be discussed in chapters 4 and 6. Figure (2.7) shows schematic zonal average potential vorticity regimes in the north Pacific, compiled by Talley (1988). The region of homogeneous potential vorticity shrinks towards the axis of the Kuroshio in the manner predicted by the theories presented below. But it only penetrates to a depth of 2.5 km, so by this criterion, the bowl

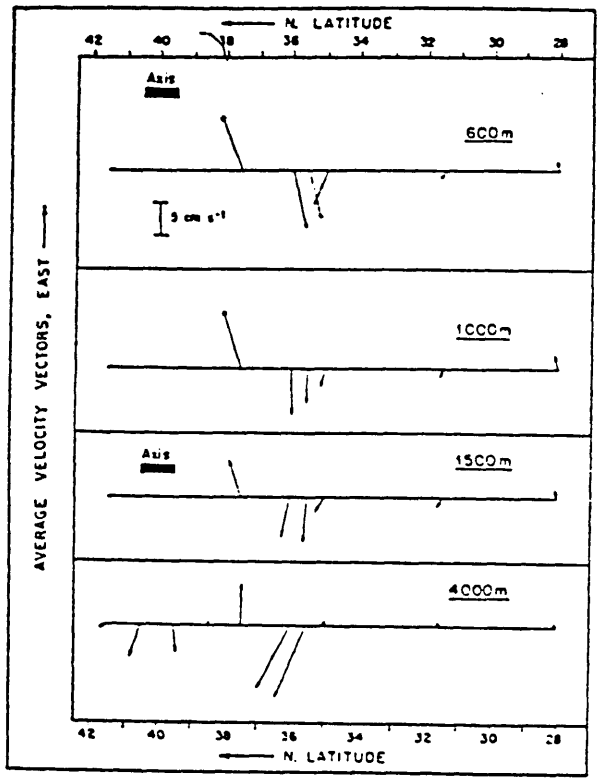

Figure 2.5: Time averaged horizontal velocity vectors at sites along 55^0 W from current meter readings reported by Schmitz (1980). The 'weakly depth dependent' nature of the westward return flow, and the counter current beneath the Gulf Stream are apparent (the range of mean positions for the axis of the Gulf Stream is shown by a horizontal bar).

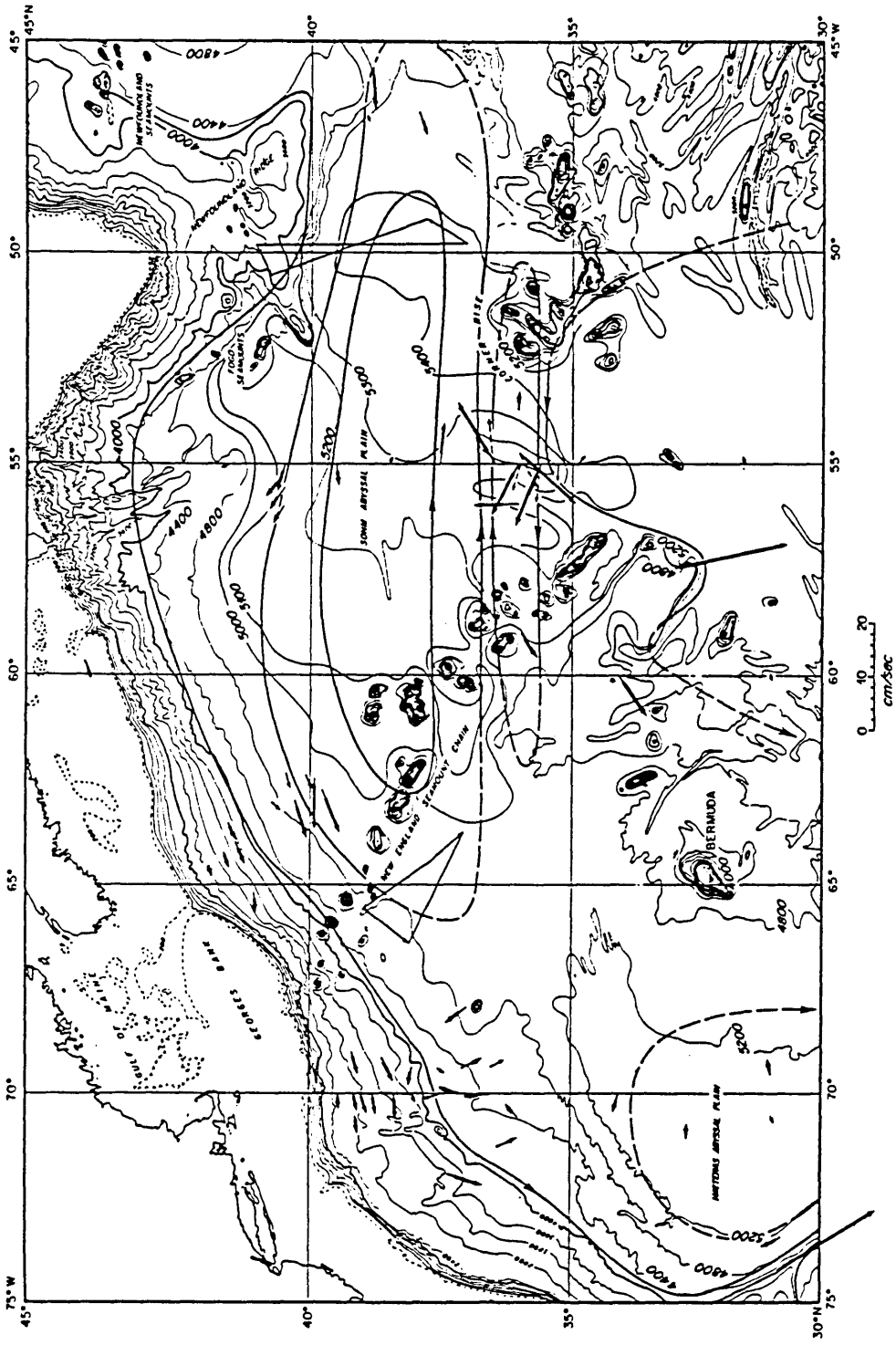

Figure 2.6: A circulation scheme for the deep flow in the western north Atlantic as inferred from long term direct measurements. From Hogg (1983).

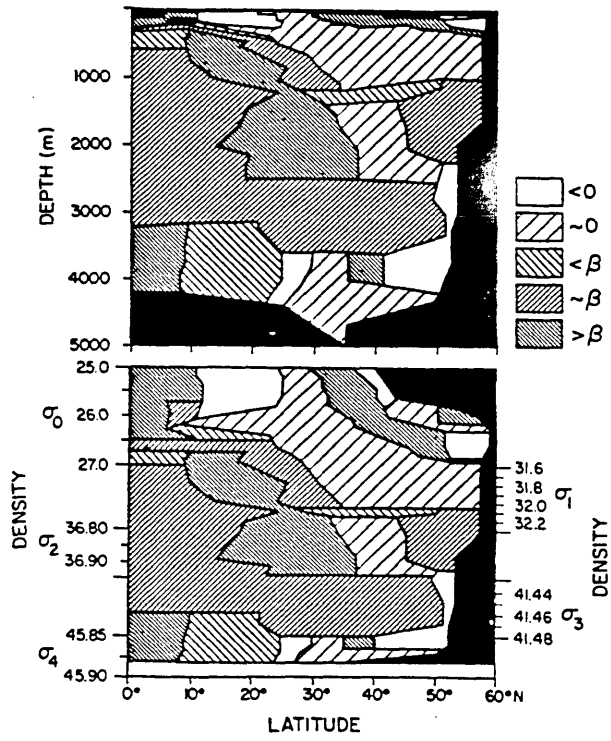

Figure 2.7: Regimes of the meridional gradient of potential vorticity, $\partial Q/\partial y$, compared to β, based on zonally averaged potential vorticity from the north Pacific (from Talley, 1988). The shallow penetration of the region of zero gradient is apparent.

does not hit the bottom (although it is possible that a uniform potential vorticity region may penetrate deeper on a scale unresolved by these data). However, bottom currents do exist in this region. Schmitz (1987) reports of large ($\sim$ 5 cm s^{-1}) stable abyssal currents which seem to bear little relation to the recirculating flow above. Whatever the origin of the abyssal Pacific currents, it is reasonable to suppose that they cannot be modelled directly by the simple theories presented below.

2.4 Partition of Mass Transport

There are two useful divisions to be made in the mass transport of the oceans. One is simply spatial: how much water goes where. The other involves depth dependence.

(a) Spatial Partition

Richardson (1985) lists the estimates of the Gulf Stream's transport between 50^0 and 70^0 W, which have been made by a variety of methods. The values vary from 79 Sv (Clarke *et al*, 1980) to 226 Sv (Robinson *et al*, 1974). The generally accepted value for the maximum transport is Worthington's (1976) value of 150 Sv, south of Nova Scotia. All these estimates suffer from the problem of differing time scales. A hydrographic section is almost synoptic, and will include eddies, meanders and embedded small scale features (although the highest frequency ageostrophic features are automatically filtered out). It is difficult to judge which of these belong to the stream and where the limits of the stream lie. Estimates based on floats have similar drawbacks although the possibility of some spatial integration exists. Current meters, on the other hand, produce a time series, but their spatial resolution is poor. Hall and Bryden (1985) overcome these problems by assuming that temperature can be used as an across stream coordinate and using the stream's own meanders to give spatial resolution to a single moored current meter array. Their estimate for the transport at 68^0 W is 94 Sv.

Richardson's (1985) estimate, based on a large scale experiment combining neutrally buoyant floats with current meter measurements, is 93 Sv for 55^0 W. This is low compared to the values mentioned above because it represents a long time average. The relevance of this to theoretical models is discussed in section (3.3).

How much of the Gulf Stream's transport can be considered part of the recirculation ?

Richardson's study reveals two counter currents, one to the north and one to the south, which reach to the ocean floor. These are the northern and southern recirculating gyres described above. Of the 93 Sv carried by the Gulf Stream, 41 are returned to the north and 29 to the south. The remaining 23 are returned further to the south in the larger scale sub-tropical gyre. These observations therefore suggest that the excess transport carried by the inertial flow is $\sim$ 40 Sv.

(b) Barotropic and Baroclinic Components

Schmitz (1980) describes the westward return flow as 'weakly depth dependent'. Yet the eastward jet itself is strongly surface intensified. Therefore there must be a baroclinic component to the recirculation at some latitude. Richardson estimates that about two thirds of the Gulf Stream's transport, and about half the transport in the two counter currents is 'bottom relative' at 55^0 W.

Since the idea of a 'level of no motion' is obviously inappropriate at least to the Atlantic recirculation, we shall use the term *baroclinic component* to mean the *bottom relative transport*, while the *barotropic component* is the *bottom flow multiplied by the depth.* It will be shown in chapter 4 that a strong relationship exists between this somewhat artificial transport partition, and a spatial partition based on the latitude at which the bowl hits the bottom, with baroclinic flow south of this latitude feeding the surface intensified eastward jet.

The Kuroshio at 152^0 E is slightly more barotropic in nature than the equivalent stage of the Gulf Stream at 68^0 W and has a shallower thermocline expression (see Hall, 1989). Further downstream, however, while the Gulf Stream intensifies and becomes more barotropic, the Kuroshio still has weak eastward bottom flow (Joyce and Schmitz, 1988), flanked by a stronger westward flow. In fact the transport at 165^0 E between 30^0 and 42^0 N is westward; about 63 Sv. This is in stark contrast with the Gulf Stream system, which shows a closed double gyre structure in the bottom flow. Hogg (1983) speculates that this difference is related to topography. He notes that the eddy energy in the deep north Atlantic increases downstream of the New England sea mounts, potentially driving the flow. At the equivalent position in the Pacific the Emperor sea mounts rise steeply from an abyssal plain. But in this case there is a downstream decrease in eddy energy,

with the topography apparently blocking rather than stirring the flow.

(c) Summary

An upper limit on the Gulf Stream's transport is $\sim$ 150 Sv. This value is reduced on time averaging. Much of this is returned in two tight recirculating gyres, one anticyclonic and one cyclonic, each carrying an excess $\sim$ 40 Sv above the linear, Sverdrup component. These recirculations have considerable barotropic components, as does the eastward flowing Gulf Stream. The eastward jet of the Kuroshio, however, lacks this barotropic intensification and closed circulation patterns for the abyssal flow in the Pacific are unclear.

Chapter 3

Models with Vertical Structure

3.1 Introduction

The homogeneous theories presented in section (1.2) have been useful in discussing the mass transport of the basin scale flows. Indeed, Sverdrup's mass transport equation (1.2.5) makes no assumption about the depth dependence of the flow. However, one of the most striking features of the ocean is its vertical structure, particularly the existence of the main thermocline: the region of strong vertical gradients of temperature and salinity which contains most of the wind driven circulation. It is desirable to build models which can represent these variations in order to understand the processes which are responsible for them. Recently, considerable progress has been made in understanding the vertical structure of ocean gyres through layered models (Rhines an Young, 1982, Luyten, Pedlosky and Stommel, 1983). These models are briefly described below as a precursor to a review of layered models of free non-linear gyres pertinent to the recirculation.

3.2 Layer Models

The concept of water being driven across latitude lines by the wind, modifying its vorticity as it goes, turns out only to be useful when considering the depth integral. In fact even in this forced region, considerable curvature of Q contours is necessary to allow the deep low to move meridionally. Otherwise the flow is confined to a shallow layer just below the Ekman layer where it can be directly forced at all latitudes (see Rhines, 1986 for a scaling

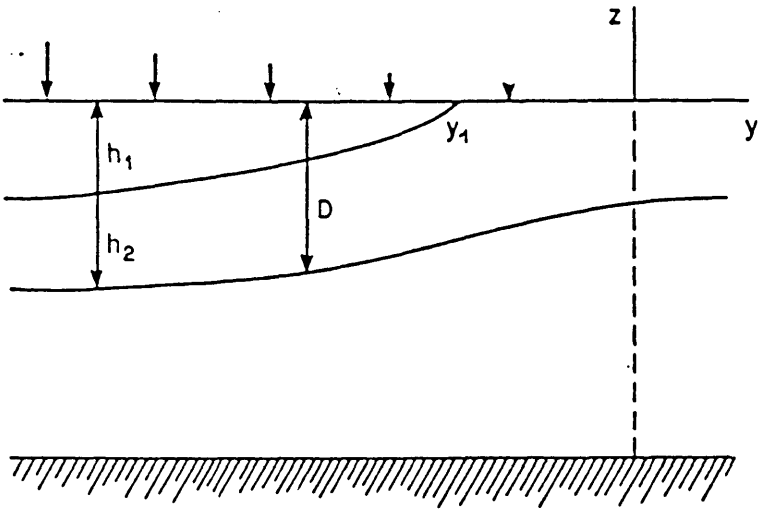

Figure 3.1: A schematic diagram of the ventilated thermocline model of Luyten, Pedlosky and Stommel (1983). The outcropping layer interfaces and the surface Ekman pumping are indicated. From Rhines (1986).

argument). In the ocean, rather than being directly forced everywhere, the thermocline flow is ventilated, as described in chapter 2. The deep curving Q contours thread back to outcrop windows at the surface. If the Q contours close off completely, then free flow becomes a possibility, and a different thermocline regime is generated. Successful layer models of these two regimes are described below.

(a) The Ventilated Thermocline

Luyten, Pedlosky and Stommel (1983) constructed a model of the eastern part of a large scale ocean gyre, in which the flow is forced by the wind. Frictional dissipation and advection of relative vorticity are considered negligible. Thus the Sverdrup constraint (1.2.5) can be applied to the depth integrated flow and the potential vorticity is simply given by $Q = f/h$, where h is the thickness of an isopycnal layer. The formulation of the model is shown in figure (3.1). Each layer outcrops between latitude lines, where it is forced by an Ekman pumping velocity. In the layer model context, the Sverdrup constraint is a summation over active layers:

$$\beta \sum_n h_n v_n = f w_E(x, y) \tag{3.2.1}$$

where n denotes layer number. Potential vorticity is conserved away from outcrop regions

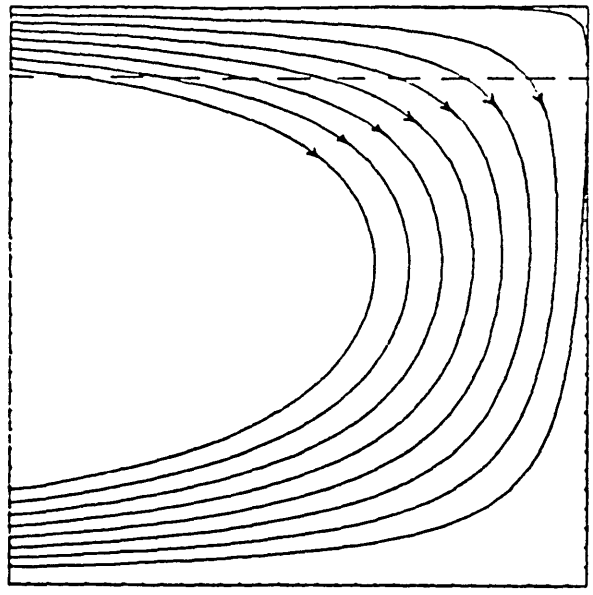

Figure 3.2: Contours of height for the lowest interface of the deepest layer of the ventilated thermocline model. These are trajectories for the lower layer flow. Notice the shadow zones to the west and on the eastern boundary. From Rhines (1986).

according to

$$\mathbf{v}_n.\nabla\left(\frac{f}{h_n}\right) = 0 \tag{3.2.2}$$

The $\mathbf{v}_n$s in the above equations can be substituted for in terms of h through thermal wind balance:

$$\mathbf{v}_n = \left(\frac{g'}{f}\right)\hat{\mathbf{k}}_\wedge\nabla h_n \tag{3.2.3}$$

The problem is solved by using (3.2.1) and (3.2.2) together to specify $h_n(x,y)$. Equation (3.2.1) is integrated from the eastern boundary and, using prior knowledge of the potential vorticity of the already subducted layers (equation (3.2.2)), the depth of the outcropping layer is found and hence its potential vorticity. When the outcropping layer is subducted to the south, it conserves this value of Q, becoming more squashed in order to offset the change in f.

A solution is shown in figure (3.2) for the total depth of the ventilated thermocline. This is a streamfunction for the lower layer flow, which outcrops north of the dashed line. South of this line the contours are also parallel to Q contours, which sweep round to allow meridional displacement of deep subducted fluid. A feature of the solution is the stagnant 'shadow zone' in the south eastern corner of the deepest active layer. In this

region, the layer is not sufficiently squashed by the flow above to allow any Q contours to connect back to the outcrop region. All Q contours in this shadow zone meet the eastern boundary so the water cannot move. Only when one is far enough west for the Ekman pumping integral to be large enough can the Q contours thread back to the outcrop.

Another shadow zone exists to the west. This region is simply not penetrated by any flow trajectories from the outcrop window of this layer. It is therefore isolated from direct wind forcing and susceptible to eddy Q homogenisation within closed Q contours. A model of this type of deep gyre is described below.

(b) Closed Wind Driven Gyres

Rhines and Young (1982a) offer an alternative to the direct ventilation of the previous model in their quasi-geostrophic layer model of closed ocean gyres. Rather than having density layers outcropping, the stratification is prescribed and the Sverdrup transport is shared between a directly forced upper layer, and a lower layer which is set into motion when q contours close to form free paths for the flow. The two layer form of equation (1.1.2) is

$$\begin{aligned} q_1 &= \beta y + L_\rho^{-2}(\psi_2 - \psi_1) \\ q_2 &= \beta y + L_\rho^{-2}(\psi_1 - \psi_2) \end{aligned} \tag{3.2.4}$$

Relative vorticity has again been neglected. If the upper layer is directly forced by the wind, and dissipation is through lateral eddy q transfer in both layers (equation (1.3.6)), then the equations of motion in the two layers are

$$\begin{aligned} J(\psi_1, q_1) &= \tfrac{1}{\rho}\hat{\mathbf{k}}.\nabla_\wedge\vec{\tau} + \kappa\nabla^2 q_1 \\ J(\psi_2, q_2) &= \kappa\nabla^2 q_2 \end{aligned} \tag{3.2.5}$$

Momentum is transferred from the upper layer to the lower layer through eddy form drag. The direct equivalence of vertical momentum transfer to lateral transfer of q is made clear by the relations:

$$\begin{aligned} \kappa\nabla^2 q_1 &= -\kappa L_\rho^{-2}\nabla^2(\psi_1 - \psi_2) \\ \kappa\nabla^2 q_2 &= -\kappa L_\rho^{-2}\nabla^2(\psi_2 - \psi_1) \end{aligned} \tag{3.2.6}$$

the right hand sides of which represent interfacial drag terms in the momentum equations. In this model, fluid is brought into motion in layer 2 through the action of eddies. A point is reached where q_2 contours close off allowing free flow. A pool of uniform q_2 then evolves,

expelling these closed contours to its perimeter. The eddy term which brought about this free flow is then 'switched off', leaving the lower layer to circulate in an equilibrium state defined by the action of eddies. This region of homogeneous free flow is impervious to influence from outside. It corresponds to the western shadow zone of the ventilated model above.

To solve equations (3.2.5) it is necessary to transform them into a set of linear equations. Rhines and Young choose to do this by imposing the Sverdrup constraint, which can be written as a barotropic mode streamfunction determined from the known wind stress.

$$\Psi = \psi_1 + \psi_2 \tag{3.2.7}$$

Substituting this into the final state of the lower layer momentum equation (in the limit of weak eddies) we obtain

$$J(\psi_2, \beta y + L_\rho^{-2}\Psi) = O(\kappa) \tag{3.2.8}$$

which implies that in the region of closed q_2 contours,

$$\psi_2 = G(\beta y + L_\rho^{-2}\Psi) \tag{3.2.9}$$

where G is an undetermined function. The form of G is also selected by the eddy terms. Equation (3.2.8), with the $O(\kappa)$ term defined as in (3.2.6), is integrated round a closed ψ_2 contour. The left hand side disappears, revealing that in this case, the integrated circulation is shared equally between the two layers, irrespective of the value of κ, and G is simply equal to $L_\rho^2/2$. ψ_2 can now be calculated and hence, from (3.2.7), ψ_1.

Figure (3.3) shows Rhines and Young's solution in each layer for a simple wind stress pattern applied to a circular patch centred on the origin of a boundless ocean. The wind stress curl is proportional to $-x$ and independent of y, integrating out to zero in the zonal direction and around streamlines and thus posing no problems requiring frictional western boundary closure. The lower layer flow is confined to the small, circular region of closed q_2 contours in the northern half of the area of upper layer flow. If the two layer model is extended to the continuously stratified case, this northward migration of the anticyclonic gyre with depth becomes clear, as seen in figure (3.4).

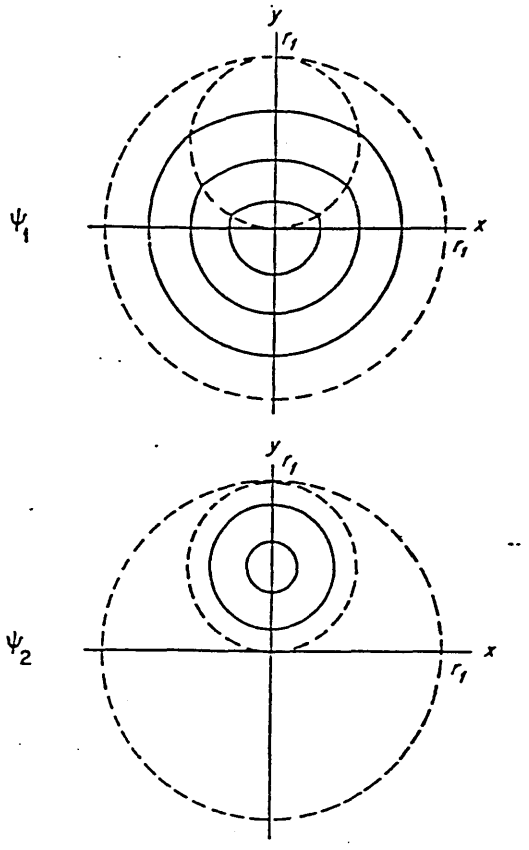

Figure 3.3: Streamfunctions from the two layer model of Rhines and Young (1982a).

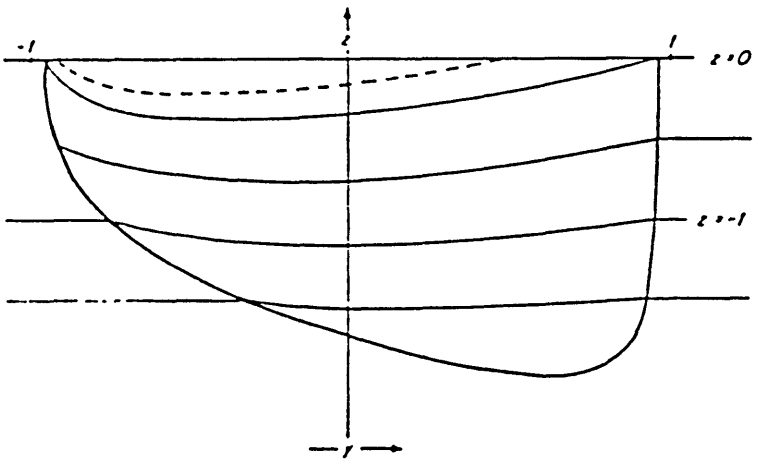

Figure 3.4: A meridional section of the continuously stratified model of Rhines and Young (1982a), showing the shape of the bowl and the northward migration of the anticyclonic gyre with depth.

3.3 Inertial Layer Models

(a) Baroclinic Fofonoff Gyres: the MN Model

Up to this point the vertical structure of ocean gyres has been discussed purely in terms of how the wind driven Sverdrup transport may be distributed in the vertical, and what the important processes are. The transport in the inertial recirculation is, however, far greater than the Sverdrup transport, as expounded in chapter 2. What is the vertical structure of the flow in a non-linear recirculating gyre ? To answer this question, the Sverdrup constraint must be abandoned and alternative ways of forcing the model adopted.

To specify the potential vorticity, given boundary conditions and a suitable balance assumption, is to specify the flow. This is the route taken by MN, MN2, Greatbatch (1987) and Cessi (1988) in setting up their analytical models of the recirculation. These models can be regarded as extensions to Rhines and Young's solutions, to the non-linear recirculation. They have the following features in common: all describe a vertical, meridional section in which the quasi-geostrophic potential vorticity is specified; they are driven by a low potential vorticity anomaly in the surface layer (determined by various means); they assume that at deep levels, the potential vorticity is homogeneous in the region of flow and they solve for the extent of this region by imposition of boundary conditions.

MN put forward a model of stacked Fofonoff gyres in which potential vorticity is set through a linear (q, ψ) relationship as in equation (1.3.16), viz

$$q = q_0 + c\psi$$

Figure (3.5) is a schematic diagram of the quasi-geostrophic layer model used in MN and MN2. It represents a vertical meridional section through a Fofonoff gyre, the position of which is shown in figure (1.4). A low value of q is given to the upper layer, representative of mode water. Thus, for continuity of potential vorticity at the southern edge of the gyre, q_0 is set to $-\beta L$ (where L is the meridional extent of the gyre). The corresponding value for the sub-polar gyre is βL, giving a realistic front in q at upper levels near the Gulf Stream (see figure (2.2a)). In the sub surface layers, it is assumed that q homogenises to the value of planetary vorticity at the axis of the eastward jet (the effects of relaxing this assumption are considered in chapter 5). This simply means that q is set equal to zero in the abyssal flow region. The value of $dq/d\psi$ is determined by the integral balance of

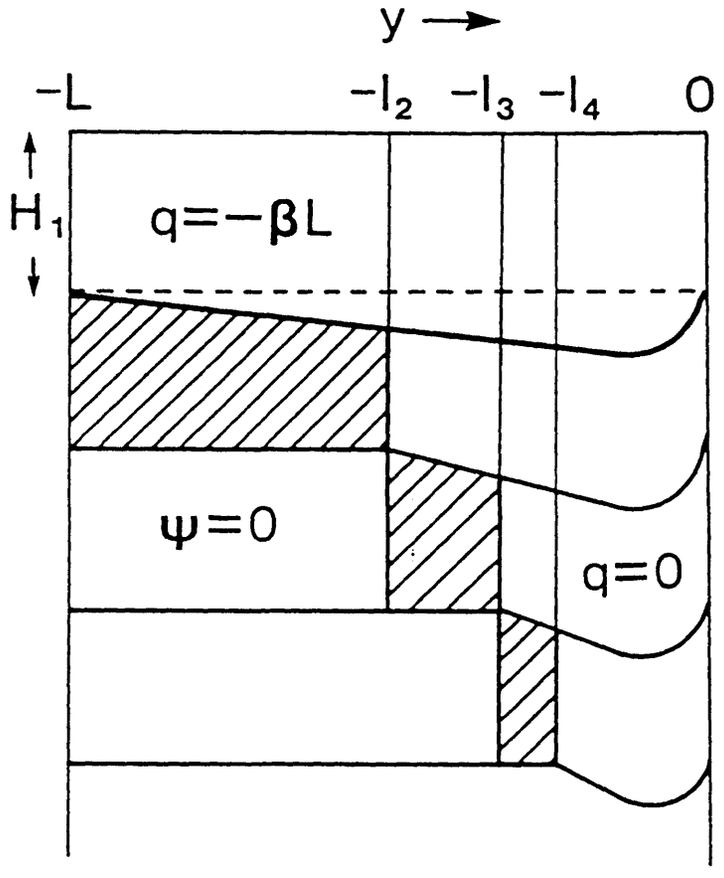

Figure 3.5: The vertical structure in MN's layer model of the recirculation. Regions of vortex squashing are shaded to represent the bowl of the circulation. North of these regions, q is homogeneous and free flow exists.

forcing and dissipation, as illustrated by equation (1.3.15). For the moment, however, we shall concern ourselves with the simpler case of uniform potential vorticity in regions of flow. (q, ψ) relationships are discussed further in section (3.3c) and chapter 4.

Returning to figure (3.5), the deep flow is set into motion through a similar mechanism to that described in section (3.2b), as follows: Layer 1 has moving fluid, with constant low potential vorticity. Its thickness increases in a linear fashion on moving northwards, as vortex stretching offsets planetary vorticity. Accordingly, the interface between layers 1 and 2 (the thermocline) is pushed down, progressively squashing the still motionless layer 2. Thus the potential vorticity in layer 2 increases at a faster rate than the beta effect and so q_2 reaches zero at $y = -l_2$. This marks the southern edge of the deep recirculating gyre. Contours of q_2 can now close off between this latitude and $y = 0$, and q_2 can homogenise to a zero value. To maintain $q_2 = 0$ against the background planetary vorticity gradient, layer 2 is now stretched until it regains its reference thickness at $y = 0$. This results in a depression of the interface between layers 2 and 3, implying motion in layer 2 and also squashing layer 3 and bringing it into motion at $y = -l_3$. The l_ns collectively define the bowl of the circulation. Figure (3.5) shows the 'hyperbolic plunge' of the bowl, with the homogeneous gyres retreating northwards with depth, and the penetration of the flow extending to infinity as the axis of the eastward jet is approached. This hyperbolic form compares well with the observations discussed in section (2.3) and shown in figure (2.3).

(b) Barotropic Flow and the Southern Boundary Condition: the CIY Model

CIY present a barotropic model in which the balance of terms in (1.1.2) is between planetary and relative vorticity, a very different emphasis to that of MN. Their model is forced by imposing anomalously low values of q on the boundaries. These q anomalies are diffused into the interior and eventually form a closed gyre with homogeneous q. They show through circulation integrals that the value of homogeneous q is a velocity weighted average of the boundary anomalies. The rationale for employing this type of forcing is that the q distribution in the recirculation is dominated by advection of q from distant sites by strong boundary currents, rather than by local forcing. This approach fails, however, to reproduce the strong minimum in q found in the gyre centre at upper levels (see figure (2.2a)) (an advantage enjoyed my MN, who model the effect of local forcing in terms of a

(q, ψ) relationship). CIY find that in their numerical integrations, a strongly forced recirculating gyre will fill the domain. If the model is less strongly forced, the southern extent of the recirculation depends on the size of the q anomaly. This dependence enters into their analytical calculations through an additional southern boundary condition, namely $u = 0$ or 'no slip'. This extra condition is required to allow the unspecified latitudinal extent of the gyre to be determined in the solution of the second order equation, (1.1.2). Whether or not it is useful to have a variable domain in the upper layers depends on the relative importance of local mechanical / thermodynamic forcing and the degree of certainty attached to the boundary conditions employed.

The choice of no slip boundary condition is justified by invoking the 'extremum principle'. CIY show through circulation integrals (see section 1.3c) that any local 'extremum' (or closed contour) in q will be eroded by eddies under the parameterisations introduced in chapter 1, and in the absence of direct forcing. If there is no flow to the south of the recirculation, then its southern edge must have a no slip character to ensure continuity of velocity. Otherwise, a forbidden extremum would result in relative vorticity and hence in q.

In the MN model, the eastward jet is assumed to have a boundary layer character and so their solutions are unable to satisfy the no slip southern boundary condition at the edge of the bowl required by CIY. Rather, at $y = -l_n$, a discontinuous jump exists in velocity at all levels. In fact, implicit in their neglect of relative vorticity at this latitude is an assumption of continuity of q through the shaded zones of figure (3.5), or to put it another way, a zero relative vorticity or 'free slip' southern boundary condition. MN argue that this is the appropriate condition to impose at the bowl. We shall return to this point in section (3.4), where the evidence from eddy resolving numerical models is noted and it is discussed in terms of a vertically continuous model in section (4.3).

(c) Models with Baroclinic and Barotropic Flow

Barotropic flow is only possible north of the latitude where the bowl hits the bottom. The question remains as to what determines the strength of the barotropic component. The bottom boundary condition usually applied in this region is $\psi_z = 0$, implying an isopycnal ocean floor. This is consistent with the spin up of the gyre from rest with $w = 0$

at the bottom. With this boundary condition, the vortex stretching term disappears from the vertical integral of (1.1.2). Therefore the depth integrated flow must be determined entirely from the remaining terms in ψ. These arise either through relative vorticity or through non-zero values of $dq/d\psi$ (or c) appearing in the form chosen for q.

In all cases, relative vorticity is essential for the closure of the circulation in the eastward jet to the north. To model this part of the gyre explicitly, relative vorticity must be included in equations (3.2.4), which are solved for a model with N isopycnal layers of constant density interval as a set of N coupled equations:

$$\begin{aligned} q_1 &= \beta y + \nabla^2\psi_1 + L_\rho^{-2}(\psi_2 - \psi_1) = -\beta L + c_1\psi_1 \\ q_n &= \beta y + \nabla^2\psi_n + \alpha_n L_\rho^{-2}(\psi_{n-1} - 2\psi_n + \psi_{n+1}) = 0 \\ q_N &= \beta y + \nabla^2\psi_N + \alpha_N L_\rho^{-2}(\psi_{N-1} - \psi_N) = 0 \quad (\text{or} = c_N\psi_N) \end{aligned} \tag{3.3.1}$$

with all sub-surface layers having $q_n = 0$ where there is flow, and $\psi_n = 0$ in the stagnant regions to the south. α_n is the ratio of the upper layer thickness to the thickness of layer n.

CIY and Cessi (1988) allow relative vorticity alone to set the transport of the barotropic component. Extending the analytical model of CIY to the baroclinic case, Cessi solved (3.3.1) for two layers, with $c = 0$ and a no slip ($\psi_y = 0$) rather than free slip ($\psi_{yy} = 0$) boundary condition at the southern edge of the deep flow. Relative vorticity, therefore, exerts its influence right out to this latitude. This alters the value of l_2 from $L/2$ in the MN model to $3L/4$ in the case of $\alpha_2 = 1$. Coupled with the presence of an ocean floor in this model, this serves to emphasise a barotropic balance to the flow, with relative vorticity offsetting planetary vorticity over most of the gyre and a strong barotropic component to the transport. The importance of vortex stretching is minimised in this study as it has no effect on the barotropic component of the flow. The processes described above, leading to the hyperbolic bowl, are relegated by Cessi to a weak 'baroclinic fringe', with most of the recirculation taking place in a 'barotropic core' north of the latitude where the bowl hits the bottom. This terminology is retained, and Cessi's interpretation of the transport in the recirculation is investigated critically in chapters 4 and 6, where the roles of relative vorticity and vortex stretching are described in full quantitative detail in a vertically continuous model.

MN2 analyse the bottom flow in terms of a 3 layer quasi-geostrophic model, where relative vorticity is neglected over the westward flowing part of the gyre and only becomes important in the eastward flowing boundary layer. This means that they have to rely on non-zero values of c to set the strength of the westward flow. Enhanced forcing is imposed in the upper layer through the relation $q_1 = -\beta L + c_1\psi_1$, and in the lower layer bottom friction is represented through $q_3 = c_3\psi_3$ in the region of bottom flow. q_2 is again equal to zero wherever layer 2 is in motion. Application of the theory embodied in (1.3.15) (where Ekman dissipation replaces wind stress forcing for the lower layers) leads to the simple constraints: $c_1 \leq 0$; $c_3 \geq 0$. To give further information about the possible values of $dq/d\psi$, (3.3.1) must be solved.

Equations (3.3.1) can be written in vector form as

$$\vec{\psi}_{yy} + L_\rho^{-2}\mathbf{A}\vec{\psi} + \beta\mathbf{b} = 0 \tag{3.3.2}$$

where $\vec{\psi}$ is the column vector $(\psi_1, \psi_2, ..., \psi_N)^T$, $\mathbf{b}$ is $(y+L, y, ..., y)^T$ and $\mathbf{A}$ is a tri-diagonal matrix involving the stretching term coefficients of ψ and the cs. In the three layer case, $\mathbf{A}$ is given by

$$\mathbf{A} = \begin{pmatrix} -(1+c_1'), & 1 & 0 \\ \alpha_2, & -2\alpha_2, & \alpha_2 \\ 0, & \alpha_3, & -(\alpha_3 + c_3') \end{pmatrix}$$

where $c' = L_\rho^2 c$. Equation (3.3.2) is solved by projecting onto normal modes and combining the particular integral ($\vec{\psi}_I$) with the complementary function ($\vec{\psi}_B$) to form the solution

$$\vec{\psi} = \vec{\psi}_I + \vec{\psi}_B \tag{3.3.3}$$

$\vec{\psi}_I$ is obtained by inverting $\mathbf{A}$ to solve

$$L_\rho^{-2}\mathbf{A}\vec{\psi}_I + \beta\mathbf{b} = 0 \tag{3.3.4}$$

and $\vec{\psi}_B$, by solving the linearly independent equations

$$\hat{\psi}_{Byy} + L_\rho^{-2}\left[\vec{\lambda}^T\hat{\psi}_B\right]^T = 0 \tag{3.3.5}$$

where $\vec{\lambda}$ is the column vector of the eigenvalues of $\mathbf{A}$ and $\hat{\psi}_B = \mathbf{E}^{-1}\vec{\psi}_B$ where $\mathbf{E}$ is the matrix of eigenvectors of $\mathbf{A}$.

Consistent with Fofonoff mode form, MN2 neglect the contribution of $\vec{\psi}_B$ to the westward flowing part of the gyre, assuming that it is only important in an eastward flowing boundary layer, with the solution of (3.3.5) decaying exponentially away from $y = 0$. To ensure westward flow under this assumption further constraints are placed on the allowed values of $dq/d\psi$. MN2 analyse the case where $\alpha_2 = 1$. The condition for westward flow is then

$$\det \mathbf{A} = \alpha_3 c_1' + c_3' + 2c_1' c_3' > 0 \tag{3.3.6}$$

since $c_1' \leq 0$ and $c_3' \geq 0$, this implies

$$0 \geq c_1' \geq -\frac{1}{2} \tag{3.3.7}$$

Equation (3.3.6) also implies a lower limit on c_3 which depends on the value of c_1. However, these limits are only meaningful if relative vorticity can be neglected out to the latitude $y = -l_3$. It will be shown in chapter 4 that c_3 can easily be zero, with relative vorticity providing the balance for the depth integrated flow rather than bottom friction. In this case, there is strong cancellation between $\vec{\psi}_I$ and $\vec{\psi}_B$ and the potentially infinite values of ψ, arising from having $\det \mathbf{A} = 0$, are avoided. Indeed, if a no slip boundary condition is to be satisfied, then the growing solution to (3.3.5) must also play a part, and the whole of the bottom flow region acquires a boundary layer character as in Cessi (1988). On the other hand, condition (3.3.7) on c_1 proves to be a realistic constraint on the upper layer forcing in the numerical inversions presented in chapter 4.

The views of the recirculation described in this section appear to be in opposition in several respects. It is hoped that the results of the next chapter will illustrate that the truth contains elements from both interpretations of equations (3.3.1).

(d) On the Interpretation of Two Dimensional Section Models

The models discussed above, and the models presented in the following chapters, are couched in terms of two dimensional inversions of specified potential vorticity distributions. They are intended to represent meridional sections through the recirculation. Wind forcing and thermodynamic processes are not considered explicitly, but their effect on the potential vorticity field is noted. It is assumed that the flow is slowly varying in the zonal direction, so zonal derivatives can be neglected. The models are also steady: time derivatives are ignored. However, it is not strictly justified to interpret the results in terms of a

time mean state. The models are intended to represent the dynamics of the Gulf Stream / Kuroshio systems. The time mean state of these systems is severely broadened and diluted by meanders which can have a similar horizontal scales to the cross stream scale represented by the models. The models should therefore be thought of as representing the time mean downstream flow, which is zonal in direction but not fixed in latitude. The interpretation of the mass transport is also a matter for careful consideration. The models represent the non-linear flow in a restricted area of the ocean in terms of an idealised potential vorticity distribution. So part of the wind driven Sverdrup transport is outside the model domain. However, the wind driven component can not easily be decoupled from the non-linear, free component of the transport as it has some effect on the potential vorticity field which is being inverted. Even in a linear, dissipative Stommel type gyre, the absolute vorticity contours do not exactly follow latitude lines, and in the ventilated models described in the last section the potential vorticity contours are swept round with the flow. It is therefore probably better to interpret the models' mass transport as an imperfect sub-basin scale representation of the total mass transport of the Gulf Stream / Kuroshio systems, rather than as a non-linear 'excess' transport. It will be seen in chapter 4 that the interpretation of the model transport has important consequences for the conclusions drawn.

3.4 Eddy Resolving General Circulation Models

Before moving on to the specification of the vertically continuous model, a brief survey is presented of the knowledge which can be gained about the dynamics of the recirculation by integrating large numerical models. The pathological problems of disparate scales in the ocean have been overcome to some extent through the use of quasi-geostrophic general circulation models. By using a 'cheap' equation set, in a reduced size ocean basin ($\sim$ 3000 km), these models can be integrated many times, allowing process studies to be carried out. The effects of the resolved $\sim$ 100 km eddies is well represented by the quasi-geostrophic dynamics, and these models can provide insight for the more idealised models considered here. The quasi-geostrophic formulation is particularly well suited to some aspects of the recirculation dynamics, such as the study of sub-basin scale isolated regions, where communication with a surface outcrop is not thought to be an important

process.

The models reviewed in this section are multi-layered, driven at the surface by a sinusoidal wind stress with mid-latitude westerlies and polar and equatorial easterlies, and retarded in the deepest layer by bottom friction. A double gyre is formed, cyclonic to the north and anticyclonic to the south with a strong eastward jet traversing the basin at its middle latitude. This jet is fed by intense western boundary currents from both gyres and the flow has a highly non-linear recirculating nature.

Figure (3.6) shows the time mean streamfunction and potential vorticity fields from the three layer integrations of Marshall, Nurser and Brugge (1988) (hereafter MNB). The latitude of the eastward jet is marked by a strong front in q with low values to the south and high values to the north. The gradient of q actually reverses on the southern flank of the anticyclonic gyre, indicating a highly unstable flow. At deeper levels, the gyres shrink towards the central latitude, much in the manner predicted by MN and MN2. In layer 2 the flow is confined to an extensive area of uniform q and in layer 3 the beta effect dominates. These fields should be compared with the observations of figure (2.2). The homogenisation of q in isolated layers is illustrated even more graphically in figure (3.7), which shows an instantaneous q field from an intermediate level of the eight layer model of Holland, Keffer and Rhines (1984). The accompanying (q, ψ) scatter plot clearly indicates that the fluid is either at rest, or in motion with uniform potential vorticity.

Closer inspection of the layer 3 streamfunction in figure (3.6) reveals the existence of four gyres. To the north and south of the two main gyres, there are two weak, counter rotating eddy driven gyres. These gyres are also a feature of the model of Holland *et al* (1984). They are not modeled explicitly in any of the theories presented above. However, their existence has implications for the choice of boundary condition at the southern edge of the deep homogeneous flow. If the possibility of flow outside the bowl is admitted, then it becomes possible for a free slip ($\psi_{yy} = 0$) southern boundary condition to be used without violating the extremum principle of CIY. The relevance of this phenomenon to the ocean is still to be investigated. In the study presented in the next chapter, the applicability of slip and no slip boundary conditions to the continuous model will be discussed and their implications explored.

Figure (3.6) also shows the (q, ψ) scatter plots from selected areas of MNB's model.

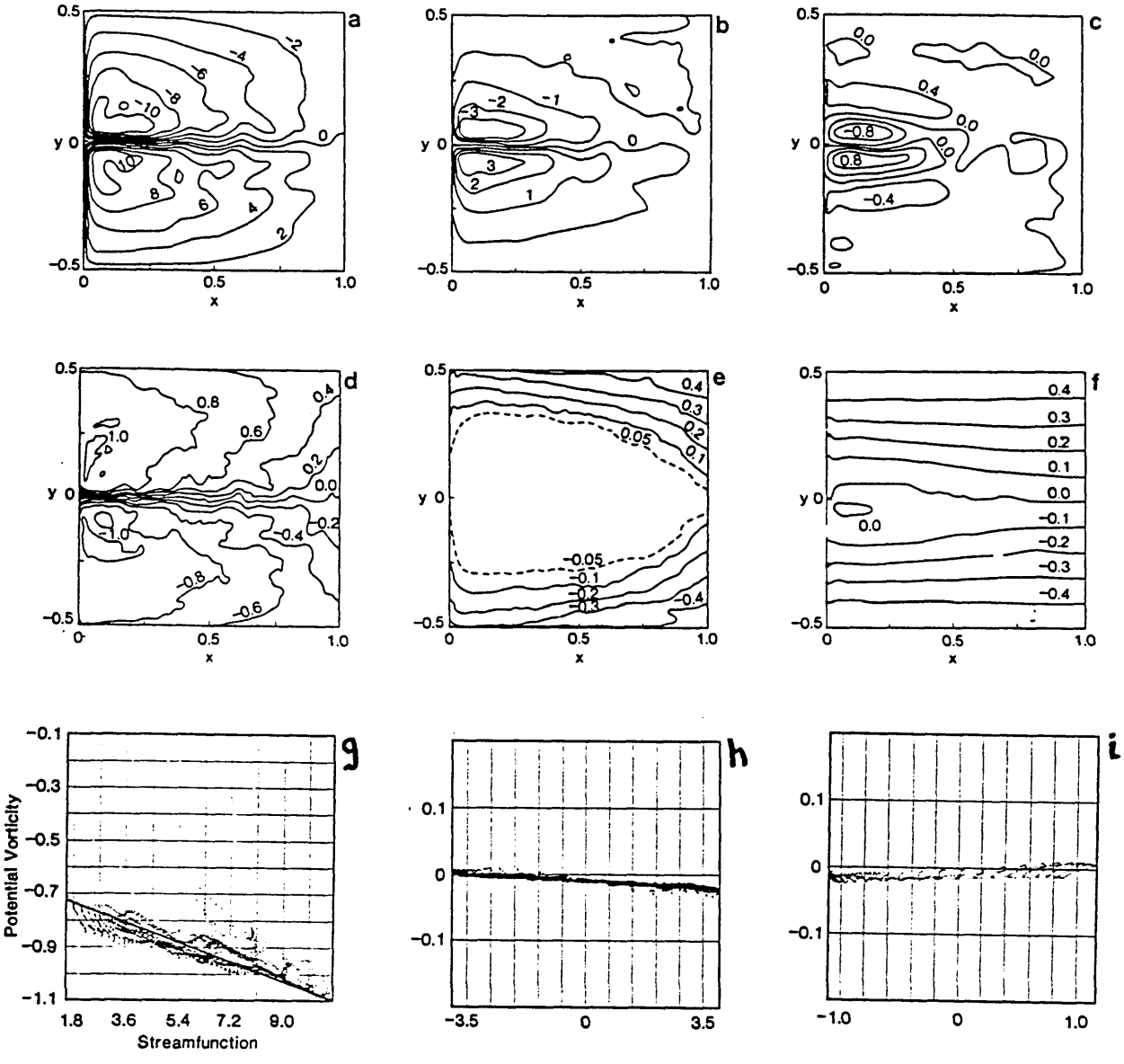

Figure 3.6: Time mean fields (non-dimensionalised) from the three layer eddy resolving quasi-geostrophic model of MNB. (a), (b) and (c) show the streamfunction (in units of a Sverdrup velocity scale multiplied by the meridional extent of the domain) for the top, middle and bottom layers respectively. (d), (e) and (f) show the potential vorticity (in units of $\beta \times$ the same length scale) and (g), (h) and (i) show scatter plots of q against ψ for selected regions of the three layers.

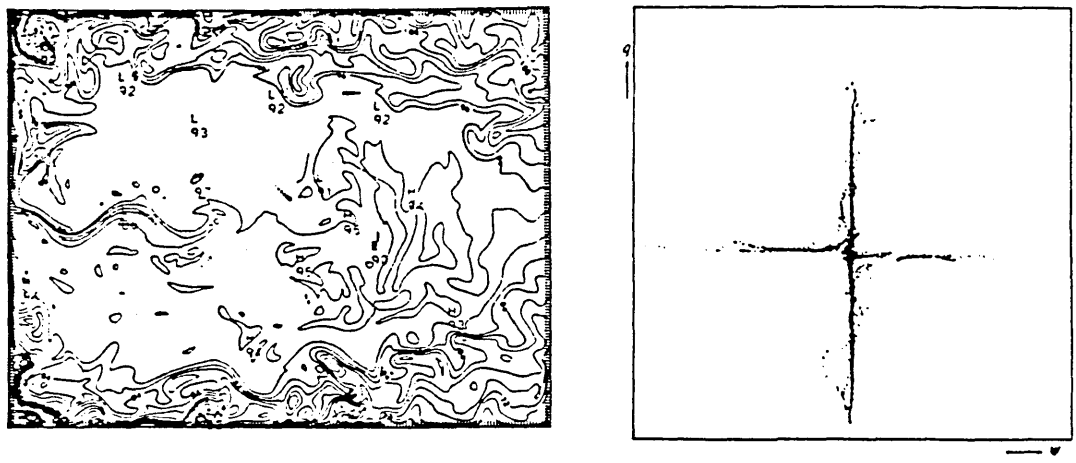

Figure 3.7: An instantaneous potential vorticity field from the third layer of the eight layer eddy resolving numerical simulation of Holland *et al* (1984), and a (q, ψ) scatter plot from the whole of this layer: either potential vorticity is uniform of the flow is stagnant.

The middle layer again shows uniform q, while for layers 1 and 3, the sign of $dq/d\psi$ vindicates the predictions made in section (3.3). The (q, ψ) relationship will be discussed in more quantitative detail in section (4.4), where comparisons with the vertically continuous model are made. Figure (3.8) shows the depth integrated transport for the three layers shown in figure (3.6). Contours are labelled in units of the linear Sverdrup component, showing an intensity of about five times the Sverdrup transport, or $\sim$ 150 Sv. Approximately half this mass transport is recirculated in the region where bottom currents exist in the same sense as the currents in the upper layers. This region can be associated with the core region referred to above, the transport returned within this region being predominantly depth independent. This partition of transport will be expanded upon in the next chapter, where differences between the MNB model and the vertically continuous model will be discussed.

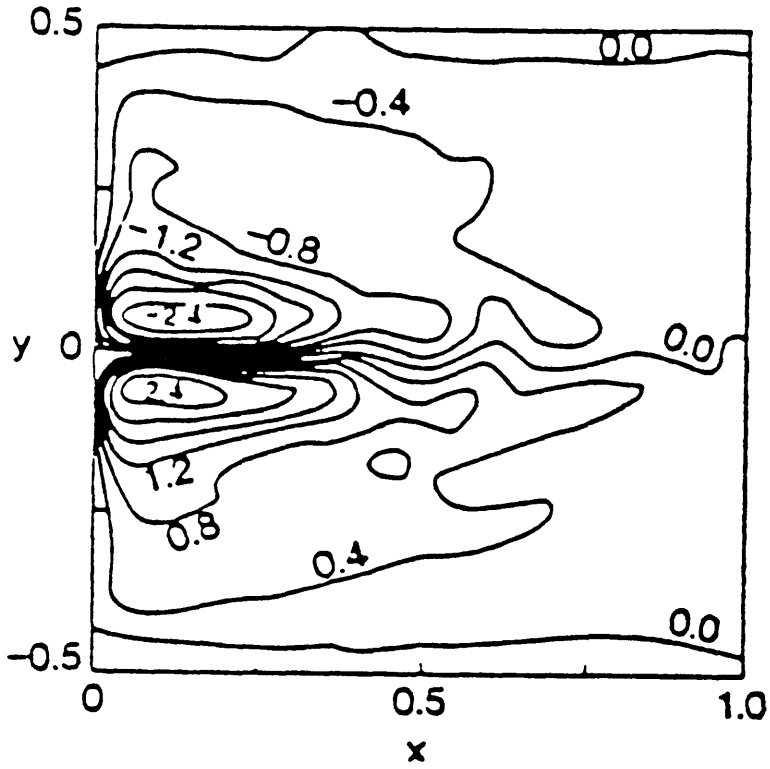

Figure 3.8: The depth integrated time mean flow from the MNB model (a sum of figures (3.6) (a), (b) and (c) weighted by the appropriate layer depths). A value of 1 corresponds to the linear, Sverdrup transport.

Chapter 4

A Vertically Continuous Quasi-Geostrophic Model

4.1 Introduction and Model Specification

In this chapter the layer models described in section (3.3) are extended to a continuous, two dimensional section. The method of prescribing the potential vorticity distribution, rather than imposing a wind stress and the Sverdrup constraint is once again utilised, and a numerical finite difference scheme is used to invert equation (1.1.2) for the flow. This high resolution, quantitative approach will help to resolve some of the apparent conflicts highlighted in the last chapter.

To understand the vertically continuous extension of figure (3.5), it is useful to ask what would happen if the number of layers became very large. Figure (3.5) consists of regions of stagnation, of vortex squashing and of stretching. As the number of layers is increased, the squashing regions become narrower. In the continuous limit, they are replaced by a line, the bowl, along which there is a discontinuity in q. This discontinuity is not dependent on the presence of relative vorticity, as is the discontinuity which results from the application of the no slip boundary condition considered in chapter 3. It is a discontinuity in the vortex stretching, arising from the fact that the smooth, squashing regions found in the layer models have collapsed onto a line. This line is the boundary between motionless water, where $q = \beta y$, and recirculating water where the flow can maintain $q = 0$ through vortex stretching and relative vorticity. On this boundary, isopy-

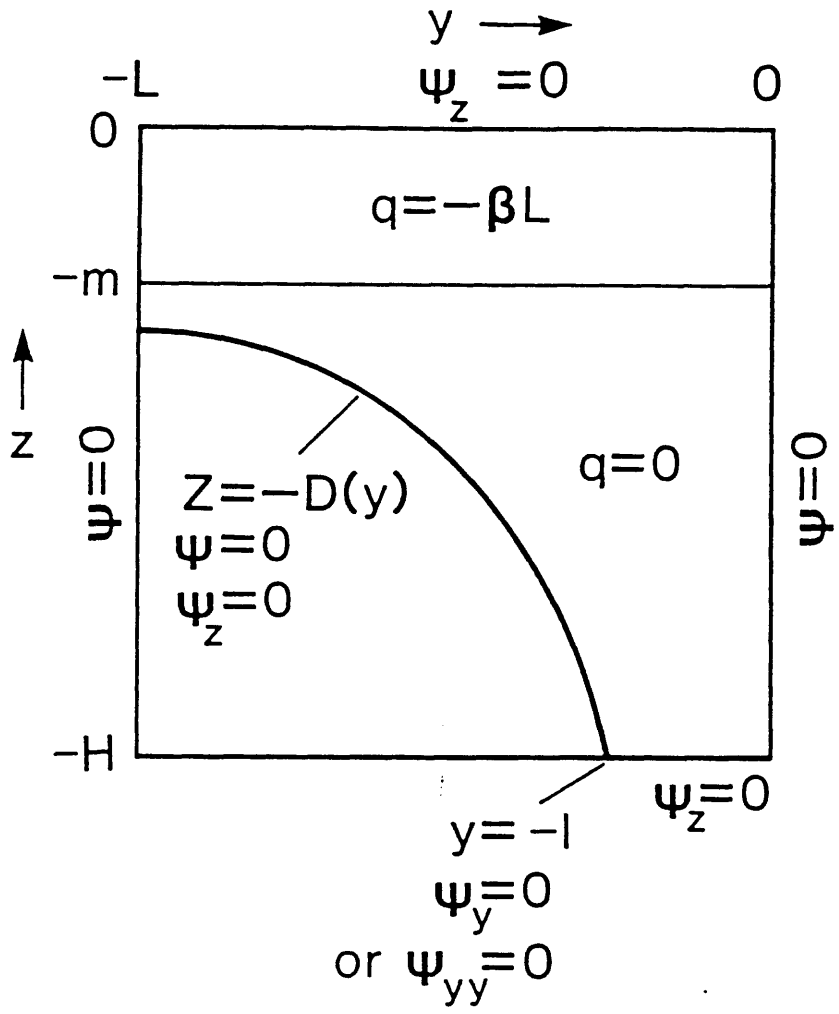

Figure 4.1: The formulation of the free boundary problem. Potential vorticity is specified above the bowl and there is no flow below. Boundary conditions are applied to close the problem and locate the bowl.

cnals are at their reference depths ($\partial\psi/\partial z = 0$). Since the surface boundary condition is $\psi_z = 0$, the vertical integral of vortex stretching vanishes at the bowl.

These facts can be used to find the position of this interface. The formulation of the problem is shown in figure (4.1). The potential vorticity is specified everywhere where there is flow as in the layer model of figure (3.5). The surface is at $z = 0$ and the low q water extends down to $z = -m$. The bowl is at $z = -D(y)$. There are three fixed boundaries with appropriate conditions while the bowl is a free boundary where extra information is needed to specify its position.

If (1.1.2) is integrated vertically from $-D(y)$ to the surface, the vortex stretching term

vanishes and one obtains

$$D = \frac{1}{|y|}\left[mL - \frac{1}{\beta}\frac{|y|}{y}\int_{-D}^{0} \nabla^2\psi \, dz\right] \tag{4.1.1}$$

If relative vorticity is neglected, then $D(y)$ simply follows the 'hyperbolic plunge' described by MN. Note that in this case, surprisingly, the depth profile is independent of stratification. A natural question to ask is: can the circulation really extend to infinite depths, and if not, does it reach the ocean floor ? Near the eastward jet, the relative vorticity integral term in (4.1.1) becomes significant and positive, tending to make the bowl more shallow. It is conceivable that it could bottom out at a finite depth.

To answer this question, the full problem must be solved by numerically inverting (1.1.2). An iterative approach has been used to find $D(y)$, in which $\psi = 0$ is imposed everywhere along the bowl and solutions are sought in which $\psi_z = 0$ is also satisfied. This is achieved by searching for vertical minima in the geostrophic energy. In cases where the bowl intersects the bottom, it becomes necessary to impose a further lateral boundary condition on the bottom flow to determine its latitudinal extent. No slip ($\psi_y = 0$) or free slip ($\psi_{yy} = 0$) conditions are applied. This point is discussed further in section (4.3). Following Gill (1984) and Nurser (1988), a vertical profile was used for N to allow the stratification to diminish realistically with depth:

$$\begin{aligned} N &= s/2h \quad &: z > -h \\ N &= s/(h - z) \quad &: z < -h \end{aligned} \tag{4.1.2}$$

where s and h are empirically derived constants (= 2.8 m s^{-1} and 150 m respectively). Full details of the method of solution are given in appendix A.

In the next section, the finite depth penetration of the flow will be exposed in a numerical inversion with a bottomless ocean. In section 4.3 an ocean floor is included allowing barotropic flow and in section 4.4 the forcing is made more realistic by imposing non-zero values of $dq/d\psi$. A brief summary is given in section 4.5.

4.2 Inversions in a Very Deep Ocean

In order to discover how deep the circulation could be expected to penetrate, equation (1.1.2) was inverted with realistic stratification, a meridional gyre extent of 1500 km and

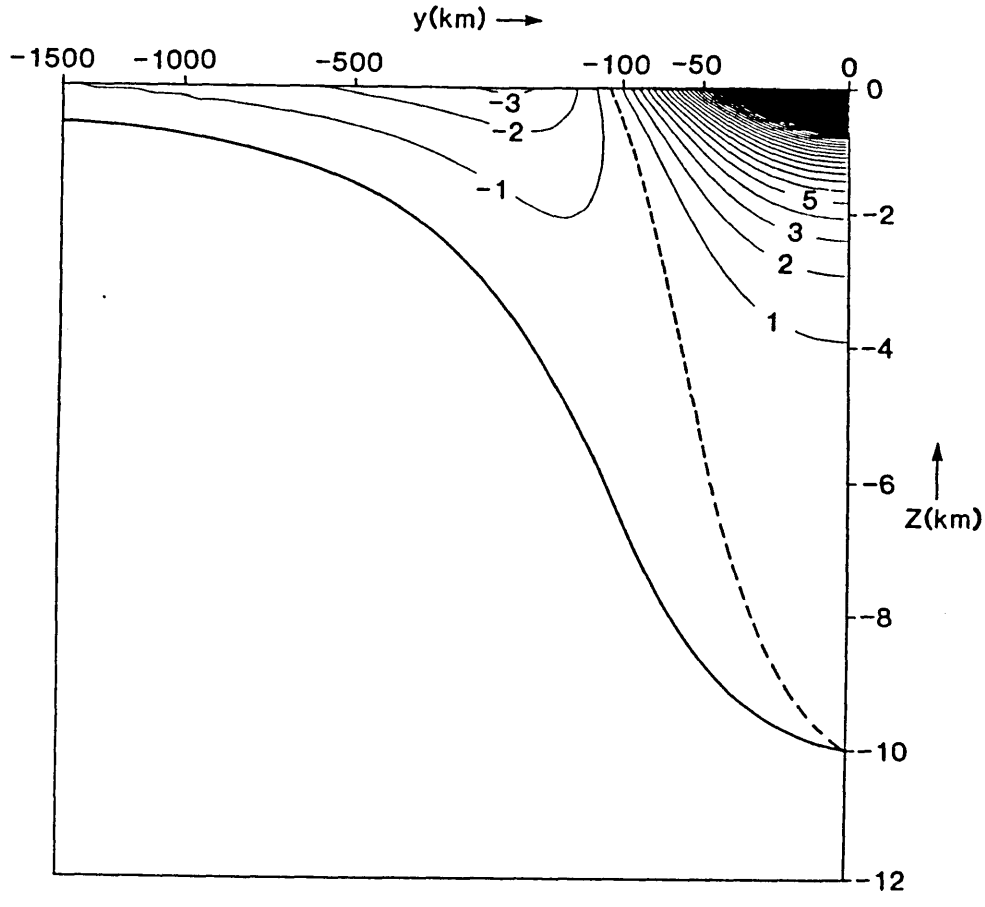

Figure 4.2: Zonal velocity section from the solution for a deep ocean. The flow extends down to 10 km. The contour interval is 1 cm s^{-1} and the maximum eastward velocity is 79 cm s^{-1}. Note that the y coordinates have been stretched to emphasise the region of the eastward jet (see appendix A).

an upper low q layer 500 m deep. The values of f_0 and β pertaining to a latitude of 40^0 N were used. The depth of the domain was allowed to become as large as necessary in order to prevent the bowl from hitting the bottom and the position of the bowl was found using the iterative procedure outlined in Appendix A. Figure (4.2) shows the solution, which consists of a strong, surface intensified eastward jet with a weak, broad return flow to the south. Note that the y coordinates have been stretched so that the eastward jet region can be clearly seen (see appendix A). As suspected, the bowl does indeed 'bottom out', the circulation penetrating to a depth of $\simeq$ 10 km below the eastward jet. So it seems likely that the circulation extends to the bottom, although it must be stressed that the penetration depth is dependent on the parameters used. The depth penetration of

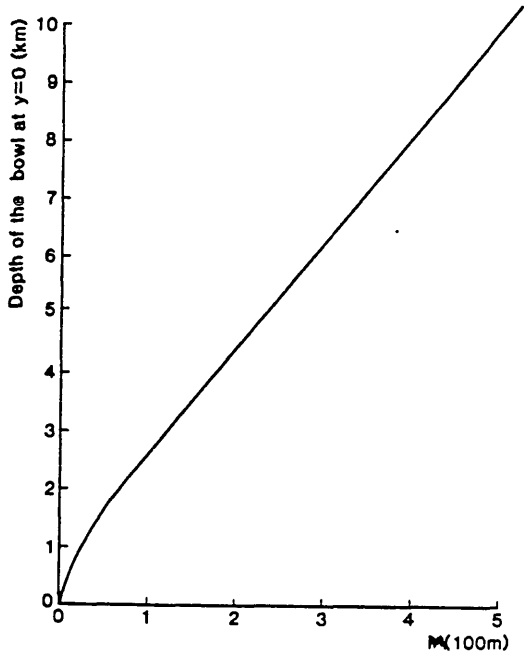

Figure 4.3: Maximum depth of the bowl plotted against the depth of the surface (low q) layer (using realistic stratification).

the flow, and its associated region of uniform potential vorticity was discussed in section (2.3) for the Gulf Stream and Kuroshio systems. The finite penetration beneath the Kuroshio could tentatively be associated with the bottoming out of this model. This idea is consistent with the notion that the poor ventilation, and relative paucity of mode water in the Pacific is responsible for this weak penetration of the recirculating flow. Figure (4.3) shows how variations in the volume of mode water, controlled by varying m, affect the depth of penetration of the flow, $D(y = 0)$. As expected the bowl gets deeper as the depth of the mode water layer increases. In fact this relationship is one of simple proportionality.

The other parameter which can be varied is the stratification, N^2. This becomes an important factor in determining both the strength of the flow and the depth of the bowl, because it sets the balance between the relative vorticity and vortex stretching terms. This should be compared with the analysis of section (4.1), where the value of N^2 has no effect on the penetration depth unless the relative vorticity term is included in (4.1.1). Figure (4.4) shows the dependence of the penetration depth on the (constant) value of N^2. In a strongly stratified ocean, the bowl becomes very shallow as relative vorticity

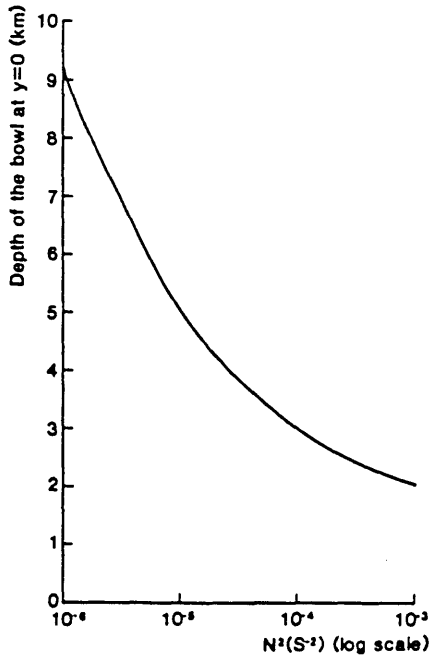

Figure 4.4: Maximum depth of the bowl plotted against the (constant) stratification, with a surface layer 500 m deep.

takes control of the dynamics with the gyre spinning very rapidly. As N^2 is decreased, the Rossby radius is reduced and relative vorticity can only exert its influence near to the axis of the eastward jet, causing the bowl to bottom out at deeper levels. The bowl bottoms out mainly as a result of the action of relative vorticity at upper levels, allowing the isopycnal at the base of the mode water layer to return to its reference depth at $y = 0$, as illustrated in figure (3.5).

These results are consistent with the simple calculations (MN, Cessi, 1988) which show that the width of the lower gyre is dependent on the strength of the upper forcing, the ratio of the layer depths and, in cases where the relative vorticity plays a role in determining the gyre width, the Rossby radius.

4.3 Inversions in an Ocean of Realistic Depth

(a) The Southern Boundary Condition in the Continuous Limit

Given the likelihood of the flow penetrating to the ocean floor, it is interesting to investigate the form and meridional extent of the bottom currents and their effect on the structure and transport of the gyre above. We shall consider two regions of the model: In

the core region, north of the latitude where the bowl hits the bottom ($y = -l$), a depth independent flow is allowed, which can enhance the transport. South of $y = -l$ is the purely baroclinic fringe region.

However, to invert for the flow in the case where the bowl hits the bottom, the question of what determines l must be addressed. The arguments for different lateral boundary conditions for layered models were given in the last chapter, but which of these conditions is the most appropriate in the continuous limit ? The position of the bowl is normally found through the knowledge that ψ and ψ_z are zero. If s is a coordinate along the direction of the bowl, then it follows from the chain rule that

$$\frac{\partial \psi}{\partial z}\frac{dz}{ds} + \frac{\partial \psi}{\partial y}\frac{dy}{ds} = 0 \tag{4.3.1}$$

on any ψ contour, including the bowl. Since ψ_z is zero on the bowl, this implies that ψ_y is also zero on the bowl, provided only that the bowl is not vertical. So the natural choice for the southern boundary condition of the bottom flow is $\psi_y = 0$, connecting smoothly onto the free boundary above. This boundary condition allows for stagnant water everywhere south of $y = -l$, while satisfying the extremum principle of CIY.

However, the evidence from eddy resolving quasi-geostrophic models (see section 3.4) is that the bottom flow has a free slip boundary at $y = -l$, with a counter rotating gyre to the south. For purposes of comparison, it would be desirable to simulate this type of flow in the continuous model without explicitly simulating the weak, eddy driven gyre. The question is, can this be done by imposing $\psi_{yy} = 0$ at $y = -l$ for the bottom flow ? It should be noted that the bowl approaches the bottom very nearly vertically, rendering the condition, $\psi_z = 0$, redundant. If this is the case, the condition $\psi_y = 0$ can no longer be directly inferred from (4.3.1), because $dy/ds = 0$. If one takes advantage of this fact to impose a free slip condition, then the bowl is, in part, no longer a 'free boundary' insofar as it has a non-zero normal derivative. It is also generally true that this type of southern boundary is unable to connect smoothly on to the true free boundary above. The discontinuity in velocity cannot follow the bowl as it becomes more slanted, without violating the condition, $\psi_z = 0$. The result is either a bowl on which $\psi_z \neq 0$ or a velocity discontinuity in the interior. This assertion is made transparent by considering a Taylor

expansion for ψ_z about the point $(y,z) = (-l,-H)$:

$$\psi_z(y,z) = \left[1 + \Delta y\frac{\partial}{\partial y} + \Delta z\frac{\partial}{\partial z} + \frac{\Delta y^2}{2}\frac{\partial^2}{\partial y^2} + \frac{\Delta y \Delta z}{2}\frac{\partial^2}{\partial y \partial z} + \frac{\Delta z^2}{2}\frac{\partial}{\partial z^2}\ \cdots\right]\psi_z(-l,-H) \tag{4.3.2}$$

where $\Delta y = y + l$ and $\Delta z = z + H$. For a free slip southern boundary condition, with a $\psi_z = 0$ bottom boundary condition in the core, the conditions at the point $(-l,-H)$ are: ψ, ψ_{yy}, ψ_z, $\partial\psi^{n+1}/\partial y^n \partial z = 0$. If we have $\psi_{yy} = 0$ it can also be assumed that all vertical derivatives of the vortex stretching term in (1.1.2) are zero at this point. Thus the only term in the right hand side of (4.3.2) which is not neglected is the term in Δz. Using (1.1.2) and neglecting vertical gradients of N^2, (4.3.2) therefore leads to

$$\psi_z = \frac{\beta l N^2}{f_0^2}\Delta z \tag{4.3.3}$$

arbitrarily close to the point (-l,-H). This quantity is non-zero, thus (1.1.2) can not be satisfied exactly in the continuous limit with a free slip boundary condition at $(y,z) = (-l,-H)$. The basic problem is that $q - \beta y$, when integrated up from the bottom is non-zero, requiring non-zero ψ_z in the absence of relative vorticity. Thus a vertical intersection of the bowl with the bottom cannot be supported in the continuous limit without relative vorticity playing a part. The discretisation of the bottom boundary condition in layered models conceals this problem, but the continuous model with a free slip boundary condition at the bottom must be regarded in the strictest sense as an approximation to the limiting behaviour of the layer models as their resolution is increased. It is possible, however, to obtain a unique and useful approximation if it is accepted that ψ_z is not exactly zero on the lower portion of the bowl (a reasonable assumption given that flow is envisaged outside the bowl in this case). $(\psi_z)^2$ can be minimised by the iteration scheme while also iterating sideways for the condition, $\psi_{yy} = 0$ at the bottom (see appendix A). This procedure has been carried out for a number of inversions presented below.

(b) Numerical Results

A similar inversion to that of figure (4.2) is shown in figure (4.5) except that in this case the ocean is 5 km deep and the flow extends to the bottom. A no slip ($\psi_y = 0$) boundary condition is applied at $z = -H$ on the southern edge of the core. North of $y = -l$, the existence of a barotropic component is clear in the velocity field of figure (4.5a). But

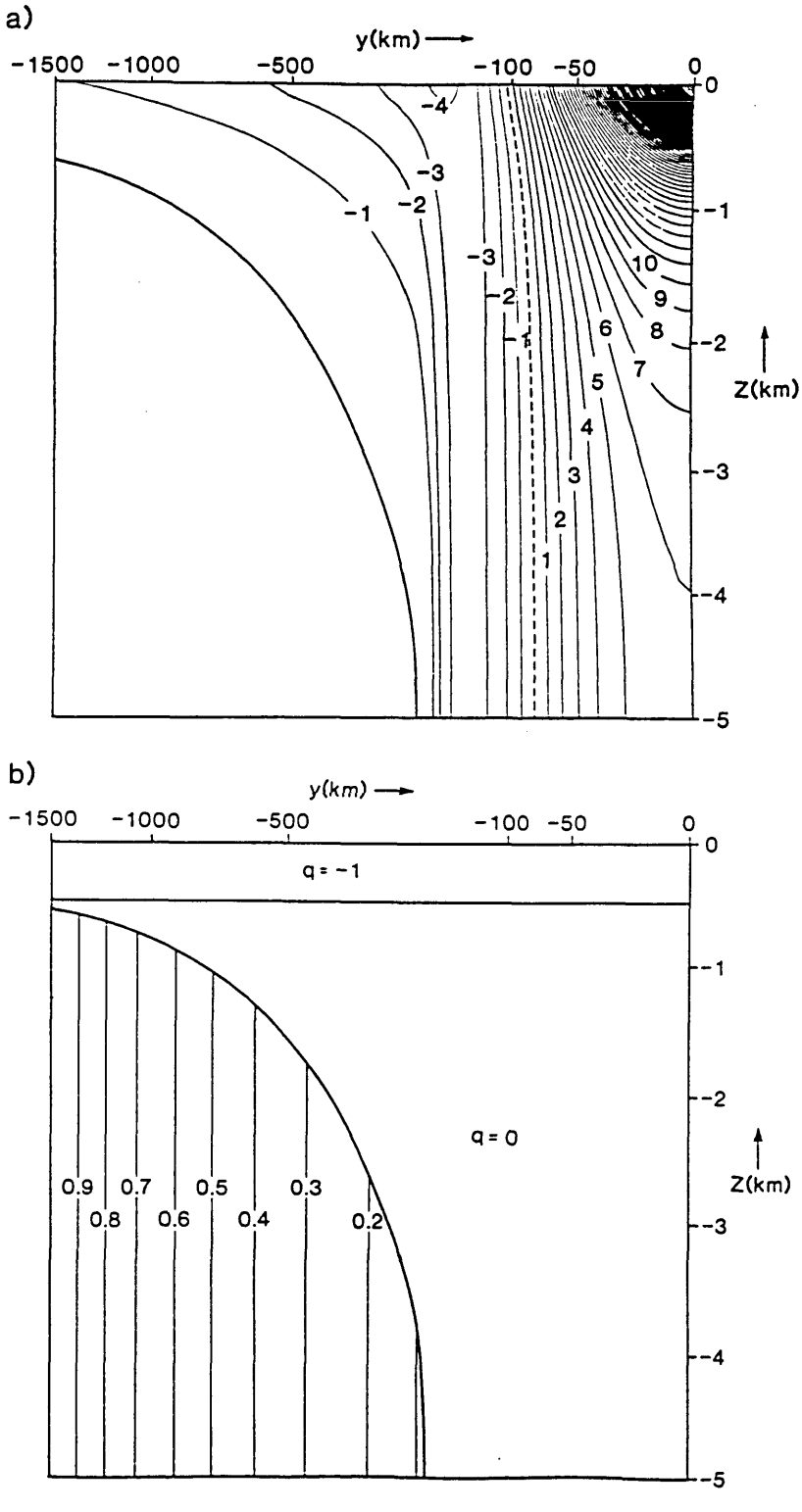
a)
y(km)
-1500 -1000 -500 -100 -50 0
0
-1
-2
-3
-4
-5
Z(km)
-4
-3
-2
-1
-3
-2
-1
1
2
3
4
5
6
7
8
9
10
b)
y(km)
-1500 -1000 -500 -100 -50 0
q = -1
q = 0
0.9 0.7 0.5 0.3
0.8 0.6 0.4 0.2
Z(km)

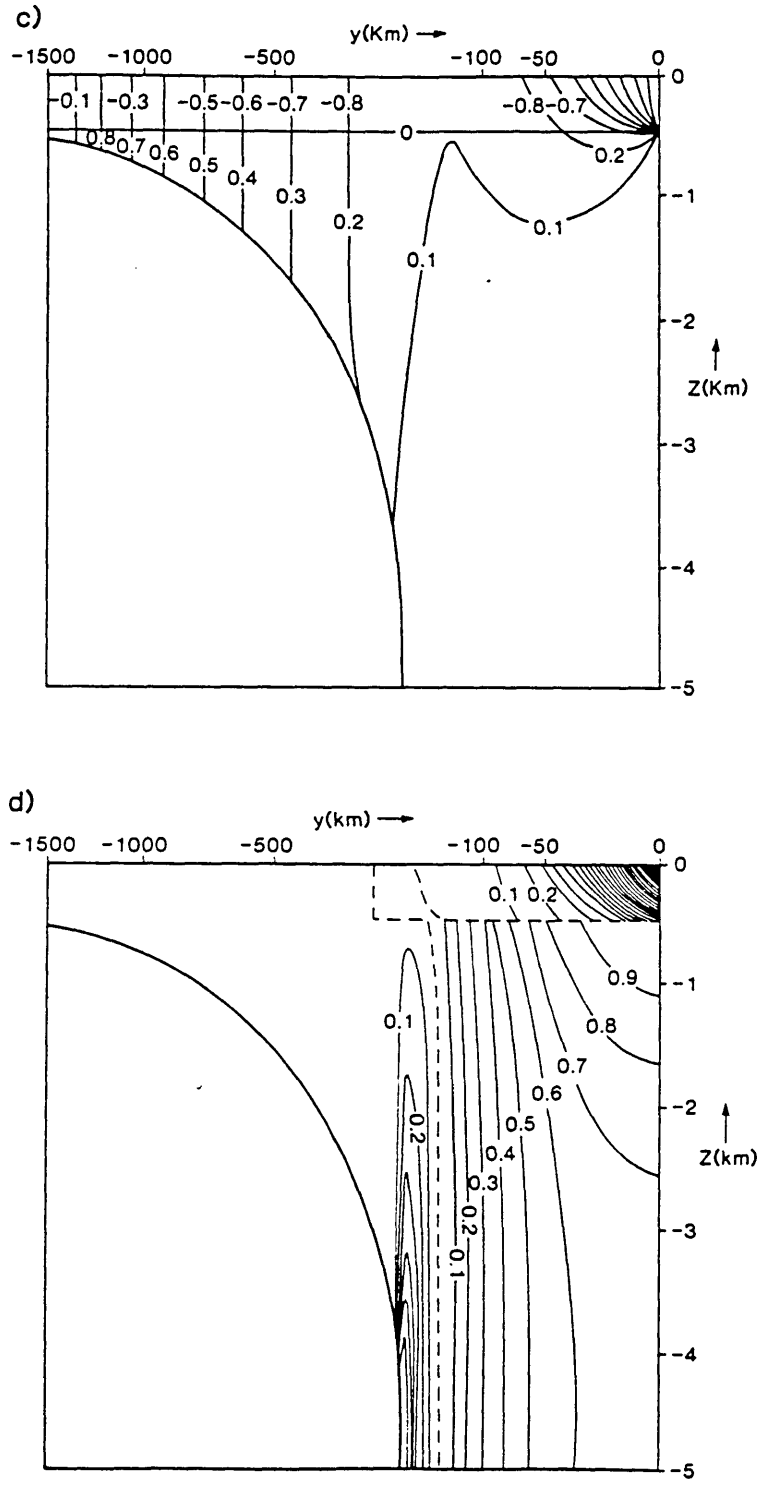

Figure 4.5: An inversion in a 5 km deep ocean with the bowl hitting the bottom. A no slip lateral boundary condition is used to locate the southern edge of the bottom flow. The core region has a latitudinal extent of 206 km. (a) Zonal velocity (cm s^{-1}). Maximum eastward velocity is 82 cm s^{-1}; (b) Potential vorticity in units of βL; (c) the vortex stretching term in (1.1.2) in units of βL; (d) the ratio of relative vorticity to vortex stretching terms. y coordinates stretched as in appendix A.

in general the depth dependent form chosen for N^2 serves to concentrate the strongest flow near the surface. Figure (4.5b) shows the potential vorticity field for reference and (4.5c) shows the vortex stretching term. By comparing these two it can be seen that the stretching simply balances the beta effect over most of the southern, westward flowing part of the gyre. Vortex stretching is important at all depths, although it disappears in the vertical integral, with negative values above $z = -m$ cancelling positive values below.Vortex stretching is the dominant dynamical process throughout the fringe and over significant regions of the core. Figure (4.5d) shows the ratio of relative vorticity to vortex stretching; $\nabla^2\psi$ only dominates in the upper reaches of the eastward jet (it is in this region that isopycnals are brought back to their reference levels, allowing the bowl to bottom out far below in the example of figure (4.2)) Although over much of the domain relative vorticity is small in absolute magnitude, it is crucial in controlling the structure of the recirculating core. Its importance relative to vortex stretching has another peak in the deep flow at the southern edge of the core, where the no slip boundary condition has been applied, implying a boundary layer structure for the deep westward as well as eastward flow.

The corresponding inversion with a free slip ($\psi_{yy} = 0$) boundary condition is shown in figure (4.6). The overall structure is similar but a discontinuous velocity is apparent at $y = -l$. In this case the core does not extend so far south and carries a smaller proportion of the transport. In the following we shall compare these two results quantitatively with a simple analysis of the barotropic mode streamfunction north of $y = -l$.

(c) Solutions for the Barotropic Mode

In the core, north of $y = -l$, the depth integral of q does not vary with y (q is uniform in y for both the upper layer and the abyssal region, and the flow extends to the bottom everywhere). Therefore, since the depth integral of vortex stretching is zero, changes in planetary vorticity must be offset by relative vorticity in a depth integral sense. So integrating (1.1.2) vertically it becomes

$$\tilde{q} = y + \tilde{\psi}_{yy} \tag{4.3.4}$$

where $\tilde{}$ denotes a depth average, and q has been scaled by βL, y by L and ψ by βL^3.

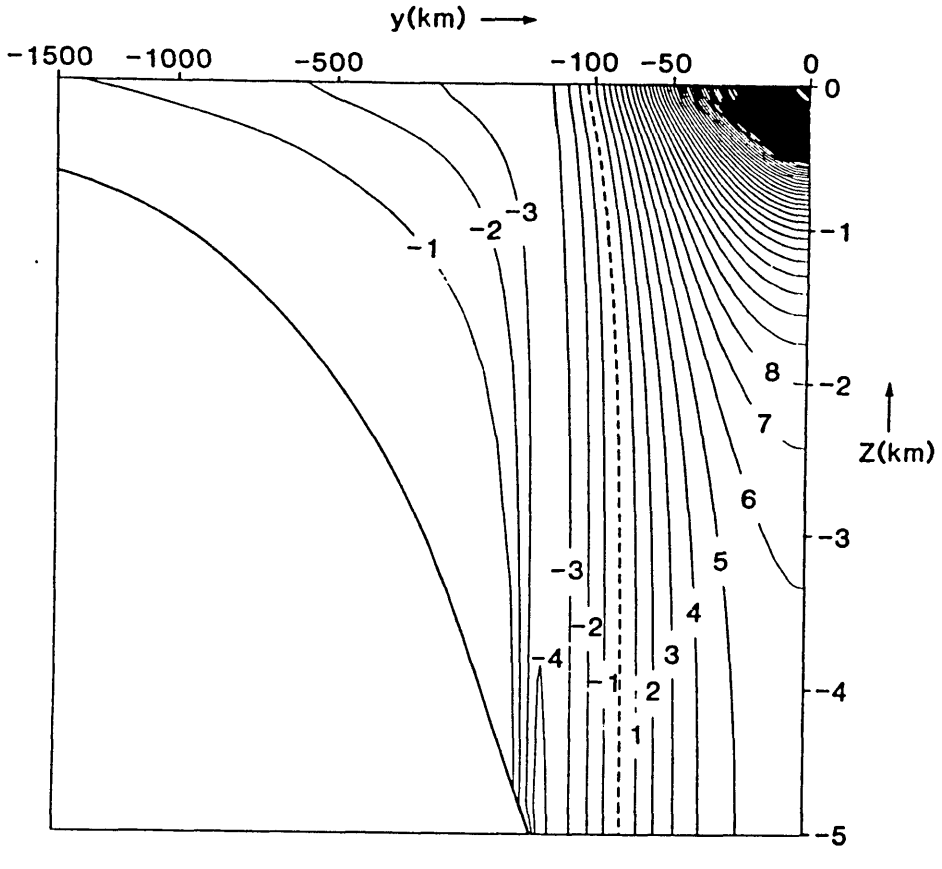

Figure 4.6: As figure (4.5a) but with a free slip lateral boundary condition at the southern edge of the bottom flow. The core is 150 km wide.

$\tilde{q} = -m/H$, where H is the depth of the ocean. Equation (4.3.4) has solution

$$\tilde{\psi} = -\frac{y^3}{6} + \tilde{q}\frac{y^2}{2} + \left[\tilde{q}\frac{l}{2} + \frac{l^2}{6} - \frac{\tilde{\psi}_F}{l}\right] y \tag{4.3.5}$$

if $\tilde{\psi} = 0$ at $y = 0$, and $\tilde{\psi}_F$ is the value of $\tilde{\psi}$ at $y = -l$. Additional boundary conditions will be used to determine l. Equation (4.3.5) can be differentiated to find the position and hence the value of the maximum depth integrated streamfunction, $\tilde{\psi}_{max}$, the barotropic mode transport. In the case when $\tilde{\psi}_F = 0$, and $\tilde{\psi}_{yy} = 0$ at $y = -l$ (free slip):

$$\begin{aligned} l &= -\tilde{q} \qquad \text{(immediately from (4.3.4))} \\ \text{and} \quad \tilde{\psi}_{max} &= -\tilde{q}^3/9\sqrt{3} \end{aligned} \tag{4.3.6}$$

If $\tilde{\psi}_y = 0$ at $y = -l$ (no slip):

$$\begin{aligned} l &= -\tfrac{3}{2}\tilde{q} \\ \tilde{\psi}_{max} &= -\tilde{q}^3/12 \quad \left(= \tfrac{2}{81}l^3\right) \end{aligned} \tag{4.3.7}$$

Equation (4.3.7) recovers the results of CIY and Cessi (1988) expressing the mass transport in terms of l. Note that there is little difference between the values of $\tilde{\psi}_{max}$ for slip and no slip conditions when it is expressed as a function of $\tilde{q}$.

It must be stressed that the predictions of (4.3.6) and (4.3.7) are only valid if the transport carried by the baroclinic fringe is negligible. However, figures (4.5) and (4.6) show that this is not the case. Table (4.1) gives values for the transport and the meridional extent of the core provided by the analysis above (where the baroclinic fringe is neglected) and from the numerical inversions. Clearly the transports given by this simple analysis are weak compared to the model's transport (the absolute value of the transport is discussed further in section (4.4)). Only in the free slip case is the gyre width correctly predicted by the analysis; the reason being that if relative vorticity is zero at the bottom at latitude $y = -l$, then the depth integrated relative vorticity can also be reasonably approximated to zero at this latitude. So (4.3.4) immediately provides a good prediction for l in the free slip case. However, $\tilde{\psi}_F = 0$ is not an appropriate boundary condition at the southern edge of the core and the zero velocity southern boundary condition is also a poor approximation for the barotropic mode. For such quantities a boundary condition applied at $z = -H$ is not equivalent to a boundary condition on the depth integrated flow. In the numerical inversions presented in figures (4.5) and (4.6) the transport in the 'baroclinic fringe' south

		$\tilde{\psi}_{max} \times 10^5$ (non-d)	$\tilde{\psi}_{max}$ (Sv)	l (non-d)	l (km)
Free Slip	Barotropic Analysis (Eq. (4.3.6))	6.42	18	0.1	150
	Numerical Inversion (Fig. (4.6))	9.65	28	0.1	150
No Slip	Barotropic Analysis (Eq. (4.3.7))	8.33	24	0.15	225
	Numerical Inversion (Fig. (4.5))	10.10	29	0.137	206

Table (4.1): A comparison of the barotropic mode solutions with the numerical inversions

of $y = -l$ is in fact very strong, and cannot be neglected. Thus, in the no slip case, the value of l given by (4.3.7) must be replaced by the appropriate solution of

$$\frac{l^3}{3} + \tilde{q}\frac{l^2}{2} - \tilde{u}_F l + \tilde{\psi}_F = 0 \tag{4.3.8}$$

(from (4.3.5)) where $\tilde{u}_F = -\tilde{\psi}_y$ at $y = -l$, and in both cases, $\tilde{\psi}_F$ must be retained in (4.3.5) when calculating $\tilde{\psi}_{max}$. If values for $\tilde{\psi}_F$ and $\tilde{u}_F$ are now taken from the numerical inversion and used in the above analysis, then excellent agreement results for the values of l and $\tilde{\psi}_{max}$.

To provide an estimate for $\tilde{\psi}_F$ which is independent of the numerical inversions, (1.1.2) can be re-written assuming ψ_{yy} can be neglected at this latitude:

$$F\psi_{zz} = q - y \tag{4.3.9}$$

where z is scaled by H and $F = (fL/NH)^2$ (constant stratification is assumed for simplicity). Solving this and integrating vertically, one obtains

$$\tilde{\psi}_F = -\frac{\tilde{q}^3}{6F}\left[\frac{1}{l^2} - 1\right] \approx -\frac{\tilde{q}^3}{6Fl^2} \tag{4.3.10}$$

So in the free slip case, $\tilde{\psi}_F = -\tilde{q}/6F$. Obviously, $\tilde{\psi}_F$ is dependent on the stratification, but reasonable values of F (~ 500) show $\tilde{\psi}_F$ to be of the same order as $\tilde{\psi}_{max}$, and therefore an important contributor to the transport. Further details of the partition of transport between fringe and core will be presented in the following section.

4.4 Inversions with a Linear (q, ψ) Relationship

The analysis above shows how the transport is controlled by the depth integrated q, and to a large extent, the stratification. It is useful for comparing the model with theory, but the inferred transports are weak compared with eddy resolving quasi-geostrophic models and with observations. The potential vorticity of the thermocline is not uniform, but exhibits a marked minimum just south of the Gulf Stream. Therefore, if the model is to represent the recirculation accurately, it must be forced with a variable upper layer q. In this section, following MN2, we consider the effect of enhanced upper forcing and bottom friction, as represented by the linear (q, ψ) relationships employed in section (3.3). We retain the notation from the 3 layer model, but for the continuous model, c_1 is applied where $z > -m$ and c_3 decays exponentially upwards from the bottom with a height scale of 500 m. Negative values are used for c_1 and positive values for c_3, as required by the conditions set out in section (3.3). An example of an inversion with non-zero $dq/d\psi$ is given in figure (4.7). The velocity and potential vorticity fields are shown; no slip conditions are imposed at $y = -l$ ($l = 225$ km); $c_1 = -400/L^2$; $c_3 = |c_1| \exp[(z + H)/500]$ and the transport is 41 Sv.

Figure (4.8) shows the dependence of the transport on c_1 and c_3. The transport has been split into two components: a purely baroclinic part, returned in the fringe (south of $y = -l$) and supplied by the surface intensified eastward jet; and the rest of the transport, returned within the core (north of $y = -l$) and almost exclusively barotropic in nature for all inversions carried out. Transport is plotted against the cube of the maximum magnitude of q in the upper layer. The linear dependence predicted in section (4.3) is still broadly adhered to. A value of $|q|^3_{max} = 1$ obviously corresponds to $c_1 = 0$, and incremental changes in c_1 are denoted by tick marks on the curve, illustrating a rapid increase in transport as c_1 is increased. Indeed an upper limit on c_1 occurs as predicted in section (3.3c). As c_1 approaches a value of about $1200/L^2$, the matrix constructed from grid point 'molecules' loses diagonal dominance and the inverter fails. It can be seen immediately that the barotropic component, excited when the bowl hits the bottom, is a major contributor to the transport of the gyre. In general, as the magnitude of c_1 is increased, the proportion of the transport carried by the core also increases, because it becomes both wider and more intense.

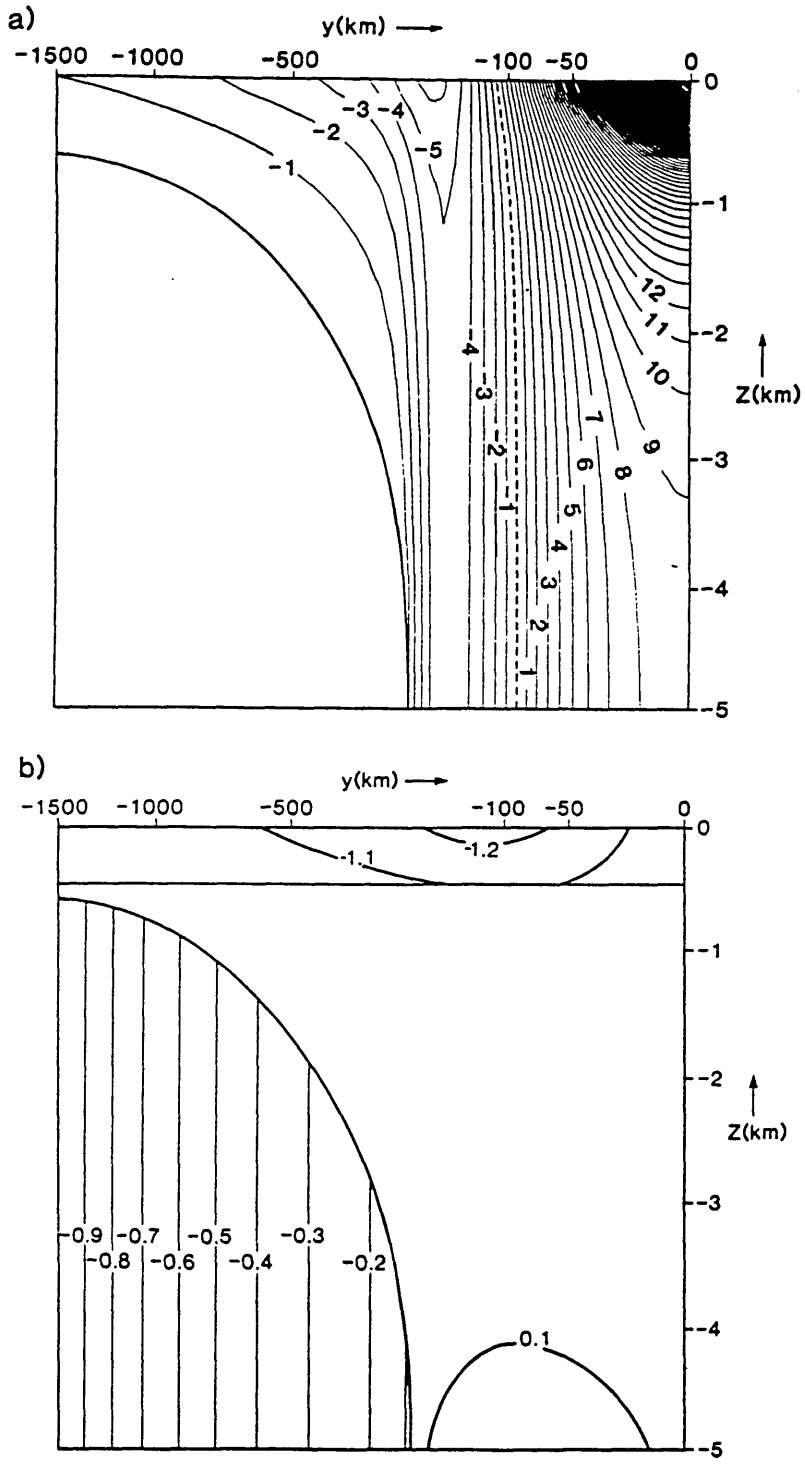

Figure 4.7: As figure (4.5) (a) and (b), but with $c_1 = -400/L^2$ and $c_3 = |c_1| \exp[(z + H)/500]$. Maximum eastward velocity is 93 cm s^{-1}. The core is 227 km wide. y coordinates stretched as in appendix A.

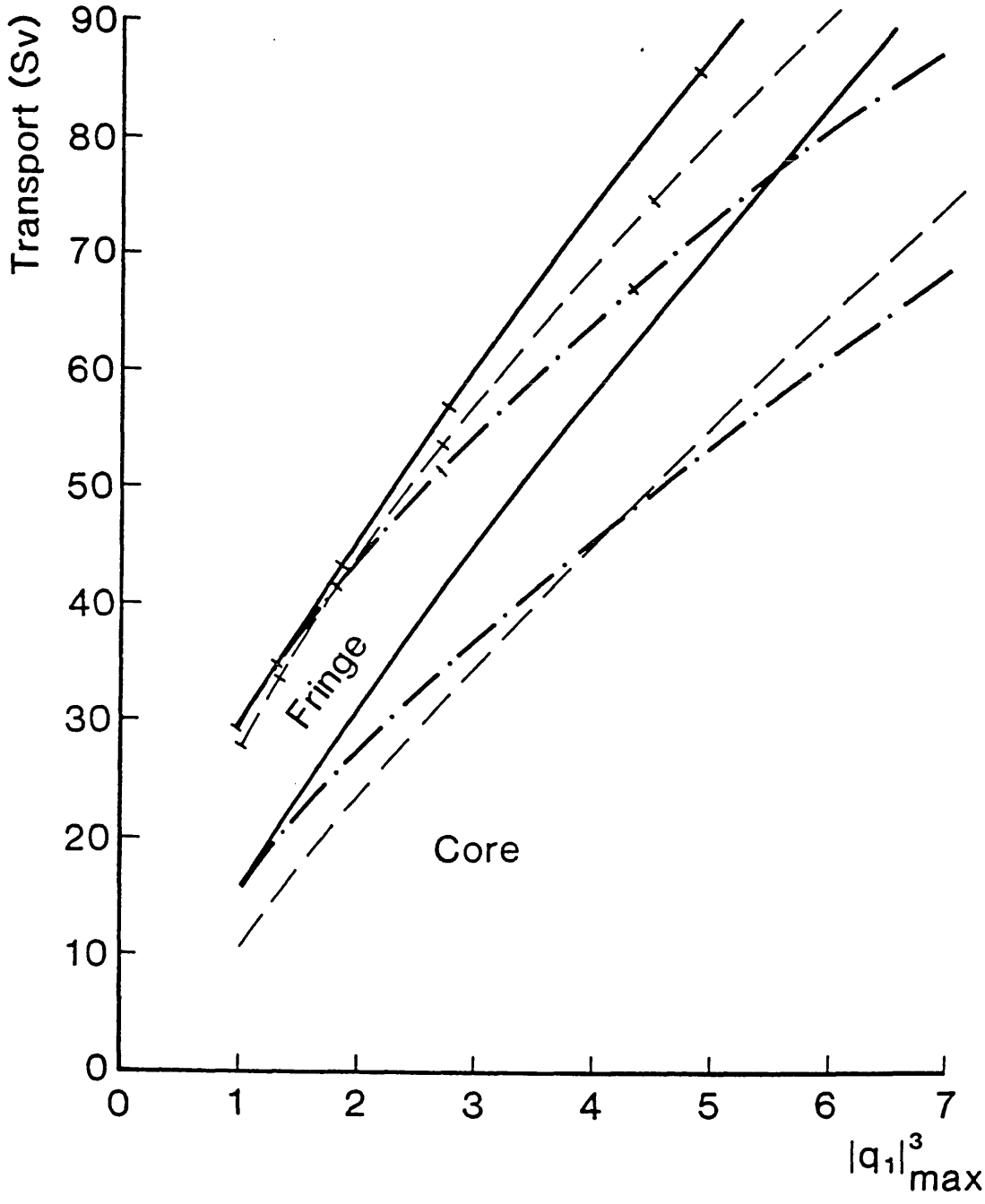

Figure 4.8: Dependence of the transport on c_1 and c_3. Transport (Sv) is plotted against the cube of the maximum magnitude of the upper q (in units of βL). The components of the transport carried by the fringe and core are shown for three models: no slip boundary condition, $c_3 = 0$ (solid lines); no slip boundary condition, $c_3 = |c_1| \exp[(z + H)/500]$ (dot-dashed lines); free slip boundary condition, $c_3 = 0$ (dashed lines). Tick marks denote increments of $200/L^2$ in the value of c_1.

Three curves are shown: two with a no slip southern boundary condition on the core and one with free slip. Of the former two, one has $c_3 = 0$ while the other has $c_3 = |c_1| \exp[(z + H)/500]$ (it is difficult to make an informed judgement on the relative magnitudes that c_1 and c_3 should have, but the eddy resolving model results (figure (3.6)) suggest that $|c_3|$ does not exceed $|c_1|$). It can be seen that non-zero c_3 causes the barotropic flow to become weaker. This is partly because the core has shrunk slightly and partly because the bottom flow has been retarded. But compared to the increase in transport effected by c_1, the decrease due to a corresponding value of c_3 is relatively small. Changing to a slippery southern boundary condition also has very little effect on the overall transport, even though the barotropic region is again less extensive in this case. However, the partition of transport between fringe and core is more sensitive to these considerations, with the fringe gaining importance if bottom friction or free slip boundary conditions are introduced.

If the model is to represent the total transport of the sub-tropical gyre (see section 3.3a), then the appropriate point to choose on the graph shown in figure (4.8) should correspond to a transport of ~ 75 Sv: the transport of one gyre in MNB's model. For this transport, c_1 takes a value of $\approx -800/L^2$, remarkably close to the value found by MNB when re-scaled to their units. There are, however, differences between the inversions and the eddy resolving model: The flow in the inversions is more barotropic for this level of transport, particularly in the no slip cases, which have a wider, stronger core. The free slip case is more directly comparable and has a more baroclinic transport with about one third of the flow returning within the fringe. It should also be noted that the eddy resolving model has a quite different upper layer potential vorticity profile, as seen in figure (3.8). The minimum in q is stronger, $-2\beta L$ as opposed to $-1.7\beta L$ in equivalent units and the southern boundary does not return smoothly to $q = -\beta L$, but has strong gradients of q. The similarity of values of c_1 for comparable transports arises from the combination of these two factors. Direct quantitative comparison of the two models is therefore more difficult than one might expect, especially with the transport so sensitively dependent on the depth integrated q. We shall return to a discussion of transport partitions in chapter 6, where a model is presented which can be compared more directly with oceanographic data.

4.5 Summary

In summary, the model has been used to illuminate the vertical structure of the recirculation. Despite the apparent dominance of vortex stretching, relative vorticity has been shown to be of importance, either in limiting the penetration depth or in controlling the depth integrated balance in the barotropic core. Both the overall transport of the gyre, and the partition of transport between barotropic and baroclinic components, has been shown to be dependent on the volume of low q water in the upper layer. For a gyre with realistic transport, the barotropic component is greater but not predominant. The effect of varying the boundary conditions at the southern edge of the barotropic recirculation has been investigated, and although it has little effect on the overall strength of the gyre, it has some impact on the latitudinal extent of the core and the proportion of the mass transport that it carries. It has also been shown that bottom friction has little effect on the transport compared to the considerable influence of imposing an upper (q, ψ) relationship of the same magnitude.

Chapter 5

Inversions with Anomalous Deep Potential Vorticity

5.1 Introduction

In the previous sections, the potential vorticity of the deep recirculating gyres has been assumed to be equal to the value of the planetary vorticity at the axis of the eastward jet. However, it is very unlikely that the entire deep homogeneous gyre should adhere strictly to this value of q. For example, it is well documented that the abyssal water of the western North Atlantic can have remote origins such as the Norwegian Sea (Hogg, 1983) with very different values of f. Its potential vorticity is also likely to be influenced by convective and thermohaline processes at distant sites. These considerations are not directly related to the position of the Gulf Stream.

It is difficult to infer a value for the abyssal potential vorticity from hydrographic sections, which is appropriate to our idealised quasi-geostrophic model, although observations suggest that the abyssal anomaly is positive (see figure (2.3b) where the deep potential vorticity contours tend to swing southwards from the axis of the Gulf Stream into the homogenised abyss). In this section we will examine the sensitivity of the above solutions to changes in the deep q. It will be seen that the structure of the solution can be modified considerably by allowing the value of deep q to depart from our reference value, and also that there is a limit on the strength of the abyssal q anomaly, above which solutions no longer exist.

The imposition of non-zero abyssal q upsets the symmetry which has so far been assumed between the cyclonic and anticyclonic recirculation gyres which flank the eastward jet to the north and south, forcing us to consider the two together. The effect on the strength and position of the two gyres, and of the eastward jet itself is considered in the following sections through a variety of models, ranging from simple calculations of bowl depth and barotropic mode (section 5.2) to solutions for the baroclinic structure in terms of a two layer model (section 5.3) and a continuous numerical inversion (section 5.4). These results are discussed in section 5.5.

5.2 Influence on the Extent and Position of Deep Gyres

Since the forcing of the sub-tropical/sub-polar gyre system is no longer antisymmetric, both gyres must now be considered together. Furthermore, it is no longer generally true that the latitude at which the upper layer streamfunction is equal to zero, marking the interface between the sub-tropical and sub-polar gyres, is at $y = 0$. However, if potential vorticity is to be conserved in steady, free flow, this gyre interface must coincide with the front in potential vorticity, where q changes from a value of $-\beta L$ (sub-tropical gyre) to βL (sub-polar gyre). This condition is therefore imposed in the models presented below: upper layer q is discontinuous and upper layer $\psi = 0$ at latitude $y = s$. The model formulation is shown in figure (5.1), with deep flow in the region $t < y < p$ and baroclinic fringes outside these latitudes.

The effect of a deep q anomaly on the shape of the bowl can be assessed by returning to equation (4.1.1). If a deep potential vorticity anomaly, $\gamma\beta L$ is assumed, where γ is a scaling factor, then (4.1.1) becomes

$$D = \frac{mL\left(\frac{|y-s|}{y-s} - \gamma\right) - \frac{1}{\beta}\int_{-D}^{0} \nabla^2\psi \, dz}{y - \gamma L} \tag{5.2.1}$$

For positive γ the bowl becomes deeper in the sub-polar gyre and shallower in the sub-tropical gyre. If relative vorticity is neglected, the sub-polar gyre now penetrates to infinite depth at $y = \gamma L$ and the solution for the depth of the bowl in the region $0 < y < \gamma L$ is not physically meaningful. However, relative vorticity cannot be neglected here, and furthermore, we expect the bowl to strike the bottom north of $y = \gamma L$ and south of $y = 0$.

To study in detail the nature of the solution in this region we can once again appeal

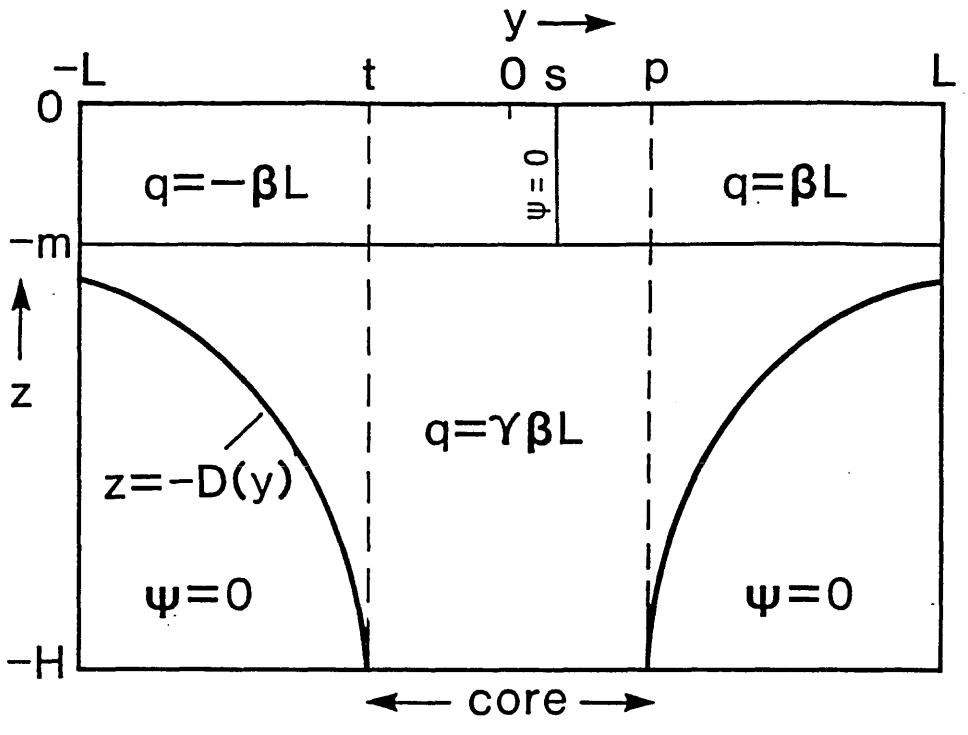

Figure 5.1: Model formulation for the double gyre problem with non-zero deep potential vorticity and variable upper gyre interface latitude. Boundary conditions as in figure (4.1).

to a depth integrated model of the barotropic core, which now consists of two counter rotating gyres. If the values of $\tilde{q}$ in the two gyres are given by

$$\begin{aligned} \tilde{q}_t &= -m + \gamma(1-m) \quad : t < y < s \\ \tilde{q}_p &= m + \gamma(1-m) \quad : s < y < p \end{aligned} \tag{5.2.2}$$

where m has now been scaled by H, and we set

$$\tilde{\psi} = \begin{cases} \tilde{\psi}_t \\ 0 \\ \tilde{\psi}_p \end{cases} \quad \text{at} \quad y = \begin{cases} t \\ s \\ p \end{cases} \tag{5.2.3}$$

then, matching $\tilde{\psi}_y$ at $y = s$ and introducing the coordinate change $y' = y - s$, the solution of (4.3.4) in the double gyre context yields

$$6(p'\tilde{\psi}_t - t'\tilde{\psi}_p) - 3(\tilde{q}_t t'^2 p' - \tilde{q}_p p'^2 t') + (t'^3 p' - p'^3 t') = 0 \tag{5.2.4}$$

It can be seen that a solution exists to (5.2.4) which is symmetrical about $y = s$, with $\tilde{\psi}_p = -\tilde{\psi}_t$, $t' = -p'$ and $s = \gamma(1-m)$. So imposing a positive value of γ is simply

equivalent to shifting coordinates so that the entire core region moves northwards. This result is in accord with equation (5.2.1), wherein the bowl becomes deeper to the north and shallower to the south. Note that the deep potential vorticity anomaly is still positive when measured relative to the latitude of the upper q discontinuity, i.e. $\gamma - s$ $(= \gamma m)$ is positive. Extra boundary conditions must be employed at t and p to allow further solutions to (5.2.4) to be found. These solutions have the core moving northwards by the same amount, but with a single gyre dominating the depth integrated flow with an eastward jet at $y = t$ or p. They do not correspond to any solutions found in the continuous model and are therefore not of interest.

The preceeding analysis provides an outline of the effect of introducing a deep q anomaly. The upper level front and gyre interface moves northwards so that potential vorticity may be conserved. The core region also migrates northwards while the baroclinic fringe becomes shallower in the sub-tropical gyre and deeper in the sub-polar gyre.

5.3 Solutions of the Two Layer Problem

The solutions for the barotropic mode within the core can, of course, tell us nothing about the vertical structure of the flow. They also rely on the restrictive assumption that $\tilde{\psi} = 0$ at $y = s$, when it is only the upper layer streamfunction which needs to be zero at this latitude.

To proceed to the baroclinic case, a two layer analytical model is examined. The solutions discussed below are essentially an extension of the solutions found by Cessi (1988) to the double gyre case with a non-zero value of q in the lower layer and an upper layer gyre interface at the variable latitude, $y = s$. Thus equations (3.3.1) become:

$$\begin{aligned} q_1 &= \beta y + \psi_{1yy} + L_\rho^{-2}(\psi_2 - \psi_1) = \tfrac{|y-s|}{y-s}\beta L \\ q_2 &= \beta y + \psi_{2yy} + \alpha L_\rho^{-2}(\psi_1 - \psi_2) = \gamma\beta L \qquad (t < y < p) \end{aligned} \tag{5.3.1a}$$

with boundary conditions

$$\begin{aligned} &\psi_1 = 0 \quad \text{at} \quad y = -L, s, L \\ &\psi_2 = 0 \quad \text{at} \quad y \le t \ \text{ and } \ y \ge p \\ &\psi_{2y} = 0 \quad \text{at} \quad y = t, p \ \ \text{(no slip)} \end{aligned} \tag{5.3.1b}$$

and continuity of

$$\psi_2,\ \psi_{1y},\ \psi_{2y} \quad \text{at} \quad y = s$$

The boundary conditions, (5.3.1b) are sufficient to solve (5.3.1a) and in addition, to determine the values of t, p and s. The equations are solved by projecting onto normal modes. Details of the method of solution are given in appendix B.

Consider first of all, the case when $\gamma = 0$ (considered in the previous chapter). We find that there are four solutions to the problem described by (5.3.1). One is trivial ($t = p = s$), one is symmetric ($t = -p$, $s = 0$) and two are asymmetric and complementary (in the sense that they map onto one another on rotation through half a circle about the origin). Figure (5.2) shows the streamfunction and potential vorticity for the symmetric solution and one of the asymmetric solutions. The streamfunction shows the familiar double gyre pattern in the symmetric case, but in the asymmetric cases, s is non zero and there is only one lower gyre which occupies the entire region $t < y < p$. In the solution shown, s is positive and the deep gyre is cyclonic. In the other solution (not shown) s is negative and the deep gyre is anticyclonic. The potential vorticity in the symmetric case shows the imposed uniform value in the region $t < y < p$ in layer 2, with discontinuities at t and p. Outside this region it returns almost linearly to the value of the planetary vorticity at the edges of the domain. In contrast, the asymmetric solution shows closed q_2 contours in the stagnant region south of $y = t$. Invoking the extremum principle, we should expect these closed contours of potential vorticity to be eliminated by eddies, and hence the solution to relax back to the symmetric state. We argue, therefore, that it is only the symmetric, 2 gyre solution which can be maintained physically.

Figure (5.3) shows the double gyre solution with $\gamma = 0.25$ and $\alpha = \frac{1}{2}$. With $\gamma > 0$, again we find that the front in q_1 shifts northwards (note that $\gamma - s$ is again positive). However, it can now be seen that although the sub-tropical gyre has expanded in the upper layer, the sub-polar gyre is dominant in layer 2, with the gyre interface moving southwards with depth. As before, there is one double gyre solution, and two single (deep) gyre solutions. As γ increases to about 0.39, the deep double gyre becomes a single cyclonic gyre which can be identified with the already existing single gyre solution. At this limit, the merged solution has no extremum in q_2. If γ is increased beyond this point, then the solution disappears immediately and no solution to the problem can be found. Evidently the continued northward shift of the homogeneous q region renders the extra boundary condition ($\psi_{2y} = 0$ at $y = t$) impossible to satisfy. For smaller values

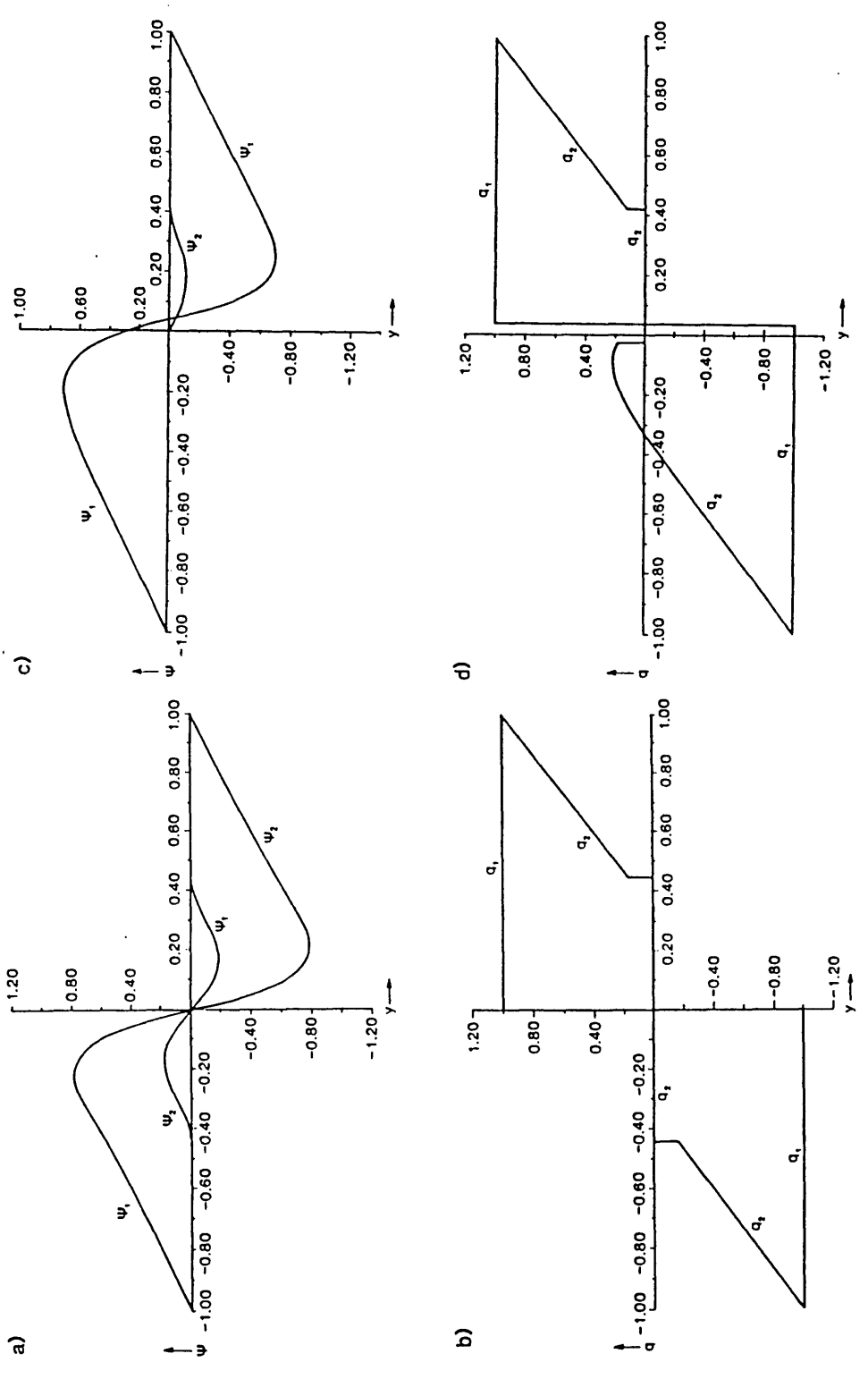

Figure 5.2: Solutions to the two layer double gyre problem with $\gamma = 0$, $\alpha = \frac{1}{2}$, $L/L_\rho = 10$. Streamfunction (in units of $\beta L_\rho^2 L$) and potential vorticity (in units of βL) are shown for the symmetric solution ((a) and (b)) and the asymmetric solution with a single cyclonic deep gyre ((c) and (d)).

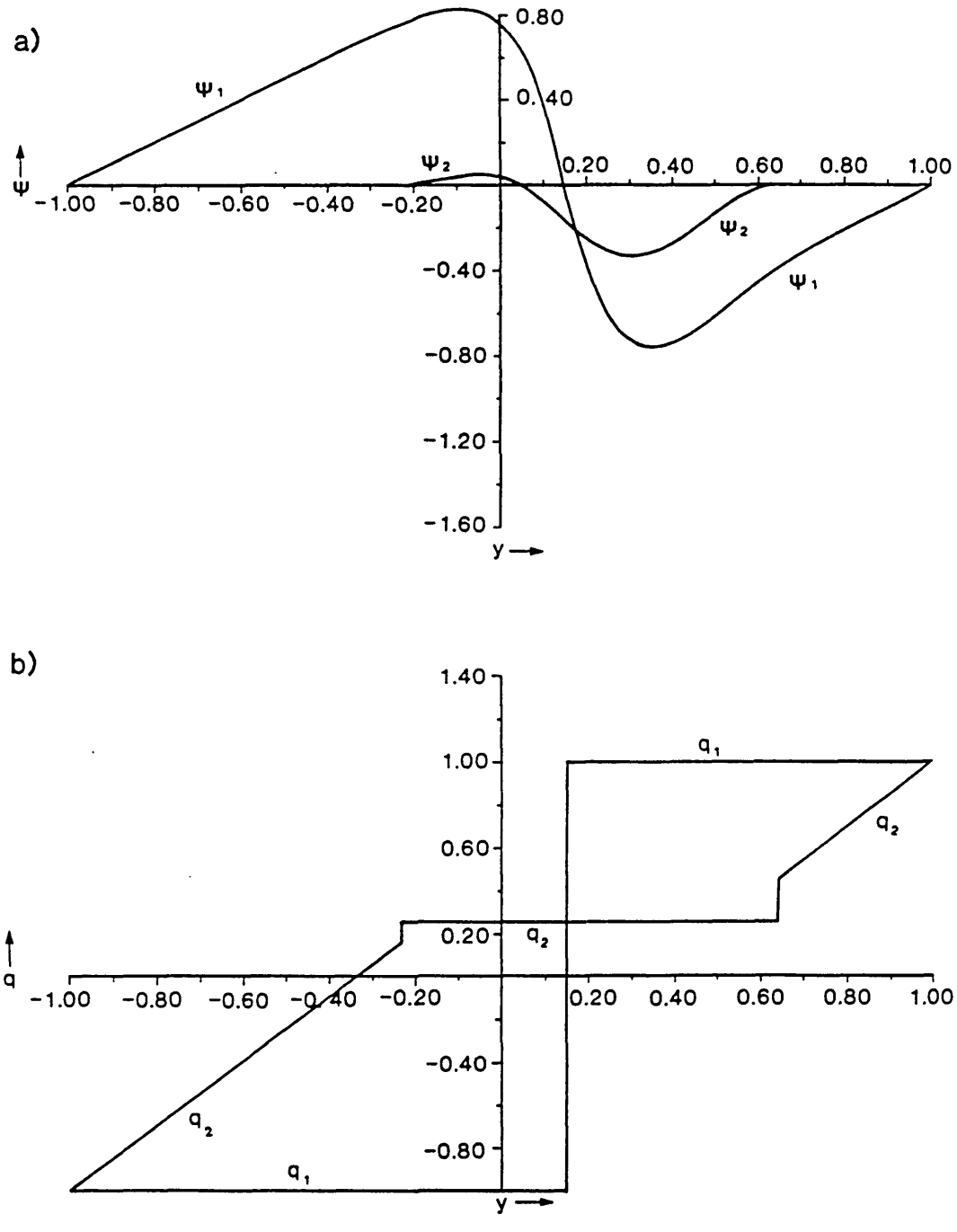

Figure 5.3: Double deep gyre solution corresponding to the solution shown in figure (5.2) (a) and (b) but with $\gamma = 0.25$.

of α (giving a deeper abyssal layer), the core region shrinks (as one would expect from the previous analysis) and the threshold value of γ is reduced: if $\alpha = \frac{1}{4}$, γ cannot exceed 0.026.

5.4 Solution Structure in the Numerical Inversions

The behaviour revealed above is also seen in the continuous model, in which a value of γ was imposed and the value of s gradually increased until precise correspondence between the upper layer q front and gyre interface, given by $\psi = 0$, was achieved. In fact the vertical structure of the flow was found to be very sensitive to γ, requiring this correspondence to be very accurate for consistent results. The results from a number of double gyre inversions show s and γ to be proportional as predicted in section (5.2). The constant of proportionality is now slightly less than $(1 - m)$ due to asymmetry between the baroclinic fringes. The values of t and p also increase linearly with γ. As s and γ are increased, the $\psi = 0$ contour, which marks the interface between the deep gyres, sweeps increasingly southwards with depth from the reference latitude, s.

Figure (5.4) shows an inversion in which the upper layer q discontinuity has been moved north to $s = 0.177$ (corresponding to a shift of 265 km). The value of γ required to ensure conservation of upper layer q was found to be 0.205. No slip boundary conditions have been applied on the bottom flow to define the position of the core and for this figure the y coordinates have not been stretched. It can be seen that the entire deep homogenised region has shifted northwards together with the upper layer gyre interface. The sub-tropical gyre has become larger and also shallower, while the sub-polar gyre is deeper, and it is this cyclonic gyre that dominates the bottom flow, with the $\psi = 0$ contour sweeping southwards with depth. At the bottom it has been displaced almost to the southern edge of the core. This corresponds to the baroclinic structure seen in the two layer model result of figure (5.3).

As γ is increased to about 0.225, the latitude where $\psi = 0$, between the two bottom gyres, becomes coincident with the southern extent of the bottom flow, and only one gyre remains. For higher values of s and γ, it becomes impossible to satisfy whatever additional boundary conditions one chooses, in order to specify this latitude. The horizontal iteration for the latitude at which the bowl strikes the bottom fails, and the southern

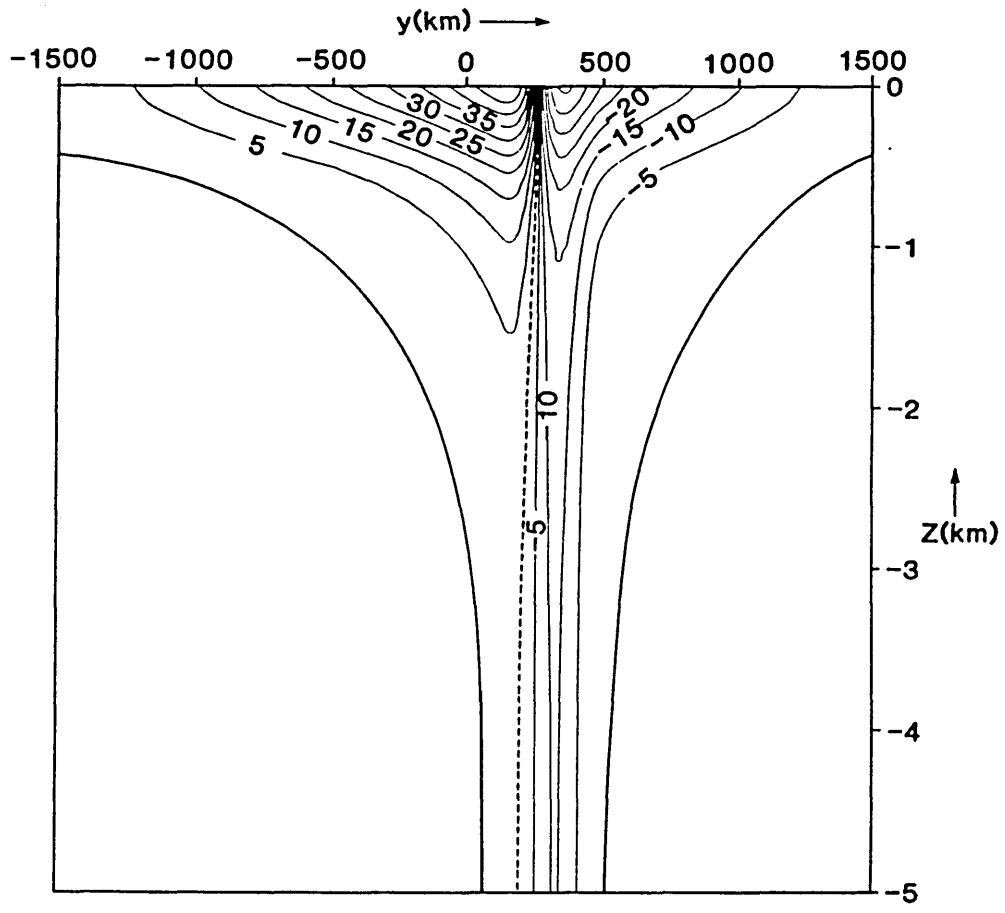

Figure 5.4: Streamfunction, ψ, (in units of βL^3) from a double gyre inversion with a deep q anomaly: $\gamma = 0.205$; $s = 0.177$ (= 265 km); $c_1 = c_3 = 0$; no slip lateral boundary conditions are applied to the bottom flow and the widths of the sub-polar and sub-tropical gyres are 330 km and 65 km respectively at the bottom. y coordinates are not stretched.

extent of the core cannot be determined. This is analogous to the response of the two layer model to increasing γ, where the solution for layer 2 reached a single gyre state and then disappeared.

5.5 Discussion

The above analysis reveals that one can expect the strength, sense and position of the abyssal recirculation to show considerable dependence not only on the surface forcing, but also on the value assumed for the deep potential vorticity. If the perturbation is positive, as implied by the observations, then the upper level gyre interface, together with the front in potential vorticity must migrate northwards. The deep flow region follows the northward shift, but the cyclonic gyre becomes stronger and more extensive than the anticyclonic gyre at depth. This result is in agreement with the abyssal recirculation scheme described in section (2.3) (see Hogg, 1983) in which the sub-polar gyre is dominant at depth.

The northward shift of the front in q can be explained in terms of a global integral constraint. If (1.1.2) is integrated over the domain of the model, we obtain

$$\int (q - \beta y)\, dA \simeq m\Delta\bar{u} \tag{5.5.1}$$

where $\Delta\bar{u}$ is the difference between the average surface layer velocities at $y = L, -L$, the only latitudes where we do not have Neumann boundary conditions. If a positive deep q anomaly is introduced, then there must be an accompanying northward shift of the upper level discontinuity in order to preserve the right hand side of (5.5.1) at a physical value. If there were no northward shift, an anomaly of $\gamma \sim 0.1$ would require this term to be orders of magnitude too large. It is clear from (5.5.1) that the northward shift in the front is dependent on the fact that the boundaries of the upper level gyres are fixed at $y = L, -L$. It could be argued that this assumption is artificial and that the boundaries of the domain should also be determined by application of further boundary conditions. This would, of course, render the problem trivial, simply shifting the origin to $y = \gamma L$. A more reasonable alternative would be to assume that the position of the eastward jet is prescribed at a fixed latitude, and allowing the domain to mutate to accommodate (5.5.1). In terms of the baroclinic structure of the flow, this option is probably equivalent to the

one pursued above.

The southward migration of the axis of the eastward jet with depth is also consistent with a positive deep q anomaly. The slope of a ψ contour is given by

$$\left(\frac{dz}{dy}\right)_{\psi\, const} = -\frac{\psi_y}{\psi_z} \tag{5.5.2}$$

and if the abyssal gyre interface is to slope southwards with depth, this quantity must be positive for the zero ψ contour. Now in the deep regions of the core, the vortex stretching term in (1.1.2) is greater in magnitude than the relative vorticity (see figure (4.5)) and will therefore have the same sign as $q - \beta y$. Since the bottom boundary condition is $\psi_z = 0$, ψ_z will also have this sign. Therefore, provided the flow is eastward, a positive deep q anomaly (relative to the latitude, s) is likely to induce a southward slope of the zero ψ contour with depth.

Finally, it is significant that in the case where $\gamma \neq 0$, solutions can only be found when the zero ψ contour hits the bottom. As γ is increased, the southern edge of the core moves northwards and the sub-tropical gyre becomes smaller. At a critical value of γ, the zero ψ contour hits the bottom at the southern edge of the core. For larger values of γ there is no solution. This is because it is impossible for the zero ψ contour to intersect the bowl south of $y = t$. In general, a zero ψ contour cannot strike a free boundary (a zero streamline on which the first normal derivative of the streamfunction is zero) except at a point where the forcing changes sign along that boundary. This result is proved by means of a Taylor expansion for ψ about a point on the free boundary (see Cessi, 1987): Consider Poisson's equation

$$Q = \nabla^2\psi \tag{5.5.3}$$

in the vicinity of a free boundary, on which

$$\psi_0 = 0 \qquad \frac{\partial^k \psi_0}{\partial s^k} = 0 \qquad \frac{\partial \psi_0}{\partial n} = 0 \tag{5.5.4}$$

where subscript 0 denotes a value on the boundary, s and n are coordinates along and normal to the boundary and k is any integer. Under conditions (5.5.4), the value of ψ at a distance δ from the boundary, ψ_δ, is given by a second order Taylor expansion about ψ_0 as

$$\psi_\delta = \frac{\delta^2}{2}\frac{\partial^2 \psi_0}{\partial n^2} \tag{5.5.5}$$

and

$$\frac{\partial^2\psi_0}{\partial n^2} = \frac{\nabla^2\psi_0}{|\nabla n|^2} \tag{5.5.6}$$

so

$$\psi_\delta = \frac{\delta^2 Q}{2|\nabla n|^2} \tag{5.5.7}$$

therefore ψ can only change sign near to the free boundary if Q also changes sign. It follows that the only latitude at which the $\psi = 0$ contour is allowed to meet the bowl is at $y = \gamma L$, where $q - \beta y$ changes sign. However if this contour slopes southward from $y = s$, and $s < \gamma L$, the above condition cannot be satisfied. In the case where $\gamma = 0$, the $\psi = 0$ contour may strike the bowl at $y = 0$, but if the abyssal potential vorticity is non-zero, the bowl cannot bottom out and the flow in both gyres must extend to the bottom.

It appears, therefore, that the symmetrical sub-polar / sub-tropical gyre system, in which the bowl bottoms out, is a singular case, for which asymmetries in the potential vorticity field cannot be supported. However, if the homogenised region extends to the bottom, the model is more robust, and can produce realistic asymmetric solutions.

In reality, bottom currents are observed in the recirculation regions of both the Atlantic and Pacific oceans. In the Pacific the bottom currents do not appear to relate systematically to the flow above, and probably owe their existence to processes not addressed in our simple model. The bottom currents in the Atlantic, on the other hand, appear to have some qualitative agreement with the above solutions, with a dominant cyclonic gyre at depth (see figure (2.6)). The explanation offered above depends on the idea of positive potential vorticity anomalies being transported to the region from distant sites at least in the creation if not the maintenance of the steady state described by the model. The larger scale abyssal flow is certainly capable of this (see McDowell, Rhines and Keffer, 1982) and even though the process of potential vorticity injection into gyres which circulate within closed potential vorticity contours can not be simulated in a steady state model, it should not be ruled out.

An alternative explanation of the deep cyclonic flow is given by Hogg and Stommel (1985), who model the abyssal recirculation in terms of uniform potential vorticity flow beneath a thermocline which surfaces. Their abyssal layer becomes thinner to the south and to the north of the upper layer outcrop because of the deep expression of the thermocline and a shoaling bottom to the north which enhances the beta effect. To ensure

mass conservation in this abyssal layer, they deduce that the relative vorticity must have a positive maximum below the outcrop, and that the deep flow must be cyclonic. Thus their deep potential vorticity anomaly must also be positive. Neglected by Hogg and Stommel is the possible importance of deep density surfaces intersecting the continental rise, allowing more freedom in the determination of the relative vorticity directly beneath the stream. The alternative offered in this chapter places more emphasis on the possible values that the deep potential vorticity may take, rather than on the gross features of the vertical extent of the deep water. The conclusion of deep cyclonic flow is still reached if the deep potential vorticity is allowed to exceed its reference value slightly.

Chapter 6

A Geostrophic Model in Isentropic Coordinates

6.1 Introduction

The results shown in chapters 4 and 5 are difficult to compare with observational data for at least two reasons:

1) The models are forced by imposing derivative quantities such as potential vorticity and (q, ψ) relationships. While this is desirable as an alternative to the Sverdrup constraint, which is unrealistic in the recirculation region, this approach to driving the model is somewhat abstract if sensitivity studies are to be usefully compared with observations.

2) The quasi-geostrophic framework places severe restrictions on the realism of the model and interpretation of the results. The linearisation of dynamic density perturbations and the accompanying lack of horizontal variations in stratification limits how representative the fields of ρ and q are.

These problems are alleviated in this chapter by adopting a less restrictive equation set. The Ertel potential vorticity (equation (1.1.1)) is inverted assuming geostrophic balance. Density is used as a vertical coordinate, allowing the forcing to enter the model by way of prescribed upper and lower boundary conditions. In particular, the top boundary condition can now be chosen as the depression of the main thermocline, a quantity which can be read directly from hydrographic sections. The Sverdrup constraint is, of course, still discarded.

In section 6.2 the model is described. Some preliminary analysis indicative of its behaviour is given in section 6.3. Numerical results are presented in section 6.4 and the effect of changing the bottom boundary condition is considered in section 6.5. In section 6.6 an inversion is presented with a thermocline shape based on hydrographic data. A brief summary is given in section 6.7.

6.2 The Model

(a) The Equations

The model described below represents an incompressible ocean which is in geostrophic and hydrostatic balance. The assumption of geostrophy, while not strictly valid everywhere in a Fofonoff gyre, is exactly satisfied on the section line considered and can be used in a diagnostic sense throughout the region since the Rossby number is small everywhere. The Ertel potential vorticity, Q, is therefore inverted for the Montgomery potential, M, the streamfunction for the geostrophic flow on a density surface, defined as

$$M = p + \rho g z \tag{6.2.1}$$

(see for example Starr, 1945). The geostrophic velocity is given by

$$\mathbf{v} = \frac{1}{\rho_0 f_0}\hat{\mathbf{k}}_\wedge \nabla M \tag{6.2.2}$$

and the hydrostatic equation can be written in terms of M, thus

$$\frac{\partial M}{\partial \rho} = gz \tag{6.2.3}$$

For our purposes, Q can be defined as the positive quantity,

$$Q = -\frac{f+\xi}{\frac{\partial z}{\partial \rho}} \tag{6.2.4}$$

where ξ is the relative vorticity in isopycnal coordinates, evaluated geostrophically. Using equations (6.2.2) and (6.2.3) this leads to the elliptic equation,

$$f + \frac{1}{\rho_0 f_0}\nabla^2 M + \frac{Q}{g}\frac{\partial^2 M}{\partial \rho^2} = 0 \tag{6.2.5}$$

It is useful to separate M into the dynamically passive and active components, M_0 and M_1. M_0 is associated with the background stratification of the resting fluid. Thus its horizontal

derivatives are zero and its derivative with respect to density gives the reference depth of an isopycnal, z_0, via equation (6.2.3). Horizontal derivatives of M_1 provide the velocity through (6.2.2) and its density derivative represents the perturbation of an isopycnal from its reference depth due to the motion field. Unlike the quasi-geostrophic equations, this perturbation need not be small. Equation (6.2.5) can now be set purely in terms of the dynamical variable, M_1.

$$-\frac{Q}{g}\left(\frac{\partial^2 M_1}{\partial \rho^2}+g\frac{\partial z_0}{\partial \rho}\right)=f+\frac{1}{\rho_0 f_0}\nabla^2 M_1 \tag{6.2.6}$$

where $\partial z_0/\partial \rho$ is a known function of ρ.

We shall now introduce the following scalings:

$$\begin{aligned} y &= y'L \\ \rho &= \rho'|\Delta\rho| \\ z &= z'H \\ M &= M'gH|\Delta\rho| \\ Q &= Q'\tfrac{f_0|\Delta\rho|}{H} \end{aligned} \tag{6.2.7}$$

The latitudinal extent, depth and top to bottom density difference of the model are given by L, H and $\Delta\rho$ respectively. Dropping primes and the subscript, 1, and considering a meridional section where zonal derivatives are neglected as before, equation (6.2.6) now becomes the model equation

$$sQ - f/f_0 = QM_{\rho\rho} + \lambda^2 M_{yy} \tag{6.2.8}$$

where s is a non-dimensional stratification parameter defined as

$$s = -\frac{|\Delta\rho|}{H}\frac{\partial z_0}{\partial \rho} \tag{6.2.9}$$

If we have uniform stratification then s is unity. λ is the non-dimensional depth average Rossby radius,

$$\lambda = \sqrt{g'H}/f_0 L \tag{6.2.10}$$

The beta plane approximation is again used to represent f. Given suitable boundary conditions described below, (6.2.8) can be inverted for M.

(b) Model Domain and Boundary Conditions

Figure (6.1) shows the specification of the model domain and boundary conditions first in physical space, and then in non-dimensional density coordinates. The uppermost density contour is defined as $\rho = 0$ and is identified with the main thermocline. All the flow in the model is therefore in the deep homogeneous Q region, beneath the mode water layer. Thus the flow above the main thermocline is not represented explicitly, rather the depth of the thermocline is used as a top boundary condition to drive the unventilated flow beneath. This enters through a Neumann boundary condition, $\partial M/\partial \rho = z_T$, the perturbation of the thermocline from its reference depth. The bottom is assumed to be a flat isopycnal with $\partial M/\partial \rho = 0$. Alternatives to this bottom boundary condition are explored in section 6.5.

To ensure mass conservation on each density surface, the side boundaries are closed streamlines with $M = 0$. Within the flow region, Q is assumed to homogenise along isopycnals to the reference value set at $y = 0$. Thus $Q(y, \rho)$ is specified as equal to $1/s(\rho)$ in this region. The southern edge of the region, the bowl of the circulation, is again determined as a free boundary on which isopycnals return to their reference depths, and at which the velocity disappears. Thus M, M_ρ and M_y are all zero along the length of this boundary with no slip at the southern edge of the bottom flow in the core (at $y = -l$). This boundary condition is used in all the inversions presented in this chapter. A simple iteration scheme is employed to find the position of the bowl, making use of the fact that the sign of M above the bowl is known. Details are given in appendix A. The y coordinate stretching is retained in order to enhance the resolution in the core (see appendix A).

(c) Background Stratification

The stratification parameter, $s(\rho)$, is equal to $\bar{N}^2/N^2(\rho)$, where $\bar{N}^2$ is the depth average value of N^2. In section 4.1, the hyperbolic form, (4.1.2), is chosen to represent realistic variations of N^2 with z. To achieve the same qualitative results in ρ coordinates, a linear expression can be chosen for $s(\rho)$. This expression must, however, satisfy the following constraint: The reference depth of an isopycnal is given by

$$z_0 = -\int_0^\rho s d\rho \tag{6.2.11}$$

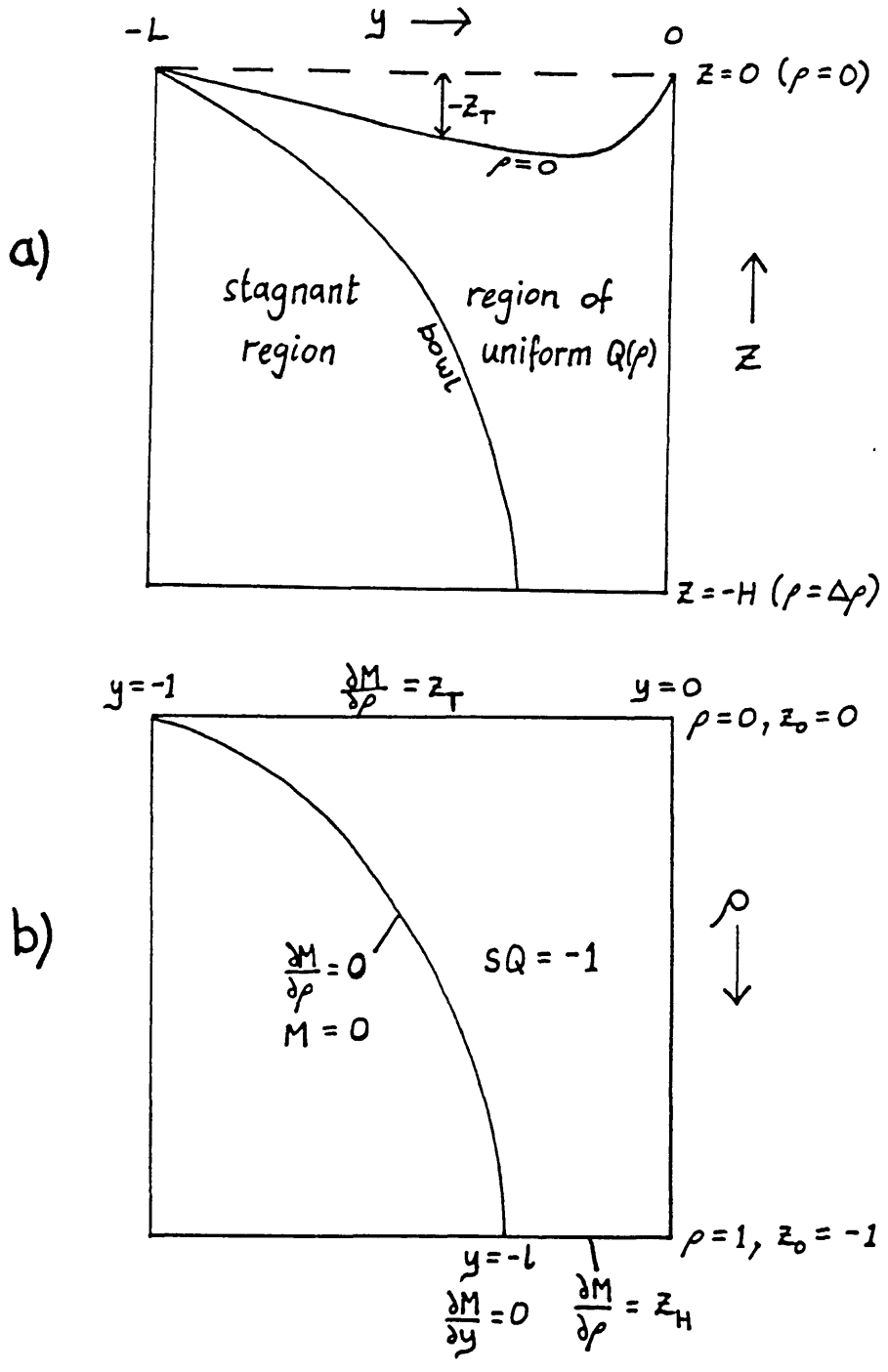

Figure 6.1: The formulation of the isopycnal model (a) with depth as the ordinate with the physical dimensions shown and (b) in the model's coordinates showing non-dimensional values and boundary conditions.

Since $z_0 = -1$ at $\rho = 1$, it follows that

$$\int_0^1 s(\rho)d\rho = 1 \tag{6.2.12}$$

The linear expression for s which satisfies (6.2.12) is

$$s = 2\rho(1 - s_0) + s_0 \tag{6.2.13}$$

where s_0 is the value of s chosen at the thermocline ($\rho = 0$).

Thus the stratification of the model is controlled by the choice of $|\Delta\rho|$ and s_0. The former controls the overall intensity while the latter controls the sharpness of its variation. The effect of varying both will be discussed below, but for realistic inversions, values of $|\Delta\rho| = 1.5\text{kg m}^{-3}$ and $s_0 = 0.05$ were chosen, implying $N^2 = 5.9 \times 10^{-5}$ s^{-2} at the thermocline and 1.5×10^{-6} s^{-2} at the bottom.

6.3 Depth Penetration and Baroclinic Flow

(a) The Depth of the Bowl

As with the quasi-geostrophic model, it is possible to solve analytically for the depth of the bowl provided relative vorticity can be neglected. If this is done, then equation (6.2.8) becomes

$$sQ - f/f_0 = QM_{\rho\rho} \tag{6.3.1}$$

setting Q to its reference value of $1/s$, we obtain

$$s = \frac{M_{\rho\rho}}{1 - f/f_0} \tag{6.3.2}$$

Integrating with respect to ρ from the thermocline to the bowl and using (6.2.11) then yields

$$z_{0B} = \frac{z_T}{1 - f/f_0} \tag{6.3.3}$$

z_{0B} is the depth of the bowl below the reference depth of the thermocline (at which $z_0 = 0$) and z_T is the perturbation of the thermocline from its reference depth. Alternative derivations of (6.3.3) are given by Nurser (1988) and MN2.

There are three things to note about equation (6.3.3):

1) If relative vorticity is neglected, we see again that the depth of the bowl is independent of the form and magnitude of the stratification used.

2) It is necessary that the thermocline should return to its reference depth at the latitude from which the value of Q has been set, i.e. $z_T = 0$ where $f = f_0$. Otherwise z_{0B} will become positive in some region. This is equivalent to the problem of non-zero deep q dealt with in chapter 5, where it was found that the upper level front needed to shift northwards to accommodate a positive deep q anomaly.

3) The presence of relative vorticity is now to a large extent implicit in this model. It is only the relative vorticity of the deep flow that has been neglected in (6.3.3) and which could conceivably modify point (2). The important contribution of relative vorticity above the thermocline is now represented in the model through the form chosen for $z_T(y)$. Indeed, it is inevitable that the bowl will bottom out at some depth even from the simple result above, provided the thermocline returns to its reference depth at $y = 0$. This is to be contrasted with the hyperbolic plunge of the previous analysis. The depth at which the bowl bottoms out will in general depend on the shape and maximum depth perturbation of the thermocline. A rough estimate of the flow penetration can be gained by considering a thermocline which returns linearly to its reference depth from a maximum depression, h_T over a scale distance for the eastward jet, δy. In this case, according to (6.3.3) the bowl will bottom out at a depth $h_T/\beta'\delta y$ where $\beta' = \beta L/f_0$. This number can be close to unity for reasonable parameters, and the influence of relative vorticity in the deep flow will be to reduce this penetration further. So again it seems possible that flow regions with uniform potential vorticity can indeed be isolated from the ocean floor in oceanographic contexts. However, in most of the numerical inversions shown below the the flow reaches the bottom, allowing a strong barotropic component to develop.

(b) The Deep Baroclinic Flow

In order to assess the strength of the baroclinic, sub-thermocline flow, (6.3.1) can be solved for M in regions where relative vorticity is negligible. In the case of uniform stratification, (6.3.1) reduces to

$$M_{\rho\rho} = G(y) \tag{6.3.4}$$

where $G = 1 - f/f_0$ or on a beta plane, $G = -\beta' y$. Applying the boundary conditions: $M_\rho = z_T$ at $\rho = 0$ and $M = M_\rho = 0$ at $\rho = \rho_B$, the solution to (6.3.4) is

$$M = \frac{G}{2}(\rho - \rho_B)^2 \tag{6.3.5}$$

where the density at the bowl is given by

$$\rho_B = -\frac{z_T}{G} \tag{6.3.6}$$

Since the stratification is uniform, (6.3.6) is simply a rescaling of (6.3.3). In general, ρ_B is a function of the strength and form of the stratification although z_{0B} is not. To find the sub-thermocline fringe transport, (6.3.5) is integrated from the thermocline to the bowl to give

$$\int_0^{\rho_B} M d\rho = \frac{|z_T|^3}{6G^2} \tag{6.3.7}$$

If this equation is fully redimensionalised, we obtain an expression for the mass transport, in Sverdrups, of the flow in the fringe, to the south of the latitude, y:

$$\text{Transport (Sv)} = 10^{-6}\frac{g f_0}{6\rho_0\beta^2}\frac{|\Delta\rho|}{H}\frac{|z_T|^3}{y^2} \tag{6.3.8}$$

Comparing (6.3.8) with (4.3.10) it can be seen that the fringe transport is still dependent on the stratification, and on the cube of a term which represents the surface forcing, in this case, z_T. Quantitative details of model transports are given in the next section.

Having established the role of the average stratification in determining the model's baroclinic transport, it remains to be seen whether the depth dependence of the stratification can also have some influence. To provide some guidance in this matter, it is convenient to consider depth dependent flow in a region where the flow reaches the bottom. If (6.3.4) is solved with $M_\rho = z_T$ at $\rho = 0$ and $M = 0$ at $\rho = 1$, and then integrated, we obtain

$$\int_0^1 M d\rho = -\left(\frac{G}{3} + \frac{z_T}{2}\right) \tag{6.3.9}$$

If, however, the stratification is a function of depth, (6.3.4) becomes

$$M_{\rho\rho} = s(\rho)G(y) \tag{6.3.10}$$

Substituting from (6.2.13) for s and using the same boundary conditions, after some simple manipulation we arrive at the following expression for the mass transport:

$$\int_0^1 sM d\rho = -\left[\frac{G}{5}\left\{1 + \frac{s_0}{2} + \frac{s_0^2}{6}\right\} + \frac{z_T}{3}\left\{1 + \frac{s_0}{2}\right\}\right] \tag{6.3.11}$$

Note that the integral has been weighted such that it is now evaluated with respect to z_0, to give a true estimate of the mass transport. For uniform stratification ($s_0 = 1$),

(6.3.11) reduces to (6.3.9) but as s_0 becomes smaller, representing a sharp decrease in stratification with depth, the depth dependent transport is diminished. In practice, for many of the inversions presented below, the baroclinic part of the flow is swamped by the strong depth independent component and varying s_0 actually makes very little difference to the overall transport of the model, but the above analysis suggests that it can have an order one effect on the baroclinic part of the flow.

(c) The Flow Above the Thermocline

The flow within the mode water layer is dynamically important, as illustrated in section (a) above, and it is a deficiency of the model that this flow is not represented explicitly. It is also to be expected that the mass transport above the thermocline should make a significant contribution to the overall model transport. It is possible to make an estimate of this component of the transport from our knowledge of the velocity and thermocline slope at the top boundary of the model.

From thermal wind balance, we can write

$$\frac{\partial u}{\partial z} = -\frac{g}{\rho_0 f_0}\frac{\partial \rho}{\partial z}\left(\frac{dz_T}{dy}\right) \tag{6.3.12}$$

Assuming a uniform stratification above the thermocline, and integrating from the thermocline to to a depth, z, we obtain

$$u(z) - u_T = \frac{N^2}{f_0}\left(\frac{dz_T}{dy}\right)[z - (z_{0T} + z_T)] \tag{6.3.13}$$

where u_T is the zonal velocity at the thermocline, z_{0T} is the reference depth of the thermocline and z_T the perturbation. Integrating again, we obtain the mass transport per unit length,

$$\int_{z_{0T}+z_T}^{0} u\,dz = \frac{N^2}{2f_0}\left(\frac{dz_T}{dy}\right)(z_{0T} + z_T)^2 + u_T(z_{0T} + z_T) \tag{6.3.14}$$

This is integrated numerically in the meridional direction to give an estimate of the transport above the model. A value of 1.6×10^{-5} s^{-2} is chosen for N^2 in this region.

6.4 Barotropic Flow and Mass Transport

(a) Solution for the Barotropic Mode

Judging from the inversions shown in chapter 4, it is to be expected that a major proportion of the flow will be carried in the depth independent component. To identify the important parameters which determine this component, the simple depth integral analysis of section 4.3(c) can be repeated for the new equation set.

Integration of (6.2.8) with respect to density from $\rho = 0$ to 1 leads to

$$\lambda^2 \tilde{M}_{yy} = z_T(y) - \beta' y \tag{6.4.1}$$

where $\tilde{}$ again denotes a depth average quantity and Q has again been set to its reference value. Note that in this case, the vortex stretching term does not disappear in the vertical integral but instead, forces the model through the upper boundary condition, $z_T(y)$, which remains to be specified. For analytical convenience we shall choose a linear ramp shape for the thermocline depression, with $z_T = 0$ at $y = -1$ and $z_T = -h_T$ at $y = 0$ (returning discontinuously to the reference depth at this latitude). Equation (6.4.1) can now be written

$$\lambda^2 \tilde{M}_{yy} = -(h_T + \beta')y - h_T \tag{6.4.2}$$

If it is assumed that all the mass transport is carried within the barotropic core (the validity of the analysis will be tested against numerical inversions below), the boundary conditions with no slip at the southern edge of the core are

$$\begin{aligned} \tilde{M} &= 0 \qquad \text{at} \quad y = 0 \\ \tilde{M} &= \tilde{M}_{yy} = 0 \quad \text{at} \quad y = -l \end{aligned} \tag{6.4.3}$$

and the solution to (6.4.2) is

$$\lambda^2 \tilde{M} = -(h_T + \beta')\frac{y^3}{6} - h_T \frac{y^2}{2} - \frac{3h_T^2}{8(h_T + \beta')} y \tag{6.4.4}$$

with

$$l = \frac{3h_T}{2(h_T + \beta')} \tag{6.4.5}$$

It is interesting to compare (6.4.5) with the expression for l given in (4.3.7). In the latter, l depends on $\tilde{q}$ and thus implicitly on the thickness of the mode water layer and on β. These dependencies arise from the assumption that $q = -\beta L$ everywhere above

the thermocline, resulting in a linear ramped thermocline depression. In (6.4.5), however, no assumptions have been made about the potential vorticity above the thermocline and the linear ramp has been imposed *a priori*. This results in a perhaps more intuitive role for β, with the core shrinking as it is increased. The core will, of course, still become larger if the thermocline depression is increased, up to a limit which violates the model assumptions.

Equation (6.4.4) can be differentiated to find the latitude at which $\tilde{M}$ is a maximum, and if this is substituted back into (6.4.4) the resulting expression for the mass transport is

$$\lambda^2 \tilde{M}_{max} = \frac{h_T^3}{12(h_T + \beta')^2} \tag{6.4.6}$$

To calculate the mass transport in Sverdrups, the right hand side of (6.4.6) must be multiplied by the factor, $10^{-6} f_0 L^2 H$. As before (equation (4.3.5)), the mass transport of the core is dependent on the cube of the surface forcing, subject to the same reinterpretation as discussed above for l. It is independent of both the strength and form of stratification used, although the problem becomes ill posed if λ is set to zero. Also, if λ gets too large, and/or h_T too small, the bowl is expected to bottom out as explained in the last section. Quantitative comparisons of (6.4.6) with numerical inversions will be presented in the next section.

(b) Inversions with a Linear Thermocline Depression

To facilitate comparison with the theory above, numerical inversions of (6.2.8) were carried out in which a linear ramp shape was chosen for the top boundary condition, $z_T(y)$. In these inversions, the thermocline returns to its reference depth over one grid point south of $y = 0$. Values of $L = 1500$ km, $H = 5$ km and $\Delta\rho = 1.5$ kg m^{-3} are used. Figures (6.2) (a) and (b) show the velocity field in density coordinates, and density contours in height coordinates respectively, from an inversion in which the thermocline was pushed down to a maximum depression, $h_T = 200$ m. The y coordinates are stretched as before (see appendix A) in figure (6.2a) but have been unstretched for the hydrographic section of figure (6.2b). The stratification is uniform so the potential vorticity is equal to 1 throughout the flow region. The broad features of the flow are the same as in the quasi-geostrophic inversions, but it should be remembered that this figure only shows

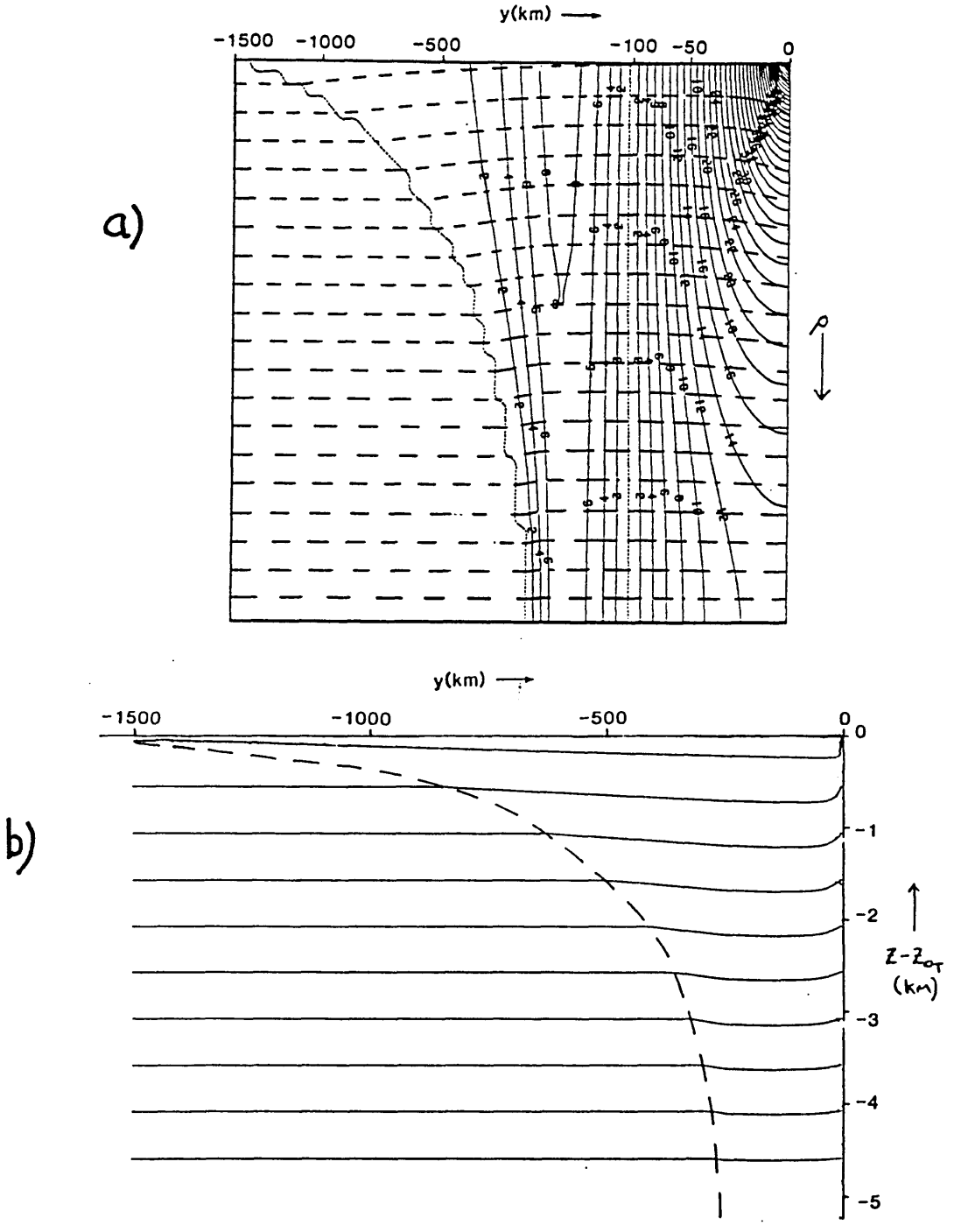

Figure 6.2: Results from an inversion with a linear ramped thermocline with a maximum depression of 200 m and uniform stratification. (a) Zonal velocity in cm s^{-1}. Density is the ordinate, varying from the value at the thermocline to this value plus $\Delta\rho$ at the bottom. Dashed lines indicate surfaces of constant depth. y coordinates are stretched as in appendix A. (b) Density contours with depth as the ordinate. The upper limit of the diagram is at the reference depth of the thermocline. y coordinates are not stretched. The bowl is indicated by a dashed line.

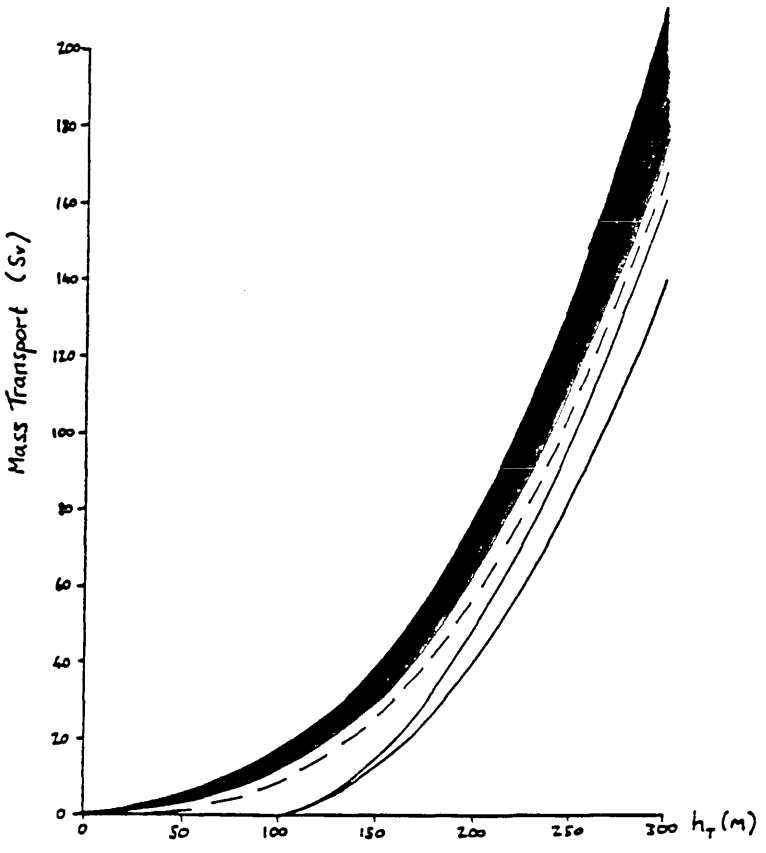

Figure 6.3: Mass transport plotted against maximum thermocline depression for the linear ramped thermocline. The shaded region represents the estimated transport above the thermocline. The lower curve is the depth independent transport beneath the thermocline and the next curve up is the sub-thermocline transport within the core. The total sub-thermocline transport (core and fringe) corresponds to the entire unshaded region. The dashed curve is the solution of (6.4.6).

the flow beneath the thermocline. The flow within the core is predominantly barotropic but a surface intensified eastward jet exists, returned mainly within the fringe. The sub-thermocline transport in this inversion is 61 Sv. The core transport, north of $y = -l$, is 47 Sv, of which 37 Sv is depth independent. The transport above the thermocline is estimated at 15 Sv, of which 4 Sv is due to the velocity shear (the first term on the right hand side of (6.3.14)). The core is 260 km wide and the maximum velocity in the jet is 84 cm s^{-1}. For this value of h_T, equation (6.4.6) predicts a mass transport of 57 Sv.

The full range of mass transport as a function of maximum thermocline depression, h_T, is shown in figure (6.3). Various curves show the different components of the sub-thermocline transport and the shaded region indicates the estimated transport above the

thermocline. The transport calculated from equation (6.4.6), appropriate to the depth independent flow, is included as a dashed line for comparison. It can immediately be seen that (6.4.6) provides a remarkably good estimate for the total transport. This is perhaps fortuitous for the region of the curve where the transport is less than about 40 Sv and the fringe transport is a large proportion of the total (the bowl actually bottoms out if h_T = 50m) but it is to be expected for the more strongly forced region when the core becomes dominant. It can also be seen from figure (6.3) that as the core becomes stronger (and wider), it starts to carry a larger proportion of the baroclinic transport and the sub-thermocline fringe transport becomes negligible. It should be noted, however, that the flow above the thermocline also makes a large contribution to the fringe transport.

(c) Inversions with a More Realistic Thermocline

In the interests of further realism, the above numerical experiments were repeated with a depth dependent stratification ($s_0 = 0.05$ in equation (6.2.13)) and a smooth, continuous thermocline depression, represented by the function,

$$z_T = h_T \sin \pi u \tag{6.4.7}$$

where u is the meridional coordinate of the stretched model grid, related to y by the expression given in appendix A. This means that the thermocline has its maximum depression, $z_T = -h_T$, in the middle of the model domain but to the north in real space (at $y = -0.2$) and results in a broader eastward jet (erring on the side of excess) and a slightly increased average thermocline depression.

Figures (6.4 a,b) show the velocity and hydrography from an inversion in which h_T = 220 m. The realistic stratification can be seen in figure (6.4b) together with the modified thermocline shape. This inversion transports 65 Sv of which 46 Sv is returned within the core and is almost completely depth independent. The estimated transport above the thermocline is 20 Sv, with 4 Sv due to the aforementioned shear component. The core is 310 km wide and the maximum velocity in the jet is now only 39 cm s^{-1}. The eastward jet is now more spread out due to the gentler rise in the thermocline. Figures (6.4) (c) (d) and (e) show further diagnostics from the model. Figure (6.4c) shows the potential vorticity, controlled by the background stratification in the flow region with $Q = 1/s$, and with sloping contours outside the flow region representing the beta effect. The terms

a)

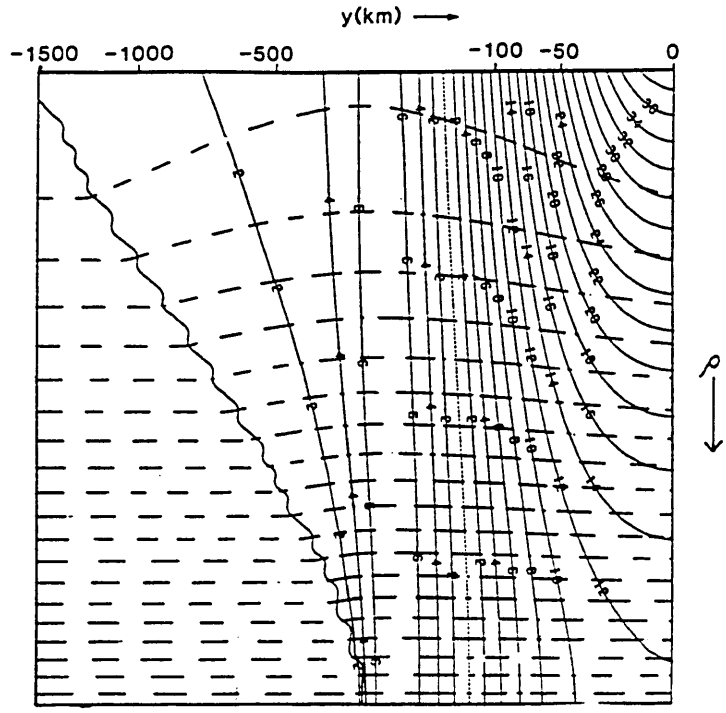

b)

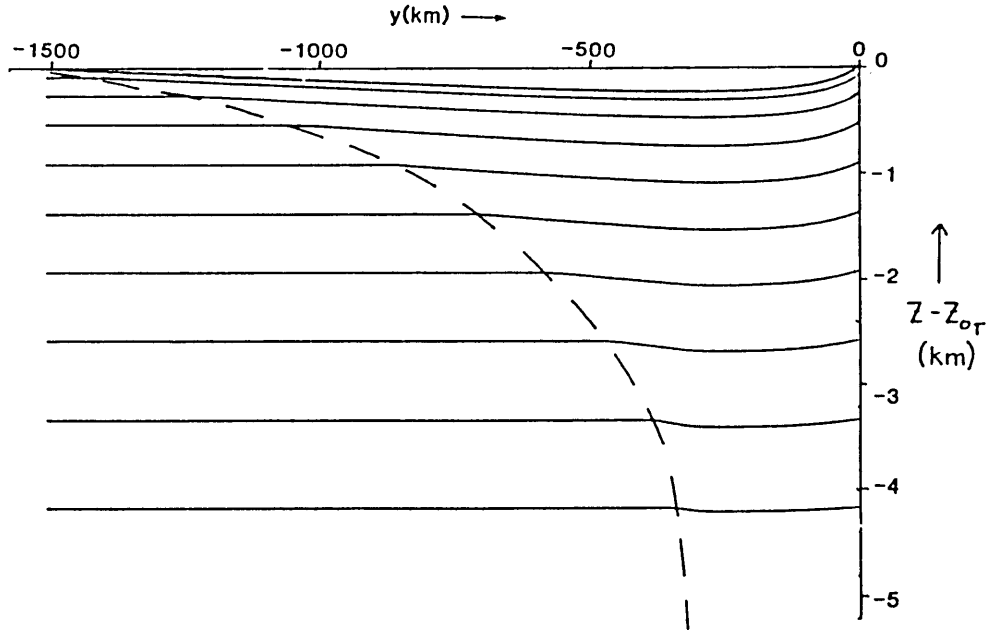

c)

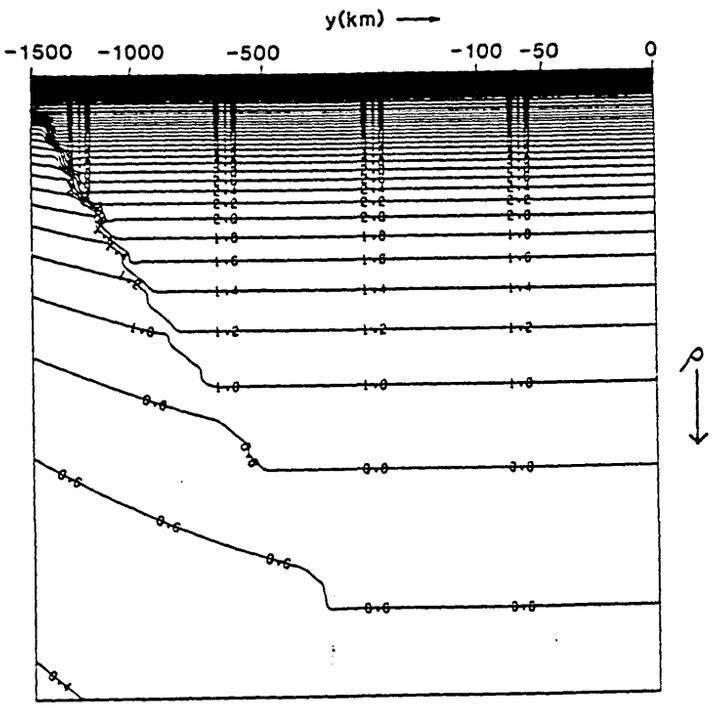

d)

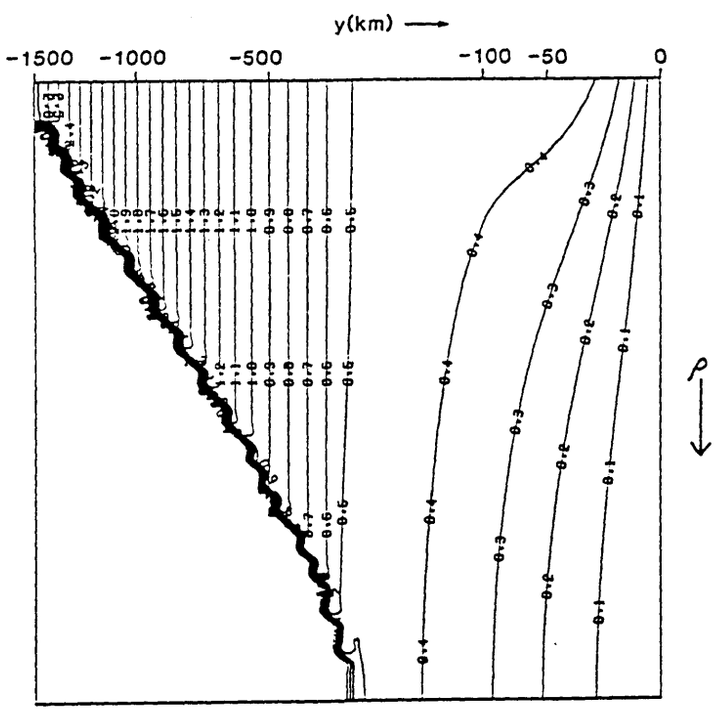

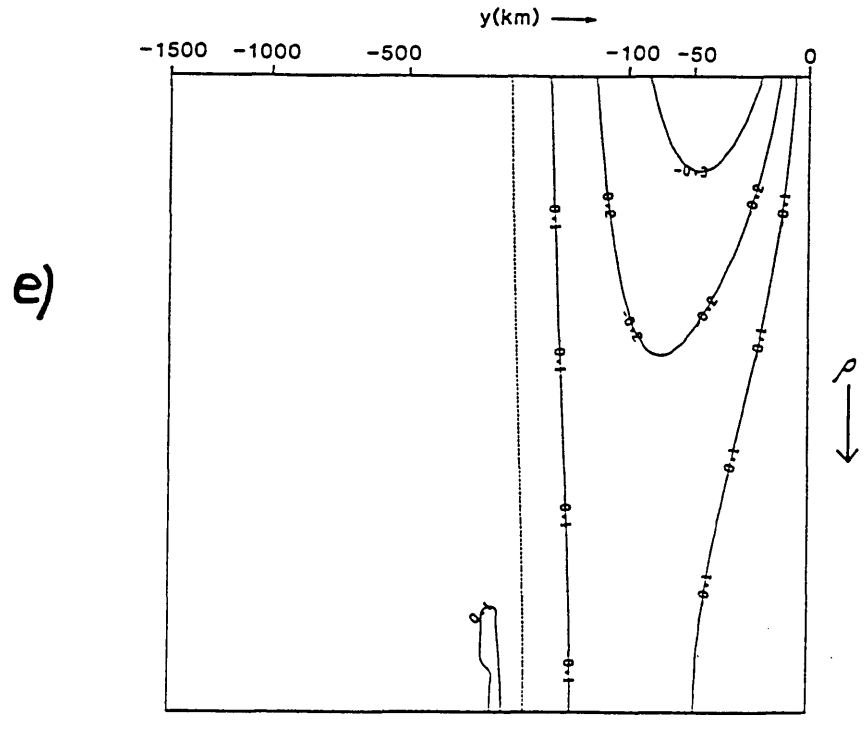

Figure 6.4: Results from an inversion with a stretched sinusoidal thermocline shape (see equation (6.4.7)) and a maximum thermocline depression of 220 m. Depth dependent stratification is used with $s_0 = 0.05$. (a) and (b) as figure (6.2). (c) Potential vorticity, Q. (d) Vortex stretching term, $QM_{\rho\rho}$ and (e) relative vorticity, $\lambda^2 M_{yy}$ all in non-dimensional units (coordinates stretched as in appendix A).

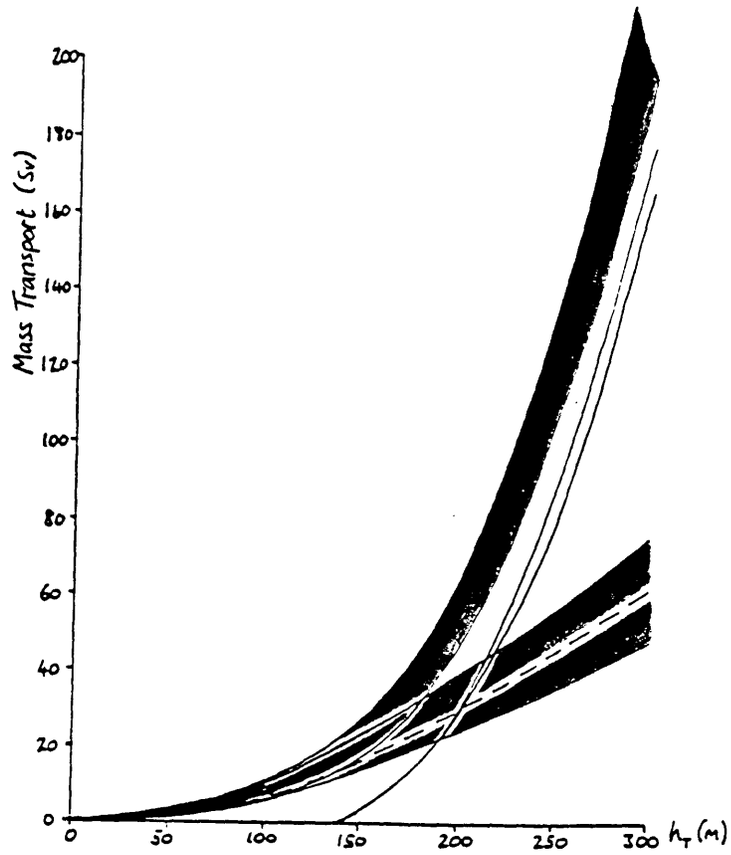

Figure 6.5: As figure (6.3) but for inversions with a stretched sinusoidal thermocline. The lower curves show results for an $M = 0$ bottom boundary condition, with the dashed curve giving the sub-thermocline transport if uniform stratification is used.

in equation (6.2.8) associated with vortex stretching and relative vorticity are shown in figures (6.4) (d) and (e). Vortex stretching is again seen to be the dominant process in the baroclinic fringe region to the south, with relative vorticity playing a role in the barotropic core, especially in the eastward jet.

The sensitivity of the transport of the model to h_T is revealed in figure (6.5), a graph similar to that of figure (6.3). It appears that the shape of the thermocline has some small impact on the strength of the flow, with the transport rising more sharply in the case where the maximum depression is further south. However, it is still the case that for realistic transports, at least the sub-thermocline transport is predominantly barotropic. Significant changes to this picture will emerge in the next section.

Parameter studies in which $\Delta\rho$ was varied by several kg m^{-3} show that this has a weak effect on the transport compared to the great sensitivity to a reasonable range of

h_T, with stronger stratification resulting in a slightly increased transport as the Rossby radius increases and relative vorticity becomes more important. The partition between barotropic and baroclinic components shows more sensitivity to stratification, with the depth independent share of the transport weakening considerably as $\Delta\rho$ gets larger.

6.5 Alternative Bottom Boundary Conditions

In all the numerical inversions discussed so far, and in the theory at the beginning of the last section, it was assumed that the bottom boundary of the ocean was a flat isopycnal. A possible rationale for making this assumption is the fact that if an ocean gyre were to spin up from rest, with zero vertical velocity on a flat bottom, then the resulting state would indeed have an isopycnal bottom. However, in reality the ocean floor is not flat; bottom friction can lead to deep Ekman pumping and the long time scales involved in setting up the baroclinic structure of the deep ocean allow for other physical processes to have important effects, neglected in the weak dynamical argument mentioned above. Bottom friction in particular has been investigated in section 4.4 by considering a (q, ψ) relationship in the deep ocean. The difficulty of assigning a value to this quantity and comparing it with measurable quantities has already been emphasised. In the framework of the new model, it is possible to obtain guidance directly from measurable quantities, such as the typical depth perturbation of very deep isopycnals in the recirculation region. In the hydrographic data taken at 52^0W (discussed further in the next section), isopycnals near the bottom of the recirculation are seen to bow downwards to extents of the order of hundreds of metres. The bottom topography also shows height variations of this order. An important question therefore arises as to the effect of changing the bottom boundary condition of the model in this manner. The following simple argument sheds light on this matter.

Consider a model in which the bottom isopycnal deviates from its reference depth by an amount $z_H(y)$. In this case (6.4.1) becomes

$$\lambda^2 \tilde{M}_{yy} = z_T - z_H - \beta' y \tag{6.5.1}$$

It can immediately be seen that if the barotropic mode is to consist of an anticyclonic gyre, with $\tilde{M}_{yy}$ negative over most of the core, then (6.5.1) places restrictions on the

possible magnitude of z_H. If z_H is negative, as suggested by the data, this limit can be written

$$|z_H| \leq |z_T| - \beta'|y| \tag{6.5.2}$$

and simply represents the value of z_H set in the one dimensional problem with no relative vorticity. This result is independent of the form used for s. Using (6.5.2) as a guide, it can be seen that if plausible values are chosen: $|z_T| \sim 0.05$; $\beta' \sim 0.3$ and $|y| \sim 0.1$, then there is considerable cancellation on the right hand side, leading to strong constraints on z_H. In general, we require that M be positive everywhere, so it is to be expected that the condition on z_H will be even more stringent than (6.5.2), which merely implies that $\tilde{M}$ is positive. The conclusion is that it does not take a very large perturbation to the bottom isopycnal to alter the barotropic component drastically.

The results of numerical inversions in which the bottom boundary condition has been set to $M = 0$, forcing the depth independent component of the flow to vanish, confirm this result. For example, in an inversion with $h_T = 220$ m in equation (6.4.7) and $s_0 = 0.05$, the maximum deviation of the bottom isopycnal is just 56 m. The corresponding transport in such inversions is, of course, purely baroclinic and greatly diminished. Its dependence on h_T is indicated through the lower curves in figure (6.5). The dashed line shows the sub-thermocline transport in similar inversions with uniform stratification, confirming the predictions of equation (6.3.11) for the baroclinic transport.

It is interesting to enquire whether it is possible to obtain a realistic transport and strong bottom currents ($\sim$ 10 cm s^{-1}, Schmitz, 1980) but with more realistic deviations of the deep isopycnals from the horizontal ($\sim$ 100 m as a conservative estimate based on hydrographic data shown in the next section). The transport is very sensitive to h_T, so it can easily be strengthened by increasing this parameter slightly. However, a very different flow pattern now emerges. This can be seen in figure (6.6), an inversion with $h_T = 330$ m and with a bottom boundary condition set through the relation

$$z_H = -h_H \sin \pi \frac{(y + l)}{l} \tag{6.5.3}$$

within the core region and $h_H = 100$ m. The resulting velocity field is far more baroclinic, with considerable baroclinic recirculation even within the core. The hydrography shows the bottom isopycnal bowing down as specified, The transport in this case is 97 Sv, with

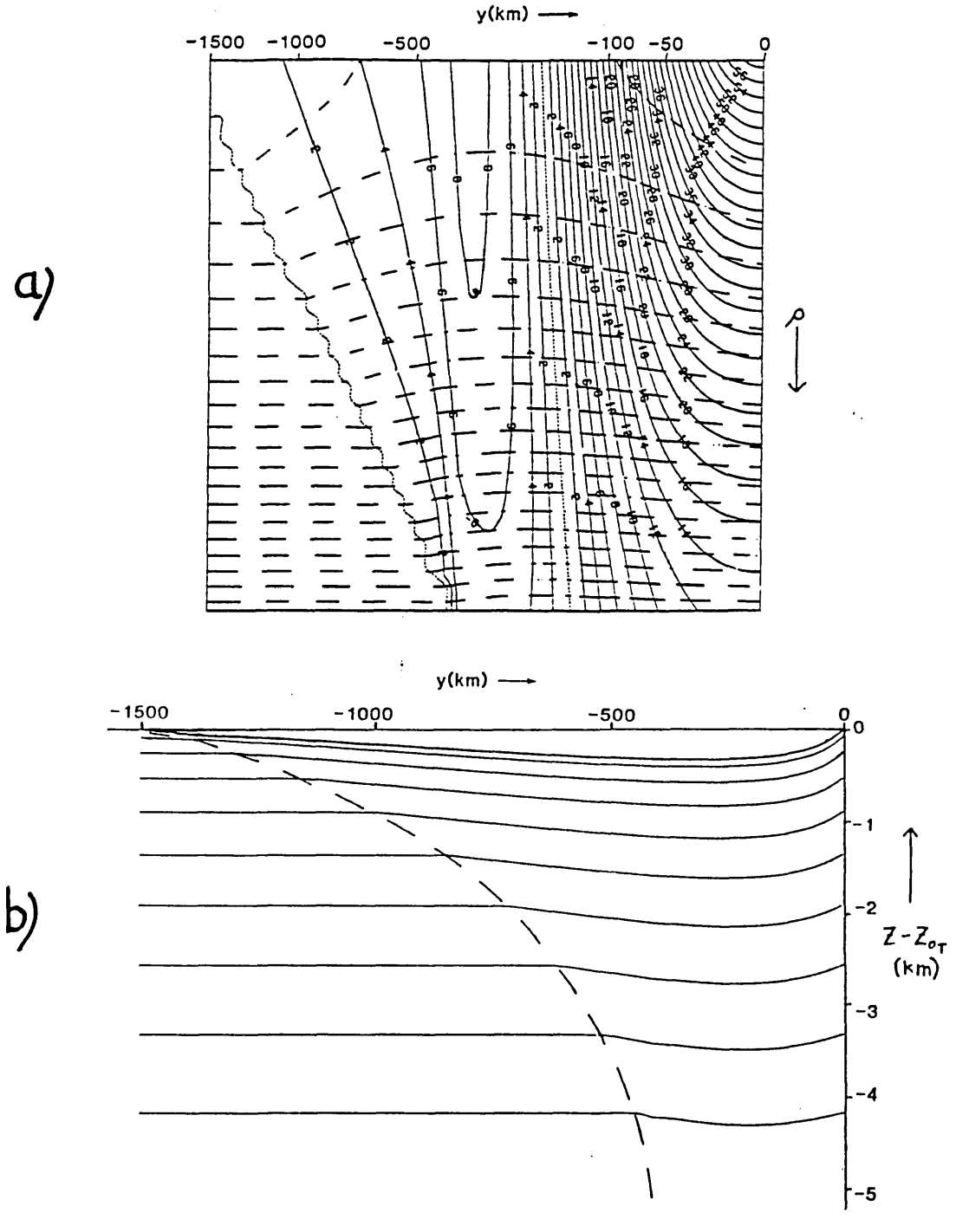

Figure 6.6: An inversion in which both top and bottom isopycnals are perturbed, by 330 m and 100 m respectively. (a) shows zonal velocity with depth contours and (b) shows the hydrography as in figure (6.2).

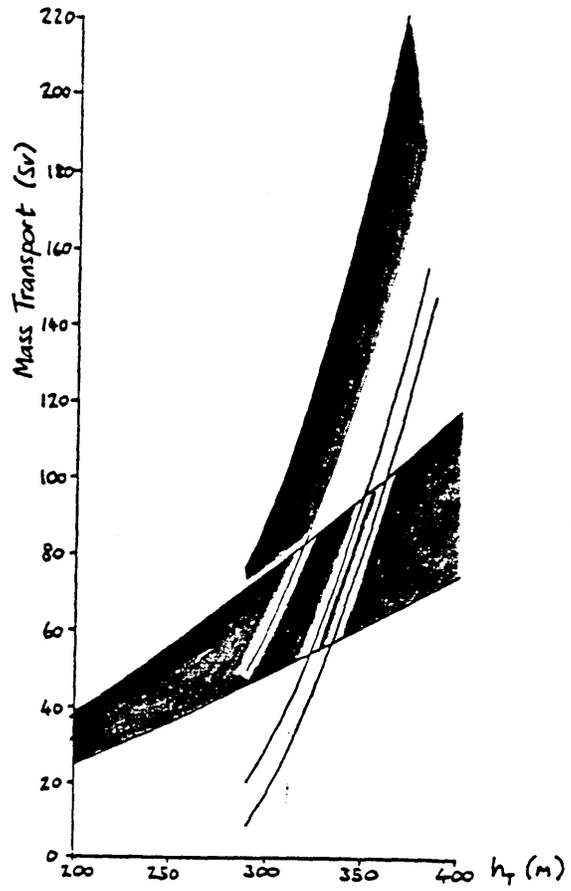

Figure 6.7: As figure (6.5) but with the bottom isopycnal depressed by 100 m according to equation (6.5.3). Lower curves show results with an $M = 0$ bottom boundary condition, continued from figure (6.5).

only 65 Sv returned within the core, of which 51 Sv is depth independent. The transport above the thermocline is estimated at 37 Sv, of which 8 Sv is due to the velocity shear. The maximum velocity in the jet is 59 cm s^{-1} and the core is 397 km wide. The transport in figure (6.6) is rather high, although not as high as it would be if the bottom isopycnal were flat (see figure (6.5)). However, the maximum westward bottom velocity is only 5 cm s^{-1}, and the depression of the bottom isopycnal is modest. The conclusion is that it is difficult to reconcile realistic bottom velocities with realistic bottom isopycnal deviations in a uniform potential vorticity model with a reasonable mass transport.

The dependence of the transport in these inversions on h_T is shown in figure (6.7). The continuation of the purely baroclinic transport curves from figure (6.5) is included for comparison. There is a lower limit on h_T, below which the deep values of M start to

become negative. Above this limit, the transport curves rise very steeply with increasing h_T with a large proportion of the transport now carried by the baroclinic flow. This highly sensitive result could be modified if some linkage between the values of h_T and h_H were imagined to exist, but this would involve further abstract physical conjecture.

6.6 A Semi-Data-Driven Inversion

The analytical functions chosen to represent the thermocline depression in previous sections have been useful for comparing the effects of the different strengths of forcing and for comparing the model with theory. However, neither gives a very satisfactory shape to the thermocline for comparison of the model with observations and in this section we shall take full advantage of our freedom to impose a realistic thermocline depression.

Figure (6.8b) shows a hydrographic section taken at 52^0W (obtained from the Rhines Atlas, University of Washinton). Deep potential vorticity contours from this section calculated by McCartney (private communication) appear to follow the density contours closely in the flow region. It is therefore interesting to carry out an investigation in which the thermocline depression is based on the shape of the $\sigma_\theta = 26.6$ contour, shown in figure (6.8a), with potential vorticity uniform on isopycnals in the flow region beneath. The meridional extent of the inversion is now 1660 km, with H and $\Delta\rho$ equal to 5 km and 1.5 kg m^{-3} respectively.

As it stands, the data presents problems if it is to be interpreted in terms of a steady model with no zonal variation. The quasi-synoptic nature of the hydrographic section means that considerable variations in thermocline depth can be seen which are not permanent or not continuous in the zonal direction. Eddies such as these, whether they are steady or transient, need to be removed to make the model more truly representative of the recirculation. It is also necessary to do this for technical reasons, because if the thermocline goes above its reference depth, M becomes negative just below the thermocline implying a locally cyclonic circulation and making it impossible to solve for the bowl. The dotted line in figure (6.8a) shows the thermocline shape which was actually used to force the model.

Another difficulty to be faced is the choice of reference depth for the thermocline. Given the actual thermocline depth, this is effectively a choice of the strength of its

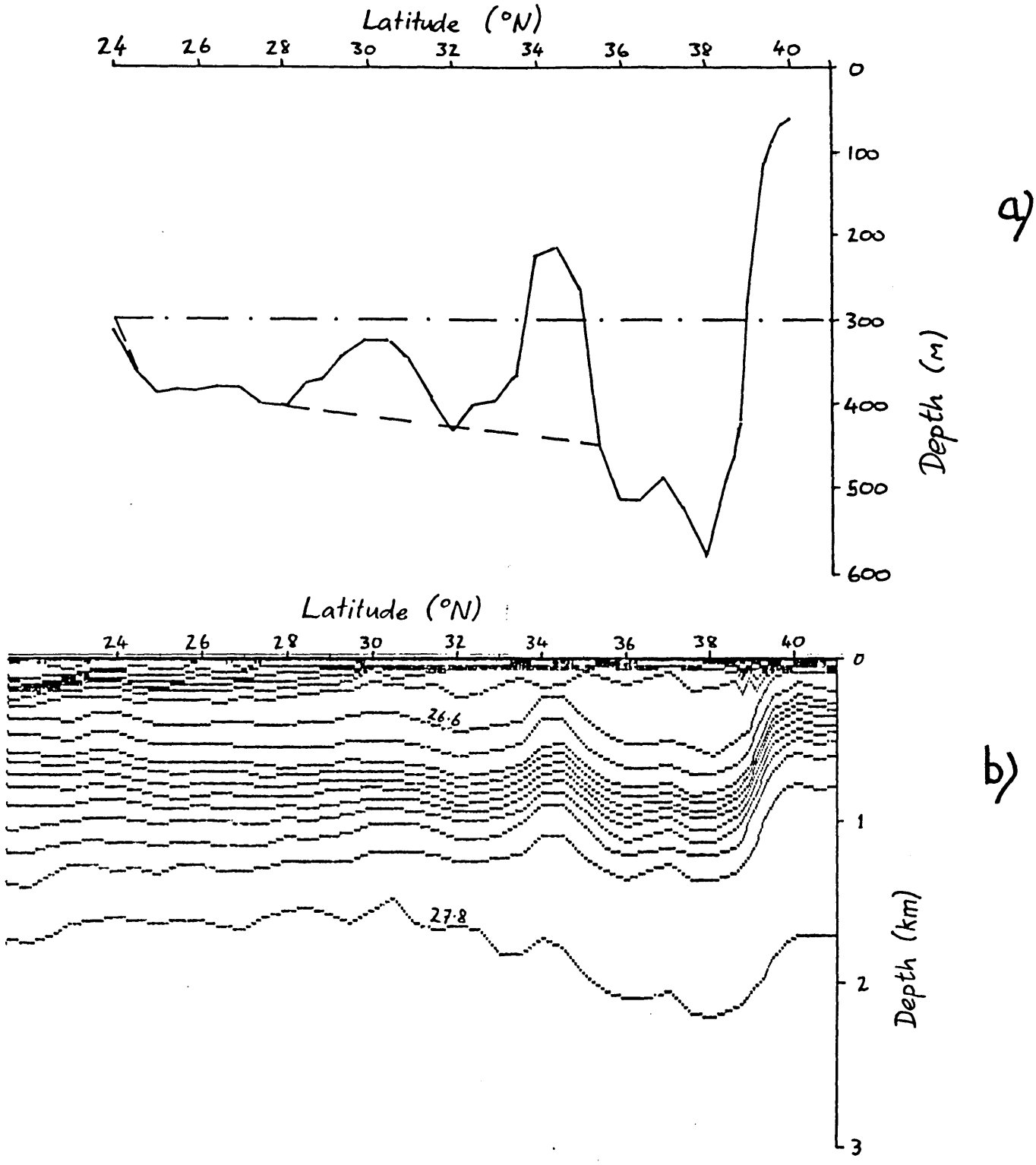

Figure 6.8: Data from a hydrographic section taken at 52^0 W (from the Rhines Atlas, University of Washington). (a) Depth of the $\sigma_\theta = 26.6$ surface, with dashed lines denoting values used to force the model (see text) and the dot-dashed line showing the reference depth chosen. (b) The full hydrographic section (contours of σ_θ).

downward perturbation, to which the transport is sensitive. This must be borne in mind when interpreting the results. The reference depth was taken to be 300 m, entering at the southern edge of the section, with the thermocline returning to this depth at the northern edge. Finally, the bottom boundary condition was imposed through equation (6.5.3) with $h_H = 50$ m in order to achieve a realistic model transport.

The results from the inversion are shown in figure (6.9). The sub-thermocline transport is 70 Sv: 52 Sv in the core of which 37 Sv is depth independent. Above the thermocline, the transport is estimated at 26 Sv; 7 Sv due to the shear component. The effect of the thermocline shape can be seen in the velocity field of figure (6.9a), with the steepening of the depression as one moves north giving rise to a tighter signature in the velocity field, which does not spread smoothly into the fringe to the same extent as in previous inversions. The maximum velocity in the eastward jet is 91 cm s^{-1} and the core is 288 km wide. As expected, the hydrography (b) (in real coordinates) bears some resemblance to the data, given that the two eddies have been removed. Vortex stretching (c) dominates the fringe, but forms a double lobed structure to balance the relative vorticity (d), which which shows maxima near the northern and southern boundaries of the core, demonstrating clearly the lack of boundary layer structure in this region at all depths. The inclusion of data has, therefore, highlighted the important qualitative features of the of the recirculation, even if we must regard the quantitative predictions of the model with the reservations mentioned above.

6.7 Summary

A geostrophic model of the recirculation has been investigated using density as a vertical coordinate. This has given us the ability to force the model in a more physically accessible way and to compare the results directly with data. The assumption of uniform potential vorticity along isopycnals beneath the thermocline has been retained and the model has been forced with various types of thermocline depression. It has been shown that it is possible for the flow to bottom out under oceanographic parameters and that the penetration and strength of the baroclinic flow is controlled by the extent to which the thermocline is depressed, with the stratification also having some effect on the later. When the flow extends to the bottom, a strong barotropic component arises, also dependent

a)

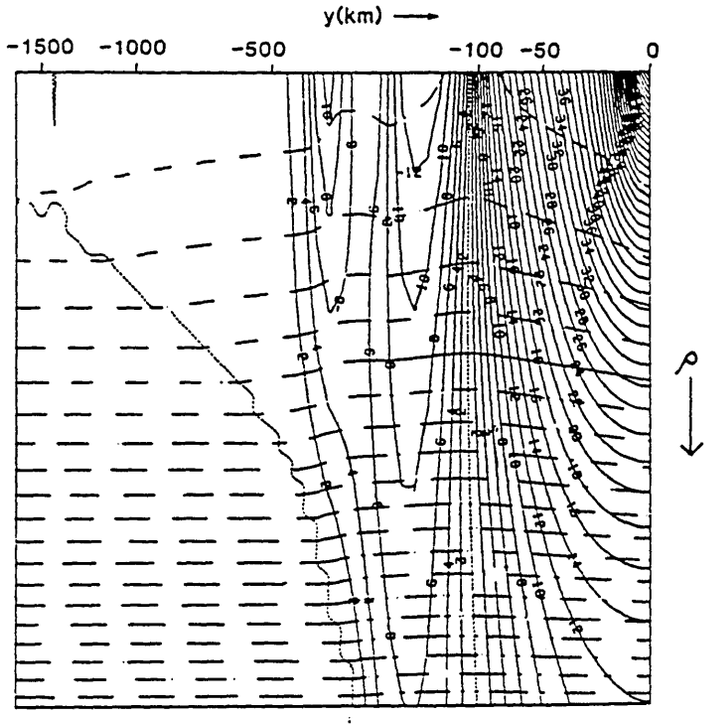

b)

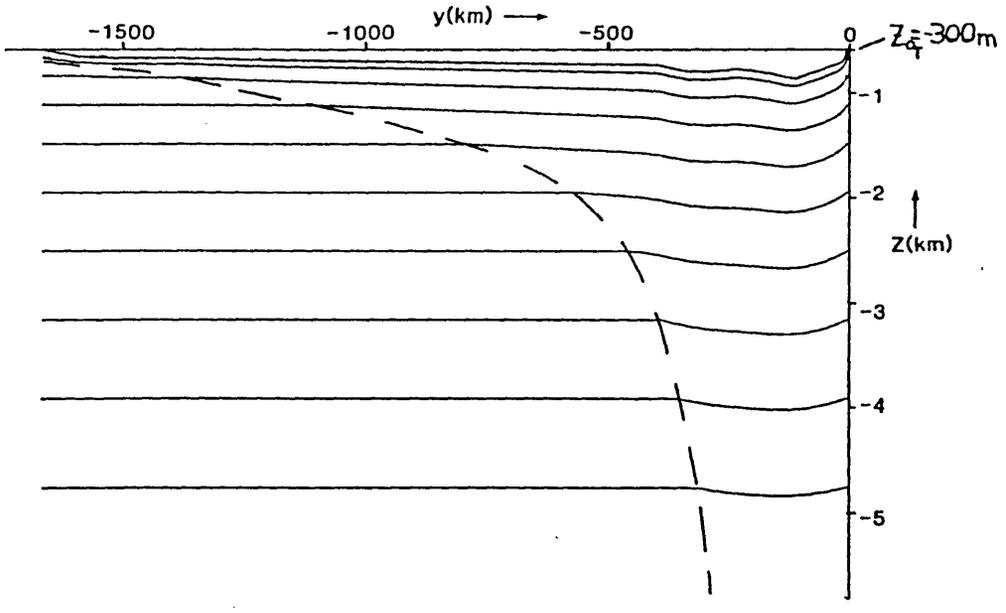

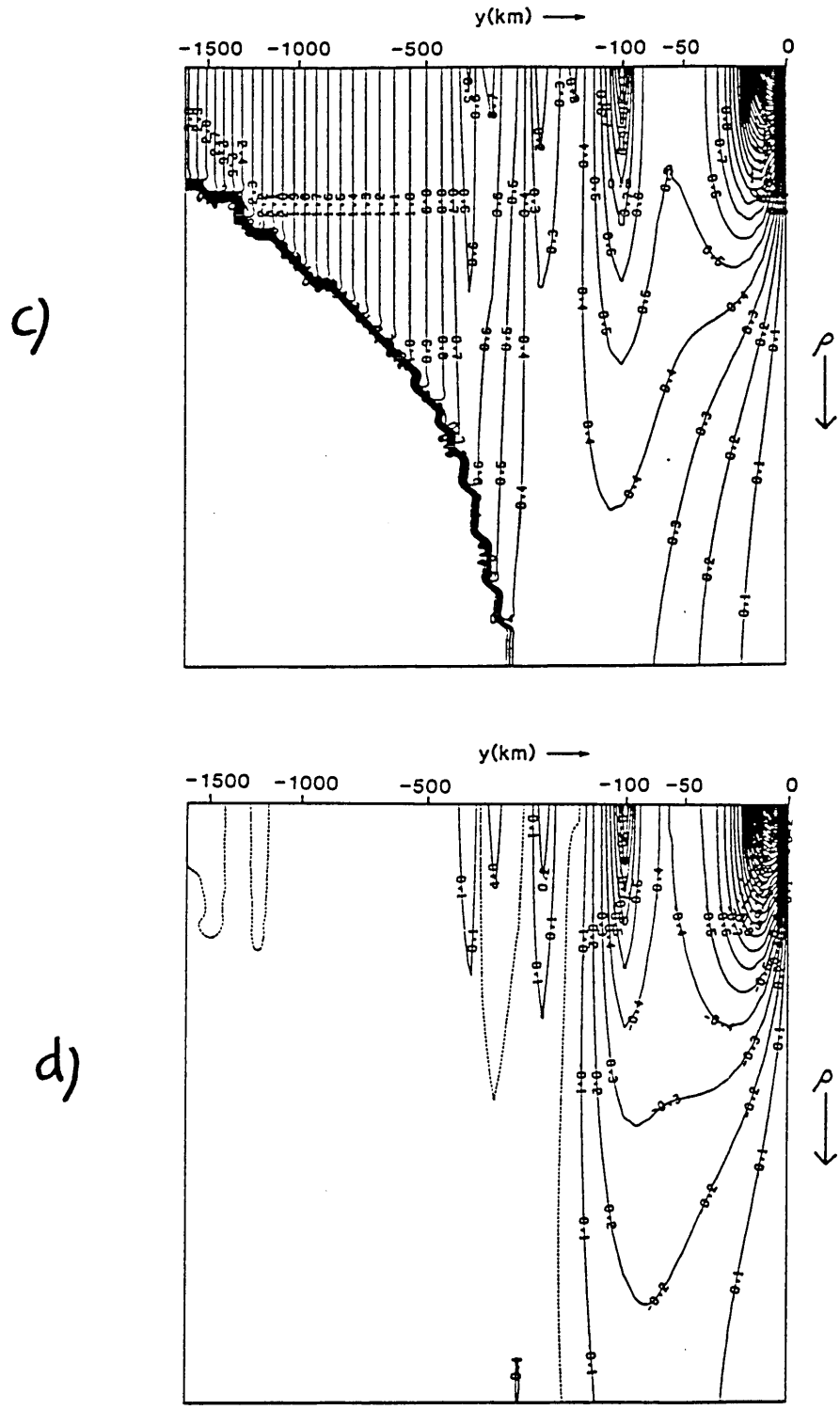

Figure 6.9: results from an inversion with the thermocline depression as in figure (6.8a) and the bottom isopycnal depressed by a maximum of 50 m. (a) Zonal velocity with depth contours. (b) The density profile. (c) Vortex stretching term. (d) Relative vorticity term. Details as in figure (6.4).

on the perturbation of the thermocline. In fact the overall transport of the model is sensitively dependent on plausible variations in maximum thermocline depression. The type of bottom boundary condition employed is also very important, with reasonable depressions of the bottom isopycnal tending to extinguish the barotropic flow leaving correspondingly small bottom velocities compared to current meter observations. Finally, it has been shown that if hydrographic data is used to guide our choice of thermocline depression, then a realistic transport can be achieved, with the realistic thermocline shape serving to emphasise the recirculating nature of the flow as opposed to a boundary layer interpretation for the eastward jet.

Chapter 7

Conclusions

A baroclinic Fofonoff gyre has been used as a basic reference point from which to describe the tight, sub-basin scale recirculating gyres found in the north western corners of the world's oceans. It was established at an early stage that it is necessary that these gyres should have some baroclinic structure, if realistic mechanical forcing and dissipation is to be balanced with eddy transfer of potential vorticity in an almost free, steady state. The remainder of the thesis has been an investigation into the precise nature of this vertical structure. Central to the studies presented above has been the assumption that potential vorticity is uniform in regions of deep flow, and that the water in these regions has been set into motion by the flow in the mechanically or thermally forced layers above. The emphasis has been on diagnosis of steady, free states, rather than on forcing mechanisms and their role in creating and maintaining these flow patterns.

Firstly, it has been shown that the abyssal flow has a finite depth penetration, and that for oceanographic parameters it is possible that this flow may not reach the bottom. This has been demonstrated in the contexts of both quasi-geostrophic and Ertel potential vorticity inversions. It is a consequence of relative vorticity, which must be present to close any type of Fofonoff gyre. This has been put forward as a possible explanation of the shallow region of uniform potential vorticity observed in the north Pacific. It should be pointed out again that these solutions are not robust to small perturbations to the value of homogeneous potential vorticity.

In regimes with stronger surface forcing, or weaker stratification, the homogeneous flow penetrates to the ocean floor. The immediate consequence of this is the emergence of

a strong barotropic component to the flow. This barotropic component is very sensitive to the surface forcing, and in some circumstances it can come to dominate the mass transport of the model. In fact, a cubic dependence on some measure of surface forcing seems ubiquitous: either on the depth integral of q in the quasi-geostrophic model, or on the depression of the main thermocline from its reference depth in the isopycnal model. This cubic dependence is not at all surprising, it was simply arrived at by solving second order linear equations. But it is significant in its relevance to the recirculation region, where these second order equations can be applied. The sensitivity of the transport to thermocline perturbation is consistent with the observed phenomenon of 'anticyclogenesis' following severe winters, when the Gulf Stream intensifies as a result of an enhanced depression of the main thermocline due to either thermal or mechanical forcing.

The existence of a barotropic component to the flow allows us to define partitions in the mass transport of the model. One such partition is between the depth independent part, and the contribution made due to velocity shear from the bottom upwards. It has been found that there is close correspondence between this partition and a spatial partition which demarkates the transport into 'core' and 'fringe' regions. The eastward jet is very surface intensified, but the recirculation immediately to the south is only weakly depth dependent, the baroclinic part of the jet being recirculated further south in the fringe where there are no bottom currents. This transport scheme is consistent with the observations of the Gulf Stream and its recirculation described in chapter 2. The precise partition of transport between fringe and core depends on a number of factors. Again the degree of surface forcing is important with more strongly forced flows tending to be more barotropic. The strength of the stratification also has some bearing on this balance with stronger stratification tending to enhance the baroclinic component.

The novel feature of the work has been the full inclusion of both the relative vorticity and vortex stretching components of the potential vorticity in a vertically continuous model. An ability to study the importance of these two terms has led to two conclusions:

1) The vortex stretching term is dominant in magnitude over almost the whole of the recirculation, although it disappears in vertical integral.

2) The relative vorticity term is vital, either in allowing the bowl of the circulation to bottom out, or in cases where bottom flow exists, in controlling the depth integral structure

over the whole of the barotropic core of the recirculation. The inversions generally demonstrate that a decaying boundary layer type structure is not applicable to the barotropic core.

To sum up: both baroclinic structure and relative vorticity are essential for any model of the recirculation based on free non-linear gyres. In this model the complementary approaches of MN and CIY have therefore been brought together, with the added advantage of high vertical resolution.

If the flow in a sub-section of an ocean basin is to be represented by solving an elliptic equation, then the solutions will be sensitive to two considerations: the nature of the field inverted and the position and conditions imposed at the boundaries. The boundaries give rise to particular problems since we do not always know where they are and exactly what conditions correspond best to the physical world. These two questions are related, as in the case of the southern boundary condition on the bottom flow, where arguments were given for the application of either free slip or no slip conditions. The total transport of the model was not sensitive to this issue, but the width and transport of the barotropic core was affected. The solutions have also shown great sensitivity to boundary conditions about which we have more information. The obvious example is the depth perturbation of the thermocline, entering as a top boundary condition in the isentropic model of chapter 6, which determined the transport of the homogenised gyre below. The solutions were also found to be sensitive to the depression of the bottom isopycnal, with feasible perturbations of deep density surfaces able to extinguish the barotropic flow brought on by the depression of the thermocline above. It was found that realistic hydrography was not easy to reconcile with realistic bottom currents in the uniform potential vorticity model.

This brings us to the first consideration mentioned above, the nature of the field being inverted. The flow field may well be sensitive to departures of the deep potential vorticity from uniformity. In chapter 5 it is demonstrated that a small, finite anomaly in the value to which the deep potential vorticity homogenises can have dramatic effects on the vertical structure of the flow. If this anomaly is positive, then a recirculation system emerges in which the surface sub-tropical gyre is strong, with a smaller counter-rotating sub-polar gyre to the north. At depth this picture is reversed, with a dominant cyclonic gyre in the core squeezing the deep sub-tropical gyre to the south. A limit exists on the deep q

anomaly which corresponds to a solution in which the bottom flow is entirely cyclonic. The solutions shown in chapter 5 are suggestive of the deep flow in the western north Atlantic and although the model is again steady and diagnostic, and does not address the question of the creation or maintenance of these flow patterns, there is circumstantial evidence of a positive deep q anomaly and ample opportunity for maintaining it in the deep north Atlantic circulation.

On the subject of comparing the model with potential vorticity distributions in the data, it has been noted that this is very difficult in the quasi-geostrophic framework. Moving to the Ertel potential vorticity in the isopycnal model of chapter 6 was a great improvement in this respect, as well as in terms of being able to force the model with real data. The 'semi-data-driven' inversion shown still carries with it the assumption of uniform deep potential vorticity, and still solves for the 'bowl' of the circulation. When looking at real potential vorticity data, the general impression is that isopycnally uniform potential vorticity does exist at all depths, bounded by some sort of bowl. Ideally, the demarkation between the flow region and the stagnant water coincides with a change in the nature of the Q contours. In density coordinates, Q contours should be flat in the homogeneous flow region, and slope at an angle given by $(\partial\rho/\partial y)_Q = -\beta N^2/f\frac{\partial N^2}{\partial\rho}$ outside this region. This angle is small enough to make location of the bowl difficult in noisy data.

The logical next step is to attempt an inversion of real potential vorticity data. This would form a very interesting extension of this work and may provide an answer to some of the questions posed above concerning uncertainties in boundary conditions, and degree of homogeneity of Q. However, this is by no means a solution to the 'level of no motion problem'. The potential vorticity field would need to include a contribution from the barotropic flow, invisible to the hydrography. It is possible to conceive of an iterative procedure which could bring forward the fields of M and Q together from initial hydrographic data to a full solution with a consistent barotropic mode, in which the Q field matches both density and momentum fields. The domain over which such an inversion could be carried out would have to be small enough to allow relative vorticity to form a significant part of the elliptic operator, and the conditions at the side boundaries would still influence the solution. Also, the two dimensional nature of the model would still give rise to the problems discussed in chapter 6. The pitfalls of attempting to recover geostroph-

ically balanced, mass conserving flow in such an 'inverse' calculation have already been encountered by Luyten and Stommel (1982).

Further desirable extensions to this model would be the explicit inclusion of the thermocline flow and the representation of outcropping density surfaces. The arguments for using an isopycnal model become considerably weaker if these things are included as the surface boundary condition is now a mixed layer density rather than the depth of an isopycnal, giving rise to considerable technical difficulties.

The ethos of forcing the model with what is known well, to deduce what is known poorly is a sound one and it should be remembered that the basic task of ocean modelling is to explain and describe the ocean circulation. A good ocean model is inspired by observations. Likewise, all data analysis contains some elements of modelling. As the extensions suggested above are added to the model, the line between modelling and data analysis will be crossed. A good oceanographer should always be aware of which side of this line he is on.

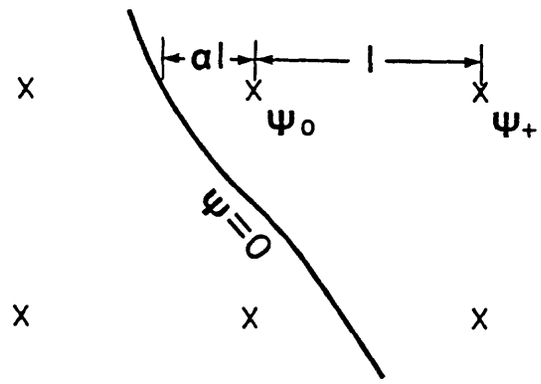

Figure A1: Grid points in the numerical inversion with the bowl passing between them.

Appendix A

The Iteration Scheme

The potential vorticity field is inverted with a free boundary (the bowl) specified at each grid point position in the horizontal and between grid points in the vertical. It is known that on this boundary, and on all grid points below it, $\psi = 0$ (see figure (4.1)). In general, the boundary will cut between grid points in the horizontal and in the vertical and this is taken into account in the finite differencing above the boundary. Consider the situation in figure (A1). A set of grid points is shown with the bowl passing between them. Outlying values of ψ can be expressed as Taylor expansions about the central grid point where $\psi = \psi_0$:

$$\psi_+ = \psi_0 + l\psi_{y0} + \frac{l^2}{2}\psi_{yy0} + O(l^3)$$

$$0 = \psi_0 - \alpha l\psi_{y0} + \frac{\alpha^2 l^2}{2}\psi_{yy0} + O(l^3)$$

Subscripts denote grid point positions, l is the non-dimensional grid spacing and α is the fraction of l shown in figure (A1). These expansions lead to the following finite difference representations for first and second derivatives at the central grid point:

$$\psi_{y0} = \frac{1}{\alpha(1+\alpha)l}\left[\alpha^2\psi_+ + (1-\alpha^2)\psi_0\right] + O(l^2)$$

$$\psi_{yy0} = \frac{2}{\alpha(1+\alpha)l^2}\left[\alpha\psi_+ - (1+\alpha)\psi_0\right] + O(l)$$

These are used to to calculate quantities on grid points just above the boundary.

The extra condition which must be satisfied at the bowl is $\psi_z = 0$. Now provided the bowl is not vertical, by the chain rule, ψ_y must also be zero at each point on the bowl

(see section 4.3a) thus we can form the following quantity,

$$\frac{1}{2}(\psi_y)^2 + \frac{f_0^2}{N^2}(\psi_z)^2 \qquad (= \text{K.E.} + \text{A.P.E.}),$$

which must be zero on the bowl. This quantity has the desirable properties of being positive definite, and non-zero everywhere except on the bowl. It is minimised just above each individual boundary point in the following way: Contours of a vertical minimum are found and the position of the bowl moved up to meet these minima in decreasing increments. It was necessary to sweep inwards from the edges of the gyres towards $y = 0$, whilst iterating upwards for the bowl, because the vertical positions of the energy minima near the eastward jet are sensitive to the solution in the interiors of the gyres. The iteration stops when when the bowl sits just below an energy minimum at each horizontal grid position. Ideally, this quantity should be zero on the bowl, and it was found to be negligible in all cases once the bowl had been located to grid point accuracy.

For cases where the bowl hits the bottom, a similar procedure was followed to find the latitudes bounding the core. The position at which the bowl intersected the bottom was moved inwards towards $y = 0$ until the required lateral boundary condition (ψ_y or $\psi_{yy} = 0$ at the bottom) was satisfied to within one grid point. In the inversions where the ψ_{yy} boundary condition was implemented, thus sacrificing exact satisfaction of $\psi_z = 0$ (see section 4.3a), the A.P.E. alone was minimised in the expression above.

In the isentropic model of chapter 6, no slip boundary conditions were used throughout and a simpler iteration scheme was employed. The finite difference formulae given above were used to calculate M, but it is known that M can not change sign near the bowl and therefore that M is positive everywhere in the sub-tropical gyre (see the arguments in section 5.5). Thus an ordinary accelerated directional scheme was used to minimise M and hence its normal derivative (ensuring that it was still positive) near the bowl.

The Coordinate Stretching

It was necessary to use an irregular grid to provide the model with sufficient resolution in the eastward flow region. The following expression was used:

$$y = 5u - 5.9253 \tanh(0.82u)$$

where y, and u are the non-dimensional northward coordinates in physical space and grid

space respectively. The numbers have been chosen such that the function is monotonic; with finite derivatives at the boundaries; with y and u equal at -1, 0 and 1 and able the stretch the middle of the double gyre in a continuous manner.

Appendix B

Method of Solution for the 2 Layer Double Gyre Problem

Equations (5.3.1) have the following solutions in four different regions:

$$
\begin{aligned}
-1 \le y \le t: \quad & \psi_1 = y + 1 + A \sinh \chi(y+1) \\
& \psi_2 = 0 \\
t \le y \le s: \quad & \alpha\psi_1 + \psi_2 = -\nu^2 \left[\tfrac{y'^3}{6} + \left\{ \tfrac{\alpha-\gamma}{1+\alpha} + s \right\} \tfrac{y'^2}{2} + By' + C \right] \\
& \psi_1 - \psi_2 = \left(\tfrac{1+\gamma}{1+\alpha} \right) [1 - \cosh \nu y'] + \nu^2 C \cosh \nu y' + (1+\alpha) D \sinh \nu y' \\
s \le y \le p: \quad & \alpha\psi_1 + \psi_2 = -\nu^2 \left[\tfrac{y'^3}{6} - \left\{ \tfrac{\alpha+\gamma}{1+\alpha} - s \right\} \tfrac{y'^2}{2} + By' + C \right] \\
& \psi_1 - \psi_2 = \left(\tfrac{\gamma-1}{1+\alpha} \right) [1 - \cosh \nu y'] + \nu^2 C \cosh \nu y' + (1+\alpha) D \sinh \nu y' \\
p \le y \le 1: \quad & \psi_1 = y - 1 + E \sinh \chi(y-1) \\
& \psi_2 = 0
\end{aligned}
$$

where $y' = y - s$, $\chi = L/L_\rho$, $\nu = \chi\sqrt{1+\alpha}$, ψ has been scaled by $\beta L_\rho^2 L$ and y by L. The above solutions yield $\psi_1 = 0$ at $y = 1, -1, s$ and ψ and ψ_y are matched at $y = s$ in both layers.

Application of the further conditions that the normal modes, and their first derivatives must match at $y = t, p$ produces eight equations in the five arbitrary constants, A to E, and cubic and hyperbolic functions of t, p and s. Five of these equations were used in a linear inversion to find the values of A to E. These values were then used in the other three equations to provide three residual functions which were then minimised by varying t, p and s (each time recalculating A to E). Mutual zeros of these three residual functions correspond to the four types of solutions for t, p and s referred to in the text.

References

Bower, A. S., H. T. Rossby and J. L. Lillibridge, 1985: The Gulf Stream, barrier or blender ? *J. Phys. Oceanogr.*, **15**, 24-32.

Charney, J. G., 1955: The Gulf Stream as an inertial boundary layer. *Proc. Nat. Acad. Sci.*, **41**, 731-740.

Cessi, P., 1987: *Ph.D Thesis, M.I.T.*

Cessi, P., 1988: A stratified model of the inertial recirculation. *J. Phys. Oceanogr.*, **18**, 662-682.

Cessi, P., G. R. Ierley and W. R. Young, 1987: A model of the inertial recirculation driven by potential vorticity anomalies. *J. Phys. Oceanogr.*, **17**, 1640-1652.

Clarke, R. A., H. W. Hill, R. F. Reiniger and B. A. Warren, 1980: Current system south and east of the Grand Banks of Newfoundland. *J. Phys. Oceanogr.*, **10**, 25-65.

Csanady, G. T., 1982: The thermohaline driving mechanism of oceanic jet streams. *J. Mar. Res.*, 40(suppl), 113-142.

Defant, A., 1961: *Physical Oceanography*, Vol. 1, Pergamon Press.

Ekman, V. W., 1905: On the influence of the Earth's rotation on ocean currents. *Ark. Mat. Astron. Fys.*, **2**(11), pp 52.

Fofonoff, N. P., 1954: Steady flow in a frictionless homogeneous ocean. *J. Mar. Res.*, **13**, 254-262.

Fu, L., J. Vazquez and M. E. Parke, 1986: Seasonal variability of the Gulf Stream from satellite altimetry. *J. Geophys. Res.*, **92**, 749-754.

Gill, A. E., 1984: On the behaviour of internal waves in the wakes of storms. *J. Phys. Oceanogr.*, **14**, 1129-1151.

Greatbatch, R. J., 1987: A model for the inertial recirculation of a gyre. *J. Mar. Res.*, **45**, 601-634.

Green, J. S. A., 1970: Transfer properties of the large scale eddies and the general circulation of the atmosphere. *Quart. J. Roy. Meteor. Soc.*, **96**, 157-185.

Halkin, D. and T. Rossby, 1985: The structure and transport of the Gulf Stream at 73^{0}W. *J. Phys. Oceanogr.*, **15**, 1439-1452.

Hall, M. M., 1989: Velocity and transport structure of the Kuroshio extension at 35^{0}N, 152^{0}E. *J. Geophys. Res.*, **94**, 14445-14459.

Hall, M. M., and H. L. Bryden, 1985: Profiling the Gulf Stream with a current meter mooring. *Geophys. Res. Letters,* **12,** 203-206.

Hall N. M. J., 1990: On the depth dependence and mass transport of recirculating mid-latitude gyres. *J. Phys. Oceanogr., (submitted).*

Hogg, N. G., 1983: A note on the deep circulation of the western North Atlantic: its nature and causes. *Deep Sea Res.,* **30,** 945-961.

Hogg, N. G., and H. Stommel, 1985: On the relation between the deep circulation and the Gulf Stream. *Deep Sea Res.,* **32,** 1181-1193.

Hogg, N. G., R. S. Pickart, R. M. Hendry and W. J. Smethie, 1986: The northern recirculation gyre of the Gulf Stream. *Deep Sea Res.,* **33,** 1139-1165.

Holland, W. R., T. Keffer and P. B. Rhines, 1984: Dynamics of the oceanic general circulation, the potential vorticity field. *Nature,* **308,** 698-705.

Hoskins, B. J., 1983: Modelling of the transient eddies and their feedback on the mean flow. *Large Scale Dynamical Processes on the Atmosphere*, B. J. Hoskins and R. P. Pearce, Eds. Academic Press. pp 169-197.

Illari, L. and J. C. Marshall, 1983: On the interpretation of eddy fluxes during a blocking episode. *J. Atmos. Sci.,* **40,** 2232-2242.

Joyce, T. M. and W. J. Schmitz, 1988: Zonal velocity structure and transport in the Kuroshio extension. *J. Phys. Oceanogr.,* **18,** 1484-1494.

Keffer, T., 1985: The ventilation of the world's oceans: maps of the potential vorticity field. *J. Phys. Oceanogr.,* **15,** 509-523.

Lau, N. C. and J. M. Wallace, 1979: On the distribution of horizontal transports by transient eddies in the northern hemisphere winter-time circulation. *J. Atmos. Sci.,* **36,** 1844-1861.

Luyten, J. R. and H. M. Stommel, 1982: Recirculation Reconsidered. *J. Mar. Res.,* **40**(suppl), 407-426.

Luyten, J. R., J. Pedlosky and H. M. Stommel, 1983: The ventilated thermocline. *J. Phys. Oceanogr.,* **13,** 292-309.

Marshall, J. C., 1984: Eddy-mean-flow interaction in a barotropic ocean model. *Quart. J. Roy. Meteor. Soc.,* **110,** 573-590.

Marshall, J. C. and G. J. Shutts, 1982: A note on rotational and divergent eddy fluxes.

J. Phys. Oceanogr., **11**, 1677-1680.

Marshall, J. C., and A. J. G. Nurser, 1986: Steady, free flow in a stratified quasi-geostrophic ocean. *J. Phys. Oceanogr.*, **16**, 1799-1813.

Marshall, J. C., and A. J. G. Nurser, 1988: On the recirculation of the subtropical gyre. *Quart. J. Roy. Meteor. Soc.*, **114**, 1517-1534.

Marshall, J. C., A. J. G. Nurser and R. Brugge, 1988: On the time mean flow of quasi-geostrophic wind driven gyres. *J. Geophys. Res.*, **93**, 15427-15436.

McCartney, M. S., 1982: The sub-tropical recirculation of mode waters. *J. Mar. Res.*, **40**(suppl), 427-464.

McCartney, M. S., L. V. Worthington and M. E. Raymer, 1980: Anomalous water mass distributions at 55^{0}W in the north Atlantic in 1977. *J. Mar. Res.*, **38**, 147-172.

McDowell, S., P. B. Rhines and T. Keffer, 1982: North Atlantic potential vorticity and its relation to the general circulation. *J. Phys. Oceanogr.*, **12**, 1417-1436.

Munk, W. H., 1950: On the wind driven ocean circulation. *J. Meteorol.*, **7**, 79-93.

Munk, W. H. and G. F. Carrier, 1950: The wind driven circulation in ocean basins of various shapes. *Tellus*, **2**, 158-167.

Niiler, P. P., 1966: On the theory of wind driven ocean circulation. *Deep Sea Res.*, **13**, 597-606.

Nurser, A. J. G., 1988: The distortion of a baroclinic Fofonoff gyre by wind forcing. *J. Phys. Oceanogr.*, **18**, 243-257.

Rhines, P. B., 1979: Geostrophic turbulence. *Ann. Rev. Fluid Mech.*, **11**, 401-441.

Rhines, P. B., 1986: Vorticity dynamics and the oceanic general circulation. *Ann. Rev. Fluid Mech.*, **18**, 433-497.

Rhines, P. B., and W. R. Young, 1982a: A theory of the wind driven ocean circulation I.: Mid-ocean gyres. *J. Mar. Res.*, **40**(suppl), 559-596.

Rhines, P. B., and W. R. Young, 1982b: Homogenisation of potential vorticity in planetary gyres. *J. Fluid Mech.*, **122**, 347-367.

Richardson, P. L., 1985: Average velocity and transport of the Gulf Stream near 55^{0}W. *J. Mar. Res.*, **38**, 111-135.

Robinson, A. R., J. R. Luyten and F. C. Fuglister, 1974: Transient Gulf Stream meandering. Part I: An observational experiment. *J. Phys. Oceanogr.*, **4**, 237-255.

Sarmiento, J. L., 1983: A tritium box model of the north Atlantic thermocline. *J. Phys. Oceanogr.,* **13,** 1269-1274.

Saunders, P. M., 1982: Circulation in the eastern north Atlantic. *J. Mar. Res.,* 40(suppl), 641-657.

Schmitz, W. J., 1980: Weakly depth dependent segments of the north Atlantic circulation. *J. Mar. Res.,* **38,** 111-133.

Schmitz. W. J., 1987: Observations of new, large and stable abyssal currents at mid-latitudes along 165 E. *J. Phys. Oceanogr.,* **17,** 1309-1315.

Starr, V. P., 1945: A quasi-lagrangian system of hydrodynamical equations. *J. Meteorol.,* **2,** 227-237.

Stewart, R. W., 1964: Th influence of friction on inertial models of oceanic circulation. *Studies in Oceanography,* pp 3-9.

Stommel, H. M., 1948: The westward intensification of wind driven ocean currents. *Trans. Am. Geophys. Union,* **29,** 202-206.

Stommel, H. M. and G. Veronis, 1980: Barotropic response to cooling. *J. Geophys. Res.,* **85,** 6661-6666.

Sverdrup, H. U., 1947: Wind driven currents in a baroclinic ocean; with application to the equatorial currents of the eastern Pacific. *Proc. Nat. Acad. Sci.,* **33,** 318-326.

Talley, L. D., 1988; Potential vorticity distribution in the North Pacific. *J. Phys. Oceanogr.,* **18,** 89-106.

Talley, L. D. and M. E. Raymer, 1982: Eighteen degree water variability. *J. Mar. Res.,* 40(suppl), 757-775.

Veronis, G., 1966: Wind driven ocean circulation - Part 2: Numerical solutions of the non-linear problem. *Deep Sea Res.,* **13,** 31-55.

Woods, J. D. and W. Barkmann, 1988: A Lagrangian mixed layer model of Atlantic 18^{0}C water formation. *Nature,* **319,** 574-576.

Worthington, L. V., 1962: Evidence for a two gyre circulation in the north Atlantic. *Deep Sea Res.,* **9,** 51-67.

Worthington, L. V., 1972a: Anticyclogenesis in the oceans as a result of outbreaks of continental polar air. *Studies in Physical Oceanography - A Tribute to George Wust on his 80th Birthday,* Vol. I, A. L. Gordon, ed. Gordon and Breach, New York. pp

169-178.

Worthington, L. V., 1972b: Negative oceanic heat flux as a cause of water mass formation. *J. Phys. Oceanogr.*, **2**, 205-211.

Worthington, L. V., 1976: On the north Atlantic circulation. *Johns Hopkins Oceanographic Studies*, Vol. VI.

Worthington, L. V. and H. Kawai, 1972: Comparison between deep sections across the Kuroshio and the Florida Current and Gulf Stream. *KUROSHIO - its Physical Aspects*, H. Stommel and K. Yoshida, eds. University of Tokyo Press. pp 371-385.